Quantitative Pipelines for Tracking and Understanding the Evolution of Cerebrovascular Atherosclerosis with Multi-contrast, Multi-time Point Vessel Wall Magnetic Resonance Imaging

Yin Guo

A dissertation

submitted in partial fulfillment of the

requirements for the degree of

Doctor of Philosophy

University of Washington

2025

Reading Committee:

Chun Yuan, Chair

Savannah C. Partridge

Ying Zheng

Program Authorized to Offer Degree:

Bioengineering

University of Washington

Abstract

Quantitative Pipelines for Tracking and Understanding the Evolution of Cerebrovascular Atherosclerosis with Multi-contrast, Multi-time Point Vessel Wall Magnetic Resonance Imaging

Yin Guo

Chair of the Supervisory Committee:

Chun Yuan

Department of Bioengineering

Given the substantial global health burden and anticipated rise in mortality rates associated with stroke, imaging of cerebrovascular atherosclerotic plaque plays a crucial role in stroke prevention efforts. Three-dimensional (3D), multi-contrast MR vessel wall imaging (VWI), applied to both carotid and intracranial arteries, offer non-invasive and comprehensive techniques to directly visualize atheromatous plaques and discern their composition, including features such as Gadolinium contrast enhancement (CE) and intraplaque hemorrhage (IPH). Particularly in longitudinal studies, this capability allows for the monitoring of lesion evolution over time, providing valuable insights into the disease process and the efficacy of medical interventions. This research presented advances in VWI analysis of both carotid and cerebral atherosclerosis and deepens our understanding of the evolution of atherosclerosis in the context of stroke.

Firstly, regarding intracranial atherosclerosis, standardized pipelines for 3D multi-planar, multi-contrast, and multi-time point imaging review were established, ensuring reproducibility in measuring plaque morphology. A novel CE map was introduced to objectively quantify plaque CE intake. In one of the first prospective studies tracking intracranial atherosclerosis evolution using 3D VWI, this research observed the evolution of intracranial plaques over a 1-year follow-up period and found that plaques progressing over time demonstrated inward remodeling and lumen loss, while regressing plaques exhibited luminal expansion. Significantly, plaque CE and diabetes mellitus were identified as biomarkers predicting plaque progression.

Secondly, tailored analysis pipelines were proposed for two complementary carotid VWI contrasts, enabling consistent measurements of vessel thickness, plaque burden, and IPH. Through a long-term prospective study spanning up to 6 years with up to 5 scans per patient, our research revealed the systemic nature of atherosclerosis, characterized by bilateral plaque evolution symmetry. IPH emerged as a significant driver of plaque progression, capable of disrupting bilateral symmetry and accelerating plaque burden increase. These findings underscore the critical importance of integrating IPH assessment into clinical evaluations of plaque progression.

Collectively, these studies establish robust quantitative methods for analyzing vessel wall imaging and provide critical insights into atherosclerotic disease progression in cerebrovascular territories. By establishing the clinical significance of imaging biomarkers like contrast enhancement and intraplaque hemorrhage, this research enables improved risk stratification and monitoring of treatment response, potentially advancing stroke prevention strategies.

Table of Contents

List of Figures

List of Tables

Acknowledgements

I would like to express my deepest gratitude to Dr. Chun Yuan for his unwavering support, mentorship, and inspiration throughout my doctoral journey. Your extraordinary research passion and incisive critical thinking have profoundly shaped my approach to scientific inquiry and will forever influence my future research endeavors and career development. Your emphasis on maintaining a comprehensive grasp of the research landscape while striving for perfection in every detail has set an exemplary standard that I will carry forward. I feel immensely fortunate to have had you as my supervisor, and your unconditional trust and steadfast support have been my continuous source of motivation to challenge myself, grow as a researcher, and contribute meaningfully to the field we both cherish.

I am also deeply grateful to my supervisory committee members—Dr. Savannah S. Partridge, Dr. Ying Zheng, Dr. Mike Averkiou, Dr. Marta Scatena, and Dr. Shuyi S. Chen—for their invaluable guidance, thoughtful insights, and constructive feedback that have enriched and strengthened my thesis work.

I am profoundly indebted to all current and former members of the Vascular Imaging Lab (VIL). Special recognition goes to Dr. Thomas S. Hatsukami, Dr. Mahmud Mossa-Basha, and Dr. Niranjan Balu for their visionary leadership in steering the lab toward exciting new frontiers and for generously dedicating their time to our weekly discussions that proved both insightful and transformative. My heartfelt gratitude extends equally to Dr. Gador Canton, Dr. Li Chen, Dr. Jie Sun, Daniel S. Hippe, and Marina S. Ferguson for their exceptional collaboration and partnership. I am also thankful to all the dedicated VIL image reviewers whose meticulous work made this research possible. Furthermore, Kaiyu Zhang, Xin Wang, Gabrielle Xia, and Zhiwei

Tan have been wonderful peers and companions throughout this journey. The VIL truly embodies the spirit of a close-knit family, bringing together remarkably kind, talented, and interdisciplinary individuals.

I would also like to acknowledge the members of the Society of Magnetic Resonance Angiography and Global Health Labs, who have been exceptional peers, cherished friends, and constant sources of inspiration. Together, we share the mission of advancing healthcare to improve lives worldwide.

This research would not have been possible without the generous financial support provided by grants from the National Institutes of Health (R01-NS092207, R01-HL103609, R01-NS125635, and R01-NS127317).

I am deeply grateful to all my friends in Seattle and from afar who have filled my life with immeasurable joy and warmth throughout this journey.

Finally, I owe my deepest gratitude to my beloved parents, whose unwavering love and steadfast belief in my dreams have been the foundation of all my achievements. I am forever grateful for the values you instilled in me and the countless ways you have shaped the person I am today.

Chapter 1 Introduction

1.1 Cerebrovascular Atherosclerosis

The human vasculature plays a critical role in maintaining the functioning of all organs by circulating blood throughout the body. Any abnormalities in the blood vessels, including arteries and veins, can lead to severe disability and even death. Cardiovascular diseases rank among the top causes of mortality globally, responsible for approximately 17.3 million deaths annually, a figure projected to rise to over 23.6 million by 2030[1].

Stroke, a devastating manifestation of vascular disease, represents a medical emergency characterized by the abrupt cessation of blood flow to the brain. This interruption can occur due to a blockage in an artery supplying blood to the brain (ischemic stroke) or the rupture of a blood vessel in the brain (hemorrhagic stroke). Responsible for 6.5 million fatalities, stroke stands as the second-leading cause of death in cardiovascular diseases[1]. Furthermore, as a primary contributor to long-term disability, survivors of stroke frequently encounter hurdles in mobility, communication, and everyday tasks, necessitating substantial rehabilitation and assistance.

Atherosclerosis, the underlying pathological process for many ischemic strokes, develops progressively through a complex cascade of events. It typically begins with damage or injury to the artery wall. With inflammation and deposition of lipid in the intimal layer, plaque forms with an increase in arterial wall thickness. Plaque buildup over time can lead to vessel stenosis and eventually occlusion, resulting in reduced blood flow and potential tissue damage. Atherosclerosis can lead to ischemic complications, such as stroke, by two mechanisms: 1) hemodynamic compromise due to development of severe stenosis or occlusion of the index

atheromatous plaque, or 2) emboli of material from the index plaque resulting in occlusion of arteries downstream[2].

The clinical significance of atherosclerosis varies considerably depending on the vascular territory affected. Intracranial atherosclerotic disease (ICAD) and carotid atherosclerosis represent two distinct but equally important manifestations of this pathological process. ICAD is particularly prevalent in Asian, Hispanic, and African American populations, accounting for up to 50% of ischemic strokes in these groups[1]. Meanwhile, carotid atherosclerosis remains a leading cause of stroke in Western populations[1]. Despite their similar pathophysiological basis, these two arterial territories present unique challenges for imaging and clinical management due to differences in vessel size, wall thickness, hemodynamics, and surrounding anatomical structures.

1.2 Imaging Atherosclerosis: Vessel Wall Magnetic Resonance Imaging

Traditional imaging approaches to assess atherosclerotic lesions have relied heavily on luminal assessment. Vascular imaging techniques, such as computed tomography angiography (CTA) and magnetic resonance angiography (MRA), are routinely used to assess stenosis and occlusion in vivo[3]. However, luminal stenosis assessment through MRA or CTA may not always accurately predict stroke risk, especially in asymptomatic or low-grade stenosis cases[4]. Studies have shown that some plaques increase in size by outward remodeling of the artery, without narrowing of the lumen area[5,6]. Such non-stenotic plaques cannot be seen by luminal imaging techniques. Hence, assessment of stenosis by angiographic imaging techniques will underestimate the presence and prevalence of these non-stenotic atheromatous lesions.

This limitation has driven the development of advanced imaging techniques that directly visualize the vessel wall rather than just the lumen. Recently, advancements in MR vessel wall imaging (VWI) sequences have facilitated the direct characterization of vessel wall pathologies in carotid and intracranial arteries within clinical settings, without the need for radiation or iodinated contrast agents[7,8]. Using post-operative specimens of carotid arteries for histopathology validation, VWI has been utilized to meticulously characterize not only the lumen and vessel wall, but also plaque components such as calcifications, lipid deposition, hemorrhage into the plaque and other matrix components.

The compositional analysis capability arises from MR VWI's capacity to integrate complementary information regarding carotid atherosclerosis within multiple contrast weightings[9]. While criteria for assessing luminal stenosis in time-of-flight (TOF) MRA are established, T1-weighted (T1w) black blood VWI serves to suppress the signal of luminal blood flow, thus facilitating direct visualization of atheromatous plaques in the vessel wall[10]. T1w VWI enables precise measurements of plaque thickness and volume. Furthermore, plaque tissue composition can be discerned and quantified through a combination of VWI contrast weightings[11]. Notably, hyperintense signals on heavily T1w sequences indicate the presence of intraplaque hemorrhage (IPH), while hypointense signals on T1w images following Gadolinium (Gd) contrast injection delineate regions of lipid-rich necrotic cores[12]. The integration of these elements, including lumen stenosis, plaque burden, and plaque tissue composition, offers a comprehensive depiction of the properties and risk profiles associated with carotid lesions, as exemplified by the recently proposed Carotid Plaque-RADS[13] approach.

While VWI techniques have been well-established for carotid atherosclerosis, their application to intracranial vessels presents unique challenges. Intracranial arteries are smaller in caliber, have

thinner walls, and follow a more tortuous course compared to extracranial vessels. Moreover, they are surrounded by cerebrospinal fluid and brain parenchyma, creating distinct imaging considerations. Lessons learned from carotid plaque imaging studies are applicable to intracranial atherosclerosis even though histological validation is challenging with cerebral vasculature. VWI of intracranial arteries is now a burgeoning field[7]. While investigators and clinicians frequently infer the imaging characteristics of plaque compositional features and the behavior of ICAD based on carotid literature, ongoing research aims to refine VWI techniques and analysis workflow tailored to the unique characteristics of intracranial vessels, promising further advancements in stroke risk assessment and management.

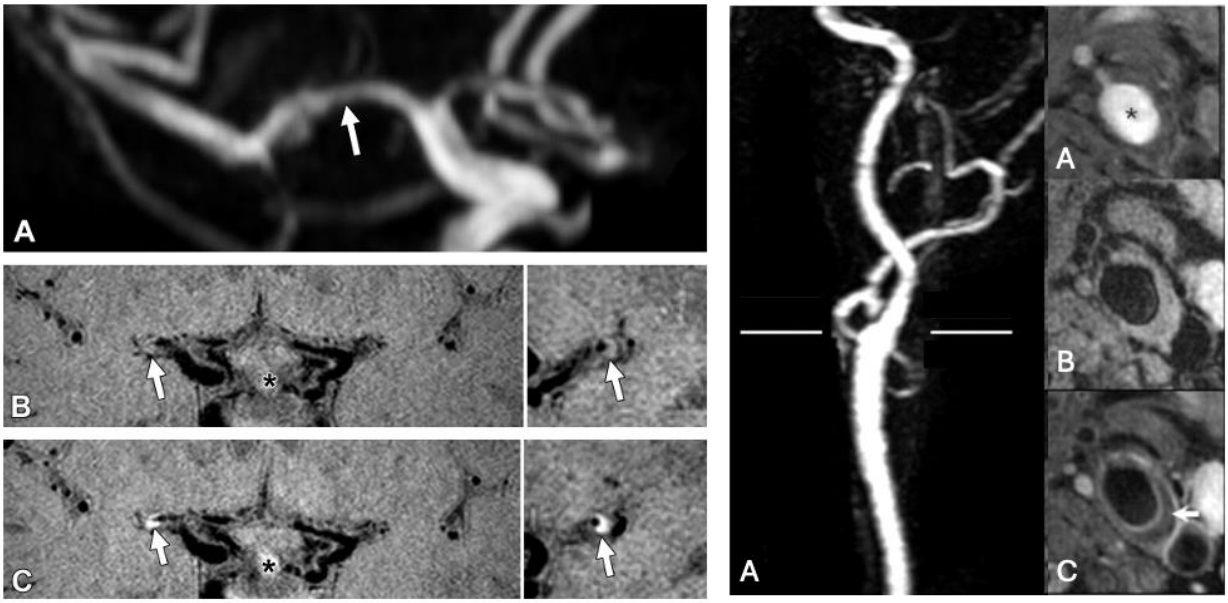

Figure 1.1 Example of intracranial and carotid MR angiography (A) and vessel wall imaging (B: pre-contrast T1w, C: post-contrast T1w) showing atherosclerotic plaques in stroke patients.

The left panel demonstrates mild to moderate stenosis of intracranial (middle cerebral) artery by MR angiography (panel A, left), but pronounced gadolinium contrast enhancement on vessel wall imaging (panel C, left) which is considered one of the features of intracranial plaque that is higher risk for stroke. The right panel demonstrates no evidence of luminal stenosis of the extracranial carotid artery (panel A, right), but presence of atheromatous plaque with a large lipid-rich necrotic core (panel C, right) which is considered to be a feature of carotid plaque that is higher risk for subsequent luminal surface disruption, intraplaque hemorrhage, and stroke[5,14].

1.3 Vessel Wall Magnetic Resonance Imaging in Longitudinal Studies

One particularly advantageous aspect of MR VWI is its non-invasiveness and lack of radiation exposure, offering unique opportunities to conduct longitudinal studies for monitoring

atherosclerotic lesions in vivo[15]. This capability allows researchers to track the natural history of atherosclerotic disease, evaluate temporal changes in plaque morphology and composition, and assess the effects of medical interventions over time. Unlike cross-sectional studies that provide only a snapshot of disease status, longitudinal VWI studies can reveal the dynamic nature of atherosclerosis, including plaque progression, regression, or remodeling in response to various factors. Furthermore, longitudinal monitoring enables the identification of imaging biomarkers and their changes that predict future clinical events, thereby improving risk stratification and potentially guiding personalized treatment decisions. The reproducibility of VWI measurements, when achieved through standardized acquisition protocols and advanced analysis methods, may further significantly enhance its value for tracking disease evolution and treatment response across patient populations.

In carotid atherosclerosis, numerous longitudinal MR VWI studies have established IPH as a critical marker of plaque vulnerability and stroke risk. Prospective studies have consistently demonstrated that patients with IPH have substantially higher rates of cerebrovascular events compared to those without IPH[16]. Recent longitudinal investigations examining IPH progression patterns have revealed that a substantial proportion of plaques with baseline IPH demonstrate persistence or expansion of hemorrhage over time, with larger baseline plaque volumes and history of smoking emerging as significant predictors of progression[17]. Technical advances in multi-contrast VWI protocols, including sequences such as MERGE[18] (motion-sensitized driven equilibrium-prepared rapid gradient echo) and SNAP[19] (simultaneous non-contrast angiography and intraplaque hemorrhage), have enabled more comprehensive assessments of carotid plaque components over time, allowing researchers to track changes in not only IPH but also calcification and lipid-rich necrotic cores[20]. For example, Zhao et al. demonstrated that intensive

lipid-lowering therapy depletes carotid plaque lipid content in a time-dependent manner, with significant reductions observed after one year of treatment and continuing through the second year, preceding overall plaque regression[21]. These longitudinal observations have significantly enhanced our understanding of plaque evolution and have informed clinical management strategies for patients with carotid atherosclerosis.

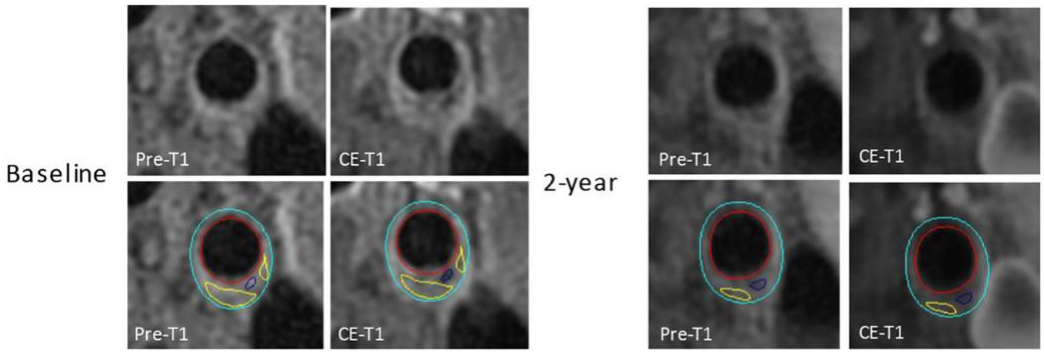

Figure 1.2 Left (baseline) and right (2-year follow-up) panels show VWI of consecutive cross-sectional images of a mixed carotid plaque in a patient undergoing intensive lipid-lowering treatment.

Contours have been added manually in the lower row of each time point (red: lumen boundary; azure: outer wall boundary). Hypointense areas indicate calcifications (navy blue contours). Non-/less-enhanced areas as compared with adjacent fibrous tissue indicate lipid cores (yellow contours). Changes in VWI signals between time points suggest a reduction in plaque wall thickness and lipid content. CE-T1 indicates contrast-enhanced T1-weighted; and Pre-T1, T1-weighted[21].

In contrast to the extensive body of literature on longitudinal carotid VWI studies, research into the evolution of intracranial atherosclerosis using VWI remains in its earlier stages. ICAD affects

a significant portion of the population and is associated with high risk of recurrent stroke (25-30%) despite optimal medical therapy[1], making longitudinal monitoring particularly important. Preliminary longitudinal VWI studies have identified Gadolinium contrast enhancement as a powerful predictor of stroke recurrence, with one study reporting a 30.3% one-year event rate in patients with enhancing plaques compared to only 6.8% in those without enhancement[22]. Additionally, enhancement patterns demonstrated disparate trends in symptomatic ICAD patients with and without stroke recurrence, suggesting their potential as prognostic indicators[23].

Emerging research has begun to identify factors associated with intracranial plaque enhancement and progression, including lipid profiles and stenosis severity[24], though longitudinal data remains limited compared to carotid studies. The continued development of intracranial VWI techniques promises to yield similarly valuable insights into disease progression and treatment response as those already established for carotid atherosclerosis.

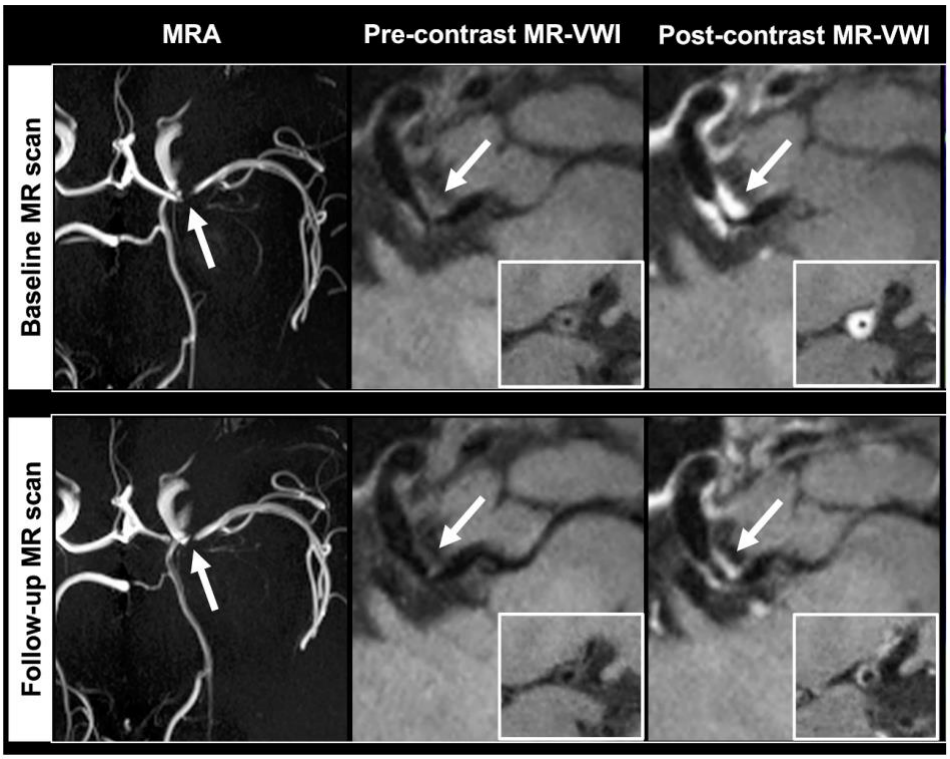

Figure 1.3 Upper (baseline) and lower (9-month follow-up) rows of panels show VWI of a plaque (arrows) at the left middle cerebral artery.

The plaque positively responded to medical therapy with smaller plaque wall volume, wall thickness and contrast enhancement[23].

1.4 Problem Statement and Research Aims

Despite significant advancements in MR VWI techniques, several critical challenges remain in the quantitative assessment of atherosclerotic disease evolution across different arterial territories. While qualitative observations of plaque features have established associations with clinical outcomes, the field lacks standardized, reproducible methods for quantitative analysis of

multi-contrast, multi-time point VWI data. This limitation hinders our ability to precisely track disease progression, evaluate treatment efficacy, and predict future cerebrovascular events.

This dissertation addresses these methodological gaps through the development and validation of novel quantitative pipelines for the analysis of VWI in both intracranial and carotid atherosclerosis. The overarching aim was to create robust analytical frameworks that enable comprehensive assessment of plaque morphology, composition, and temporal evolution, thereby enhancing our understanding of the natural history of atherosclerotic disease and its response to treatment.

For intracranial atherosclerosis, this research first established MOCHA (multi-planar, multi-contrast and multi-time point plaque characterization), an integrated workflow for automated registration, artery tracing, and multi-planar reformatting of vessel wall images that significantly improves the reproducibility of plaque detection and quantification. Building on this foundation, a novel semi-automated method was developed for the visualization and quantification of Gadolinium contrast enhancement in intracranial plaques, providing objective measures of plaque vulnerability that correlate with stroke risk. These methodological advances then enabled the first prospective longitudinal study using 3D vessel wall MRI to investigate the temporal evolution of intracranial atherosclerotic disease, revealing significant associations between diabetes, baseline contrast enhancement, and plaque progression patterns.

In the domain of carotid atherosclerosis, this dissertation developed and implemented deep learning-based segmentation pipelines for accurate and efficient delineation of vessel walls and IPH from multi-contrast VWI. These tools facilitated the longest-duration longitudinal study of carotid plaque dynamics to date, demonstrating that IPH persists over extended periods and

significantly accelerates plaque growth compared to lesions without hemorrhage. This finding has important implications for risk stratification and treatment selection in patients with carotid atherosclerosis.

Collectively, the quantitative methodologies and clinical insights presented in this dissertation represent significant contributions to the field of cerebrovascular imaging. By enabling more precise characterization of atherosclerotic plaque features and their evolution over time, this work establishes a foundation for improved risk assessment and personalized management strategies for patients with cerebrovascular disease. Furthermore, the validated analysis pipelines developed herein provide valuable tools for future research and clinical applications in the ongoing effort to reduce the global burden of stroke.

Bibliography

1. Benjamin, E. J. *et al.* Heart Disease and Stroke Statistics—2017 Update: A Report From the American Heart Association. *Circulation* **135**, e146–e603 (2017).
2. Bentzon, J. F., Otsuka, F., Virmani, R. & Falk, E. Mechanisms of Plaque Formation and Rupture. *Circulation Research* **114**, 1852–1866 (2014).
3. Kwon, S. U. *et al.* Efficacy and Safety of Combination Antiplatelet Therapies in Patients With Symptomatic Intracranial Atherosclerotic Stenosis. *Stroke* **42**, 2883–2890 (2011).
4. Wasserman, B. A., Wityk, R. J., Trout, H. H. & Virmani, R. Low-Grade Carotid Stenosis. *Stroke* **36**, 2504–2513 (2005).
5. Dong, L. *et al.* Geometric and Compositional Appearance of Atheroma in an Angiographically Normal Carotid Artery in Patients with Atherosclerosis. *American Journal of Neuroradiology* **31**, 311–316 (2010).
6. Sun, J. *et al.* Characterization of non-stenotic plaques in intracranial arteries with multi-contrast, multi-planar vessel wall image analysis. *Journal of Stroke and Cerebrovascular Diseases* **31**, 106719 (2022).
7. Mandell, D. M. *et al.* Intracranial Vessel Wall MRI: Principles and Expert Consensus Recommendations of the American Society of Neuroradiology. *American Journal of Neuroradiology* **38**, 218–229 (2017).
8. Saba, L. *et al.* Carotid Artery Wall Imaging: Perspective and Guidelines from the ASNR Vessel Wall Imaging Study Group and Expert Consensus Recommendations of the American Society of Neuroradiology. *American Journal of Neuroradiology* **39**, E9–E31 (2018).
9. Cai, J.-M. *et al.* Classification of Human Carotid Atherosclerotic Lesions With In Vivo Multicontrast Magnetic Resonance Imaging. *Circulation* **106**, 1368–1373 (2002).

10. Yarnykh, V. L. & Yuan, C. Multislice double inversion-recovery black-blood imaging with simultaneous slice reinversion. *Journal of Magnetic Resonance Imaging* **17**, 478–483 (2003).
11. Saam, T. *et al.* Quantitative Evaluation of Carotid Plaque Composition by In Vivo MRI. *Arteriosclerosis, Thrombosis, and Vascular Biology* **25**, 234–239 (2005).
12. Yuan, C. *et al.* Contrast-enhanced high resolution MRI for atherosclerotic carotid artery tissue characterization. *Journal of Magnetic Resonance Imaging* **15**, 62–67 (2002).
13. Saba, L. *et al.* Carotid Plaque-RADS: A Novel Stroke Risk Classification System. *JACC: Cardiovascular Imaging* **17**, 62–75 (2024).
14. Qiao, Y. *et al.* Intracranial Plaque Enhancement in Patients with Cerebrovascular Events on High-Spatial-Resolution MR Images. *Radiology* **271**, 534–542 (2014).
15. Shi, Z. *et al.* Progression of Plaque Burden of Intracranial Atherosclerotic Plaque Predicts Recurrent Stroke/Transient Ischemic Attack: A Pilot Follow-Up Study Using Higher-Resolution MRI. *Journal of Magnetic Resonance Imaging* **54**, 560–570 (2021).
16. Schindler, A. *et al.* Prediction of Stroke Risk by Detection of Hemorrhage in Carotid Plaques: Meta-Analysis of Individual Patient Data. *JACC: Cardiovascular Imaging* **13**, 395–406 (2020).
17. Mingming, L. *et al.* Predictors of Progression in Intraplaque Hemorrhage Volume in Patients With Carotid Atherosclerosis: A Serial Magnetic Resonance Imaging Study. *Front. Neurol.* **13**, (2022).
18. Balu, N. *et al.* Carotid plaque assessment using fast 3D isotropic resolution black-blood MRI. *Magnetic Resonance in Medicine* **65**, 627–637 (2011).

19. Wang, J. *et al.* Simultaneous noncontrast angiography and intraPlaque hemorrhage (SNAP) imaging for carotid atherosclerotic disease evaluation. *Magnetic Resonance in Medicine* **69**, 337–345 (2013).
20. Canton, G. *et al.* Pathophysiology of carotid atherosclerosis: Calcification, intraplaque haemorrhage and pulse pressure as key players. *European Journal of Radiology* **178**, 111647 (2024).
21. Zhao, X.-Q. *et al.* Magnetic Resonance Imaging of Intraplaque Hemorrhage and Plaque Lipid Content With Continued Lipid-Lowering Therapy: Results of a Magnetic Resonance Imaging Substudy in AIM-HIGH. *Circulation: Cardiovascular Imaging* **15**, e014229 (2022).
22. Kim, J.-M. *et al.* Intracranial plaque enhancement from high resolution vessel wall magnetic resonance imaging predicts stroke recurrence. *International Journal of Stroke* **11**, 171–179 (2016).
23. Xiao, J. *et al.* Disparate trends of atherosclerotic plaque evolution in stroke patients under 18-month follow-up: a 3D whole-brain magnetic resonance vessel wall imaging study. *Neuroradiol J* **35**, 42–52 (2022).
24. Woo, N.-E. *et al.* Factors for Enhancement of Intracranial Atherosclerosis in High Resolution Vessel Wall MRI in Ischemic Stroke Patients. *Front. Neurol.* **11**, (2020).

Chapter 2 Multi-Planar, Multi-Contrast and Multi-Time Point Analysis Tool (MOCHA) for Intracranial Vessel Wall Characterization

This chapter presents the development and evaluation of MOCHA, an image analysis pipeline designed for comprehensive atherosclerotic plaque assessment in 3D intracranial vessel wall MRI. The MOCHA pipeline addresses critical challenges in intracranial vessel wall imaging through four integrated steps: 1) multi-contrast and multi-time point image registration, which enables seamless comparison of different contrast weightings and longitudinal data that would otherwise be misaligned due to patient movement and repositioning; 2) automated artery tracing and labeling that systematically maps the complex cerebrovascular tree, enabling comprehensive detection of atherosclerotic plaques that may occur anywhere along the intracranial circulation; 3) generation of tailored multi-planar reformats that transform naturally tortuous and tapering arteries into intuitive, standardized viewing planes for consistent analysis; and 4) human visual inspection to validate the pre-processed images. Through rigorous scan-rescan evaluation in patients with intracranial atherosclerotic disease, we demonstrate MOCHA's excellent reproducibility for both qualitative plaque detection and quantitative measurements of plaque morphology. These findings establish MOCHA as a reliable tool for identifying and characterizing atherosclerosis along multiple intracranial arterial segments, with significant potential for clinical applications in assessing plaque morphology, composition and monitoring disease progression longitudinally.

Indeed, MOCHA has served as the robust basis for the contrast enhancement mapping methodology presented in Chapter 3 and enabled us to conduct one of the first longitudinal

studies of intracranial atherosclerosis described in Chapter 4. Beyond atherosclerosis, ongoing studies utilizing MOCHA are investigating other intracranial vasculopathies, including vasculitis, reversible cerebral vasoconstriction syndrome (RCVS), and moyamoya disease, demonstrating its broad applicability in cerebrovascular imaging research.

The work presented here is reproduced and adapted from: Guo, Yin, et al. "Multi-planar, multi-contrast and multi-time point analysis tool (MOCHA) for intracranial vessel wall characterization." *Journal of Magnetic Resonance Imaging* 56.3 (2022): 944-955.

2.1 Introduction

Intracranial atherosclerotic disease (ICAD) is a leading cause of stroke worldwide, accounting for approximately 10% of ischemic strokes in the United States and 50% in Asia[1,2]. In recent years, intracranial vessel wall magnetic resonance imaging (IVW) has been used for ICAD evaluation[3]. IVW provides qualitative and quantitative evaluation of vessel lumen and wall, providing novel assessment that can help characterize and differentiate various intracranial vasculopathies, including ICAD[3–7]. In a clinical or research setting, IVW analysis is frequently enhanced through the analysis of multi-contrast acquisitions that often includes time-of-flight (TOF) MR angiography (MRA) and the use of contrast agent[3,5–8]. Furthermore, considering patients with ischemic stroke attributable to ICAD carry a risk of recurrent stroke of 12%, the need for serial IVW follow-up of ICAD is critical[2].

3D IVW with isotropic resolution shows clear advantages over 2D acquisition techniques, and is increasingly adopted in both research and clinical applications[3,5,9]. However, despite its promise for improving ICAD diagnosis and treatment, systematic evaluation of intracranial arteries with 3D multi-contrast serial IVW poses many challenges, making routine clinical adoption difficult. Atherosclerotic plaques may involve multiple intracranial arterial segments, necessitating a thorough screening of the entire cerebrovascular tree for both stenotic and non-stenotic plaques, since non-stenotic lesions are not readily detectable on CT angiography (CTA) or MRA[3]. Intracranial arteries are tortuous with natural tapering, and therefore, tailored multi-planar reformatting (MPR) is often required for better assessment of artery remodeling and disease extent[10–13]. Intracranial plaques are small lesions and thus require precise image registration to combine information from multiple contrast weightings for accurate characterization of the lesions, or to compare serial scans to quantify changes over time[14,15].

Previous IVW studies assessing ICAD have demonstrated good reliability in both plaque detection and lesion measurements[8,13,16–18]. In these studies, reviewers manually drew a centerline in every artery segment of interest to generate cross-sectional MPRs of a single contrast weighting, which is not well suited for either multi-contrast or a serial imaging study. A dedicated IVW image analysis pipeline is essential to improve diagnosis and management of ICAD and to streamline clinical workflow.

The purpose of this study was to propose a new IVW analysis pipeline, namely Multi-planar, multi-contrast and multi-time point analysis tOol for intracranial vessel wall CHAracterization (MOCHA), and to evaluate its feasibility in serial IVW studies in patients with ICAD.

2.2 Methods

2.2.1 Study population

Informed consent was obtained from all subjects after institutional review board approval.
In this study, subjects were selected from the cohort recruited as part of the 3D vessel WALL Imaging (WALLI) study (R01 NS092207)**.** Details on the inclusion and exclusion criteria can be found in Mossa-Basha et al[8]. In brief, all subjects had known atherosclerotic lesions within the cerebrovascular tree, as clinically detected based on the presence of stenosis on clinical luminal imaging, the presence of two or more risk factors for atherosclerosis (age >50 for men or >60 for women, hypertension, diabetes mellitus, hyperlipidemia, obesity, or smoking) and no clinical evidence for other intracranial vasculopathies.

2.2.2 Image acquisition

All examinations were performed on a 3T whole-body scanner (Ingenia CX, Philips Healthcare; Best, the Netherlands) with a 32-channel head coil. All IVW sequences were based on a Volume ISotropic Turbo spin echo Acquisition (VISTA) sequence and employed fat suppression and Cartesian UnderSampling with Target Ordering Method (CUSTOM) acceleration with Self-supporting Tailored k-space Estimation for Parallel imaging (STEP) reconstruction[19,20]. Imaging parameters are provided in Table 2.1. Delay Alternating with Nutation for Tailored Excitation (DANTE) pre-pulses were additionally applied for blood suppression for the PD-VISTA acquisition[21]. Pre-contrast T1-VISTA, PD-VISTA, and 3D-TOF were obtained then post-contrast T1-VISTA was also acquired after single-dose gadolinium contrast injection (0.1 mmol/kg of Prohance at 2cc/s followed by bolus of equal volume of saline), 3-min post-injection. For each subject, two repeated 3D-IVW scans were performed within two weeks.

Table 2.1 MRI protocol

Sequence	**Pre-T1 VISTA**	**PD VISTA**	**Post-T1 VISTA**	**3D-TOF**
Orientation	**Coronal**	**Coronal**	**Coronal**	**Axial**
FOV (mm)	180 × 180 × 40	180 × 180 × 40	180 × 180 × 40	190 × 190 × 72
Resolution for acquisition (mm)	0.5 × 0.5 × 0.5	0.5 × 0.5 × 0.5	0.5 × 0.5 × 0.5	0.5 × 0.5 × 1
Resolution for reconstruction (mm)	0.25 × 0.25 × 0.25	0.25 × 0.25 × 0.25	0.25 × 0.25 × 0.25	0.25 × 0.25 × 0.5
Bandwidth (Hz/pixel)	620	625	620	289
TR (msec)	800	2000	800	15
TE (msec)	26	36	26	3.5
Flip angle (°)	Varies	Varies	Varies	18
Echo train length	30	60	30	NA
Averages	2	2	2	1
Scan time (min:sec)	5:03	5:38	5:03	5:15

2.2.3 MOCHA workflow

The scan and rescan IVW images were processed using the MOCHA pipeline, which includes automated and integrated steps of 1) multi-contrast and multi-time point image registration, 2) artery tracing and labeling on TOF MRA, and 3) generation of tailored MPRs, followed by 4) human visual inspection to validate the resulting pre-processed images (Figure 2.1(a)). These steps are described in detail in the following paragraphs. MOCHA pre-processing and visual inspection were performed by a technologist, independent of the subsequent image analysis.

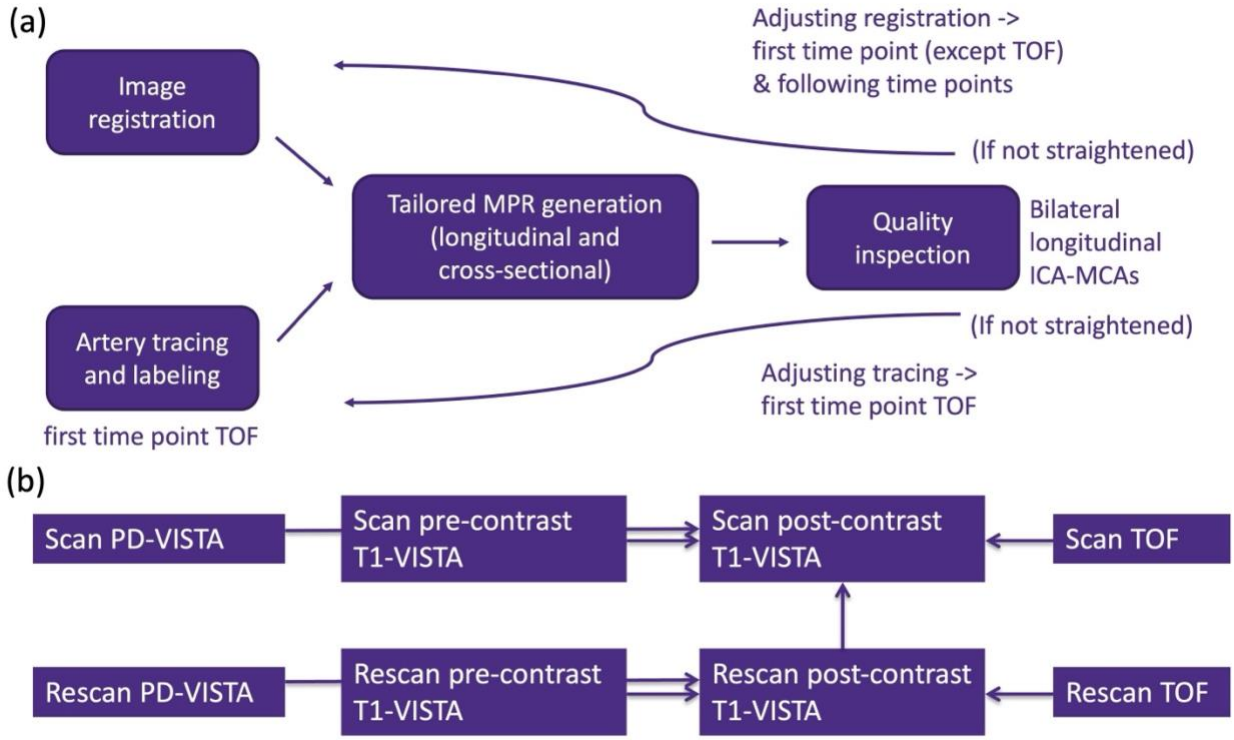

Figure 2.1 a) MOCHA flowchart. (b) Automatic IVW registration scheme. Arrow pointing from A to B indicates 'A is registered to B'.

Image registration. Automatic 3D rigid registration of multi-contrast, multi-time point images to a reference scan was performed, using mutual information[22] as the similarity metric, by the open-source package SimpleITK[23]. Figure 2.1(b) shows the registration scheme of pre- and post-contrast T1-VISTA, PD-VISTA and TOF images at two time points. In this study, the post-contrast isotropic resolution T1-VISTA sequence was selected as the reference due to its clear lumen and wall boundaries[24] and higher signal-to-noise ratio. If post-contrast T1-VISTA was not available, pre-contrast T1-VISTA was used. When multiple time point scans were present, the corresponding post-contrast T1-VISTA image was registered to the post-contrast T1-VISTA image of the first time point, and then within each multi-contrast scan session, registration was performed in a pair-to-pair manner. Finally, images were automatically realigned into the same orientation and resampled into the same resolution as the isotropic reference scan.

Artery tracing and labeling. An open-curve active contour model (iCafe) was used to automatically identify artery centerlines from the TOF MRA[25] acquired at the first time point. In order to identify intracranial artery segments, vessel landmarks were computed by maximum a posteriori estimation[25] automatically, and the following vessel segments were labeled: basilar artery (BA), V4 vertebral arteries (VA), distal cervical and intracranial internal carotid arteries (ICA), M1/M2 middle cerebral arteries (MCA), A1/A2 anterior cerebral arteries (ACA) and P1/P2 posterior cerebral arteries (PCA). Figure 2.2 demonstrates the 14 landmarks and 11 segments analyzed in this study. A reviewer (GC, 12 years of vascular MR imaging experience) edited the centerlines and landmarks as needed to correct errors from the automatic processing. This tracing and labeling of the entire intracranial vascular tree generated a template for interactive analysis in subsequent steps.

Generation of tailored MPRs. For each vessel segment, coordinates of the centerline were used to interpolate to multi-contrast, multi-time point images for generation of longitudinal MPR images, which can be considered as perpendicularly stacked profiles of cross-sectional slices along the centerline with a gap of one pixel. Rotation of profiles in each cross-sectional image led to rotational MPR views for display of the specified arterial segment. Selected vessel trace, cross-sectional and longitudinal MPR views were all synchronized by viewing angles and slice positions, with multiple contrast weightings side by side, in a specially designed graphical user interface (GUI, Figure 2.3), dedicated for an interactive visualization and quantification.

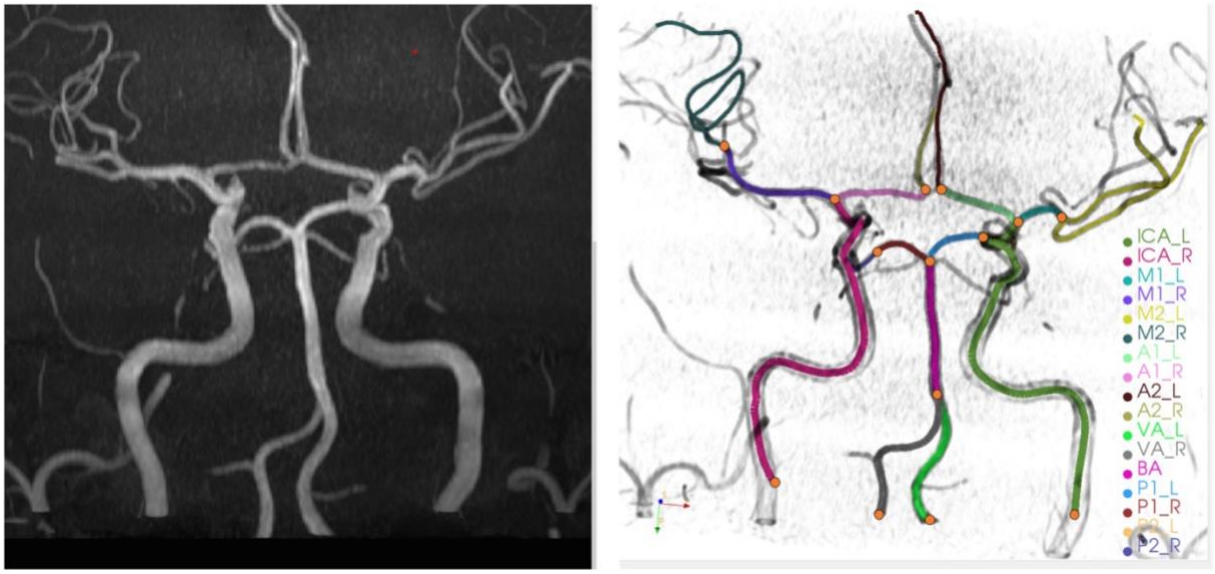

Figure 2.2 Demonstrations of the artery landmarks (in orange) and vessel segments (marked in various colors) used in this study.

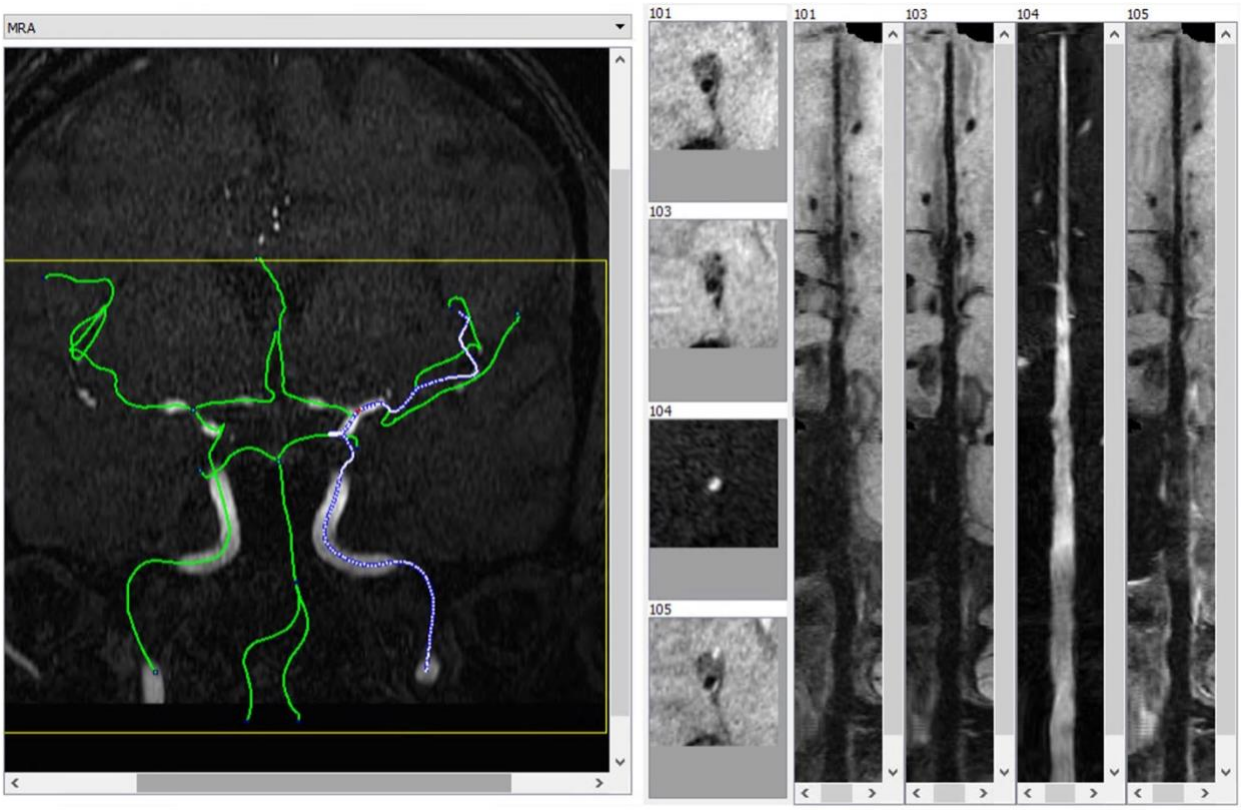

Figure 2.3 The interactive analysis GUI with synchronized vessel traces (left), cross-sectional (middle) and longitudinal MPR views (right, S101: pre-contrast T1-VISTA; S103: PD-VISTA; S104: TOF; S105: post-contrast T1-VISTA) for the left ICA-MCA segment

Quality inspection. Longitudinal MPR images of bilateral ICA-MCA segments were visually inspected (YG, 3 years of experience with medical image processing) to ensure success of the workflow. The ICA-MCA segment was selected for its longer length permitting assessment of a range of vessel diameters along its course. A straightened display of the ICA-MCA segment from the first time point reformatted TOF showing arterial tapering was used to validate artery tracing, and similar straightened displays of other contrasts and time points were used to ensure good image registration (Figure 2.4).

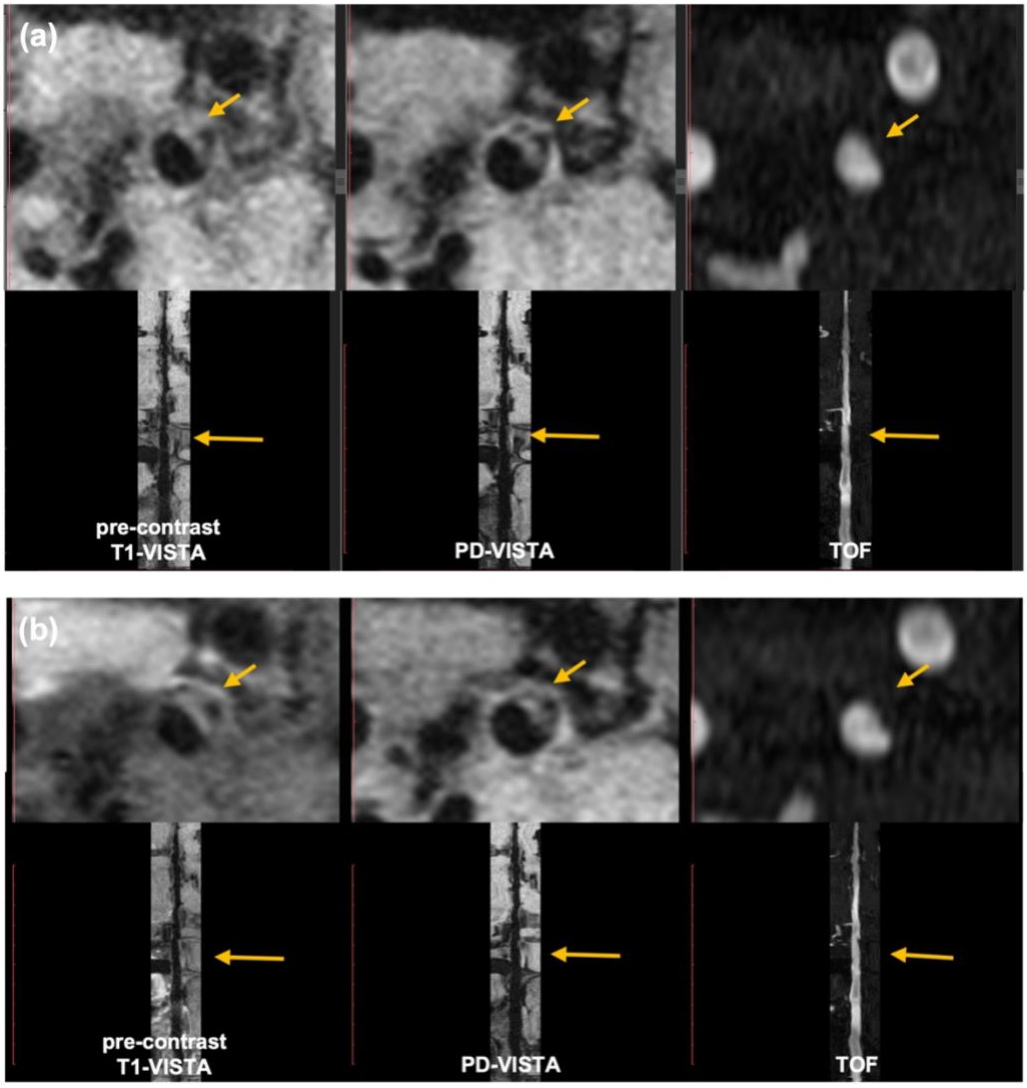

Figure 2.4 Representative stenotic supraclinoid ICA lesion with inward remodeling detected in both the scan (a) and rescan (b) MR sessions.

The arrows point to the eccentric plaque encroaching the lumen area (Top: cross-sectional view, bottom: longitudinal view)

2.2.4 Image analysis

Segments of all subjects were randomized and analyzed independently. A total of 15 individual vessel segments were independently analyzed for each subject: proximal segments (the BA, V4 VAs, intracranial ICAs (further subdivided into petrous, cavernous, and supraclinoid segments)) and distal segments (M1/M2 MCAs, A1/A2 ACAs and P1/P2 PCAs). All the reconstructed cross-sectional and longitudinal MPR images of pre-contrast T1-VISTA, PD-VISTA, TOF and post-contrast T1-VISTA were displayed interactively (Figure 2.3).

For each segment, atherosclerotic lesions were identified on the MOCHA generated longitudinal and cross-sectional MPR images following the criteria described by Mossa-Basha et al[8]. In summary, a segment was considered to have a lesion if it showed stenosis or irregularity on luminal imaging and/or wall thickening on T1 pre- and post- contrast VISTA, or circumferential enhancement and/or wall thickening without stenosis. Only slices with identified lesions were outlined for quantitative lesion assessment: lumen and outer wall boundaries were manually traced (GC, twelve years of experience in vascular MR imaging) along the interfaces between lumen and wall and between wall and surrounding tissues, respectively. One reader (GC) contoured the lumen and outer wall on the cross-sectional MOCHA images from the first scan and the results were reviewed by a second reader (JS, twelve years of experience in vascular MR imaging) following an established peer-review protocol to reach consensus in the identification of the luminal and outer wall boundaries. After two weeks, the primary and secondary readers performed the same analysis but on the MOCHA images from the second scan. Both readers were blinded to scan and clinical information.

The length of each plaque was calculated from the number of consecutive cross-sectional slices with lesion multiplied by slice thickness. For each cross-sectional slice with lesion, the following

morphological measurements were generated: the maximum wall thickness (i.e., the maximum value of the distance between lumen and outer wall contours), the lumen area (i.e., the area inside the luminal contour), the wall area (i.e., subtracting the lumen contour area from the outer wall contour area) and normalized wall index (i.e., the ratio of the wall area to the outer wall contour area). In addition, we measured mean signal intensity (SI) of the vessel wall within each slice on pre- and post-contrast T1-VISTA images to calculate the contrast enhancement ratio as follows:

$(SI_{post} - SI_{pre})/SI_{pre}$

To assess operator-dependent factors in image pre-processing and inter-rater agreement in plaque measurement, the MOCHA workflow was applied again in these subjects with a different reader (DBG, 3 years of experience in vascular imaging) editing the vessel traces and labels. Then, a new pair of readers performed the image analysis following the same review procedure described above; that is, a reader (DBG) determined the presence of atherosclerotic plaques and contoured the lumen and outer wall of 20 randomly selected plaques, and the resulting contours were peer-reviewed by another reader (MMB, 17 years of experience in vascular imaging). Plaque quantitative morphological measurements were then calculated at 1) all matching slice locations and 2) 3 consecutive cross sections with the largest normalized wall index. Both measurement approaches were employed to evaluate the robustness of plaque quantification: measurements at all matching slice locations provide comprehensive assessment of plaque burden along the vessel segment, while measurements at the 3 consecutive cross-sections with the largest normalized wall index focus on the most stenotic region, which is clinically most relevant, and account for potential spatial misalignment that may occur when the vessel centerline is re-edited by a different reader.

2.2.5 Statistical analysis

All statistical analyses were performed using R (version 3.5.1). Scan-rescan reproducibility of detecting plaques with MOCHA was summarized using percent agreement and Cohen' κ. κ - values of agreement between 0 and 0.20 were defined as poor agreement; 0.21 and 0.40 as fair agreement; 0.41 and 0.60 as moderate agreement; 0.61 and 0.80 as good agreement; 0.81 and 1.0 as excellent agreement [8]. When comparing morphological and contrast enhancement measurements, the intra-class correlation coefficient (ICC) was obtained from a two-way mixed model. Confidence intervals for the overall ICC were calculated by bootstrapping. An ICC value of less than 0.4 was considered poor agreement, a value of 0.4–0.75 was considered good agreement, and a value of 0.75 or greater was considered excellent agreement[13]. Bland-Altman analysis was also used to determine the scan-rescan reproducibility.

2.3 Results

IVW from 11 subjects were included in this study (68±10 years old, 6 males). Post-contrast T1-VISTA sequence was not available for one subject due to difficulties with intravenous line placement for the contrast injection. MOCHA images of these 11 subjects were generated and all passed visual inspection.

In four subjects, bilateral distal V4s were not included due to lack of coverage in at least one scan. On TOF, the left ACA was occluded in one subject; the left PCA and right ACA were occluded in another subject; the left ICA (petrous, cavernous, and supraclinoid) and MCA were occluded in a third subject. These 11 segments were excluded and therefore, a total of 150 paired segments were analyzed for scan-rescan reproducibility.

With MOCHA, readers achieved consistent identification and delineation of plaques. In terms of plaque detection, there was excellent scan-rescan agreement (92.7% agreement, $\kappa = 0.822$). The agreement is 94.3% for proximal segments ($\kappa = 0.863$) and 90.3% for distal segments ($\kappa = 0.761$). A total of 43 plaques were identified in both scans (24 in proximal segments, 19 in distal segments). 11 plaques were identified in one of the two scans (5 in proximal segments, 6 in distal segments). Representative lesions identified of supraclinoid, MCA, ACA, PCA, BA segments were shown in Figures 2.4 and 2.5.

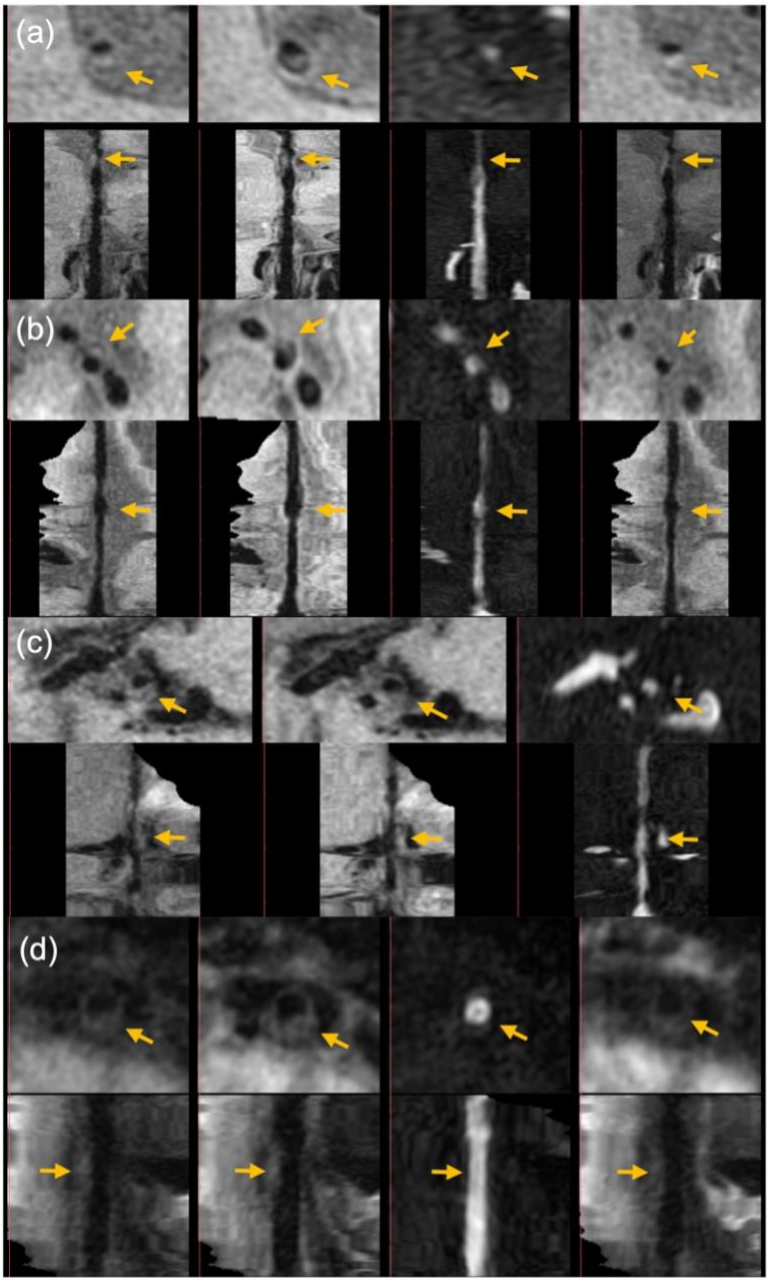

Figure 2.5 Representative lesions in distal segments (a: MCA, b: ACA, c: PCA, d: BA) identified using MOCHA (Top: cross-sectional view, bottom: longitudinal view).

The four panels display images from left to right: pre-contrast T1-VISTA, PD-VISTA, TOF, and post-contrast T1-VISTA. Note that in panel (c), the subject did not receive contrast injection, therefore post-contrast T1-VISTA images were not available for this case.

The measurements of morphology and contrast enhancement of these 43 detected plaques along with their corresponding ICC values are summarized in Table 2.2. The subject (with 9 plaques) without the post-contrast T1-VISTA sequence was excluded in the calculation of contrast enhancement ratio. Each of the assessed indices had an ICC greater than 0.90. The Bland-Altman plots for mean lumen area, maximum wall thickness, normalized wall index, and mean enhancement ratio, respectively, for all the identified plaques are shown in Figure 2.6. There was no bias observed on the Bland-Altman plots.

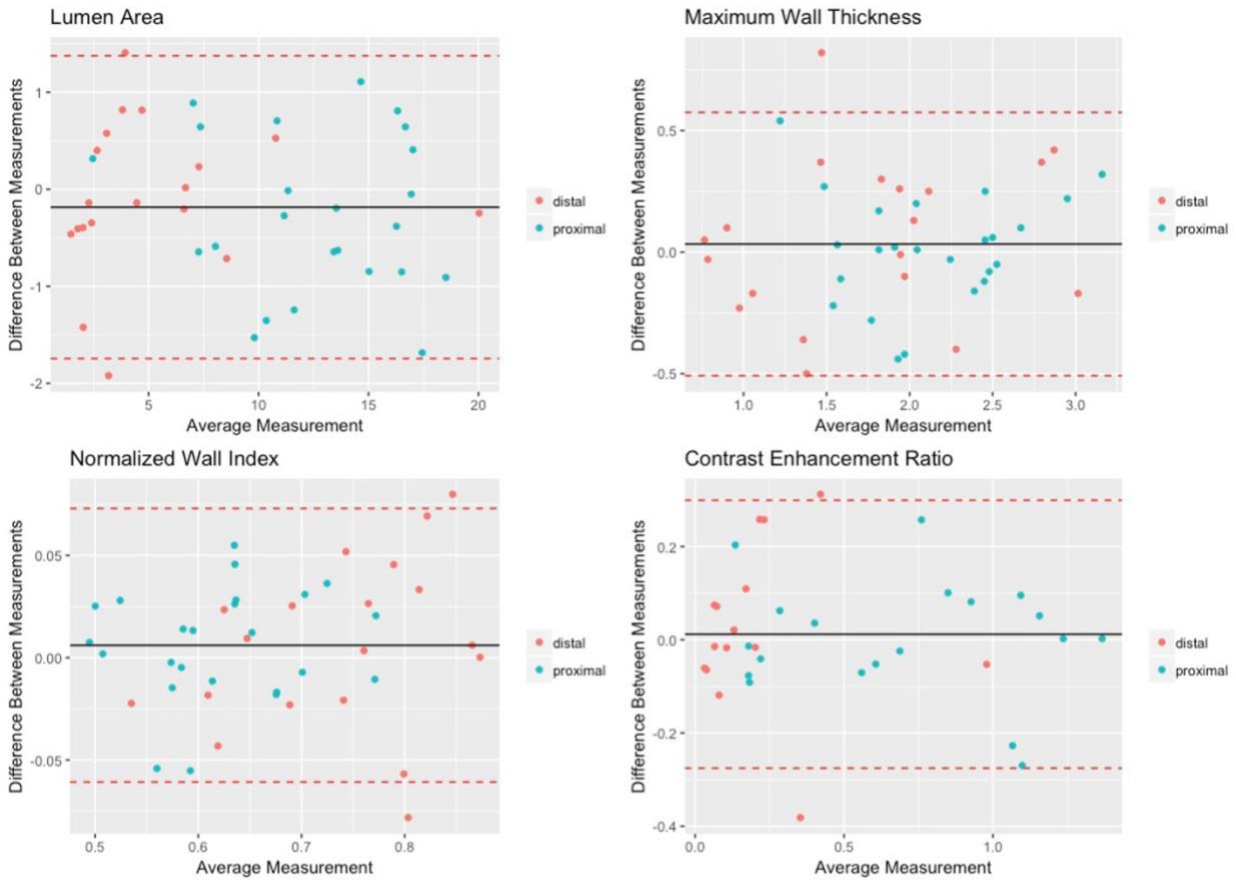

Figure 2.6 Bland-Altman plots for lumen area (mm^2), maximum wall thickness (mm), normalized wall index and contrast enhancement ratio

The inter-rater reproducibility of morphological measurements of the 20 plaques demonstrated good to excellent agreement, as summarized in the Table 2.3.

Table 2.2 Morphological measures and enhancement ratio of plaques, and corresponding scan–rescan reproducibility using MOCHA

	First Scan	Secnd Scan	ICC	95% CI
Plaque length (mm)	2.81 ± 1.85	2.64 ± 1.84	0.953	(0.915,0.974)
Maximum wall thickness (mm)	1.97 ± 0.65	1.93 ± 0.61	0.904	(0.831,0.947)
Mean lumen area (mm^2)	9.23 ± 5.64	9.41 ± 5.72	0.990	(0.981,0.994)
Mean wall area (mm^2)	13.08 ± 5.14	13.14 ± 5.04	0.969	(0.943,0.983)
Normalized wall index	0.68 ± 0.11	0.67 ± 0.10	0.947	(0.905,0.971)
Enhancement ratio	0.48 ± 0.42	0.47 ± 0.43	0.942	(0.888,0.971)

Table 2.3 Morphological measures of plaques and corresponding inter-rater reproducibility using MOCHA

	All matching slices				3 consecutive slices with largest normalized wall index			
	1st Reader Group	2nd Reader Group	ICC	95% CI	1st Reader Group	2nd Reader Group	ICC	95% CI
Plaque length (mm)	2.32 ± 0.93		NA		NA			
Maximum wall thickness (mm)	2.14 ± 0.55	2.22 ± 0.52	0.578	(0.202, 0.807)	2.02 ± 0.46	2.07 ± 0.50	0.705	(0.377, 0.878)
Mean lumen area (mm^2)	9.69 ± 5.15	9.45 ± 4.88	0.982	(0.957, 0.993)	8.85 ± 4.59	8.46 ± 4.75	0.951	(0.878, 0.981)
Mean wall area (mm^2)	14.74 ± 4.22	15.43 ± 5.48	0.701	(0.393, 0.869)	15.25 ± 4.65	15.86 ± 6.19	0.800	(0.549, 0.919)
Normalized wall index	0.68 ± 0.09	0.69 ± 0.07	0.789	(0.547, 0.910)	0.68 ± 0.08	0.70 ± 0.06	0.792	(0.534, 0.916)

2.4 Discussion

This study demonstrates how MOCHA, a pipeline that includes multiple functional units, facilitates both qualitative and quantitative analysis of intracranial vessel wall MRI. MOCHA allows a comprehensive analysis of IVW through an integrated, streamlined, and optimized approach of displaying multi-planar, multi-contrast, multi-time point views of specified vessel segments in an interactive fashion. With further validation and future clinical implementation, MOCHA will be able to standardize IVW review and streamline radiologist workflows. Through a systematic and synchronized review of multi-contrast IVW datasets, lesions can be detected and characterized more accurately and efficiently. Through multi-time point review, serial evaluation will also become more consistent and faster. The standardization of IVW review will lead to user-to-user consistency in radiology reporting in the clinic, resulting in increased radiologist comfort in IVW interpretation and, in turn, in increased ordering-provider reliance on and adoption of the technique. MOCHA also has the potential to expand beyond ICAD assessment, to include vasculopathy differentiation, an application where IVW has already shown drastic improvements over conventional imaging techniques[4,26,27].

Despite the promise of IVW for improving ICAD diagnosis, characterization and serial evaluation, analyzing such high-resolution, 3D multi-contrast datasets pose significant challenges. Most previous studies did not use specialized software but relied on PACS DICOM viewers to review IVW data[8,18,28]. A few studies used commercial software such as VesselMass for vessel wall segmentation[6,7,13,17]. Thus far, a dedicated software that provides automatic 3D IVW pre-processing, for comparison with multiple viewing angles, artery segments, image contrast and scanning time points, was not yet achieved. Guggenberger et al. proposed a framework for IVW visualization by semi-automatically extracting MPR reformats from 3D

black-blood CS-SPACE (Compressed Sensing - Sampling Perfection with Application optimized Contrasts using different flip angle Evolution)[29]. However, the reliability of this pipeline was not evaluated (especially in vessels with smaller dimensions), and there was no functionality for registration of multiple contrasts or time points.

Scan-rescan reproducibility is a principal requirement for an imaging workflow to be used in serial examination review. Our results show excellent scan-rescan reproducibility in evaluating ICAD of major intracranial arterial segments for subjects, both qualitatively and quantitatively. Identifying lesions with MOCHA reported higher percent agreement and Cohen' κ compared with a previous study[8] using a generic DICOM viewer software. In terms of measuring plaque morphology, there were studies[13,17] showing comparable or better ICCs to our study but only with a single contrast weighting. Furthermore, in our study, the number of consecutive slices (i.e., plaque length) analyzed in the two scans was decided independently as a morphological measurement based on lesion identification, while it was either pre-determined or resolved in consensus in previous studies. Plaque length measurement was highly reproducible.

The inter-rater reproducibility results show good to excellent agreement between measurements from the two image reader teams. Our plaque burden results agree with those achieved in the ARIC study[9] with respect to plaque burden, though we achieved excellent reproducibility in the lumen area measurements. This excellent inter-rater reproducibility lumen area measurement was also achieved in the symptomatic cohort study by Zhang and collaborators[17], who also reported good to excellent reproducibility in plaque burden. Our results showed lower reproducibility of plaque burden compared to theirs, both in the whole plaque[17] and when focusing on the slice with highest plaque burden[13]. Their higher inter-rater reproducibility results might be due to the better surrounding tissue suppression in the segments where their analyzed plaques are mainly

localized, namely the MCA, BA, and VA, whereas 50% of the 20 plaques included in our analysis are located in the ICA, specifically the cavernous ICA, characterized by poorer contrast resolution between the arterial wall and surrounding venous compartment, especially on post-contrast imaging.

There are four distinct advantages of MOCHA: 1) the technique provides automatic artery tracing, labeling and extraction of arterial segments of interest from the complex intracranial cerebrovascular tree; 2) rotational longitudinal MPR views provide comprehensive display of selected arteries; 3) simultaneous cross-sectional views allow consistent display and contouring for vessel wall feature extraction and quantification; and 4) a precise registration scheme ensures identical physical location is aligned from images of different contrast weightings and time points. High reproducibility of analyzing IVW shown in this study supports the reliability of MOCHA's pre-processing workflows and can help realize the above-mentioned benefits.

The simultaneous and interactive display of longitudinal and cross-sectional MPR views is a unique aspect of MOCHA. Readers have access to the display where the vessel center points, cross-sectional slice locations and MPR viewing angles are synchronized. Readers can scroll through and rotate the MPRs to fully appreciate vessel wall remodeling and the extent of disease. In addition, readers are no longer required to traverse image slices to locate one segment of interest at a time, since segments of intracranial arteries are automatically traced and labeled through mapping of the cerebrovascular tree. By selecting a segment of interest using a specially designed GUI, both original and reformatted images of that segment are displayed. All these integrations are desirable for an efficient and effective review experience.

The value of the comprehensive display is further demonstrated by the fact that both stenotic and non-stenotic ICAD lesions may be assessed using MOCHA. While stenotic ICAD can be

identified using MRA such as TOF, non-stenosing ICAD lesions are difficult to detect unless IVW from all the artery segments are assessed. Previous studies show that the prevalence of intracranial atherosclerotic plaques detected with IVW appears to be >2-fold higher than with angiographic imaging[30]. If untreated, these plaques may progress and lead to ischemic events. Analyzing the entire arterial tree using tailored MPRs may minimize the number of missed non-stenotic plaques (Figure 2.7). MOCHA streamlines this review process and may help clinicians more comprehensively, accurately, and efficiently assess IVW for non-stenotic ICAD.

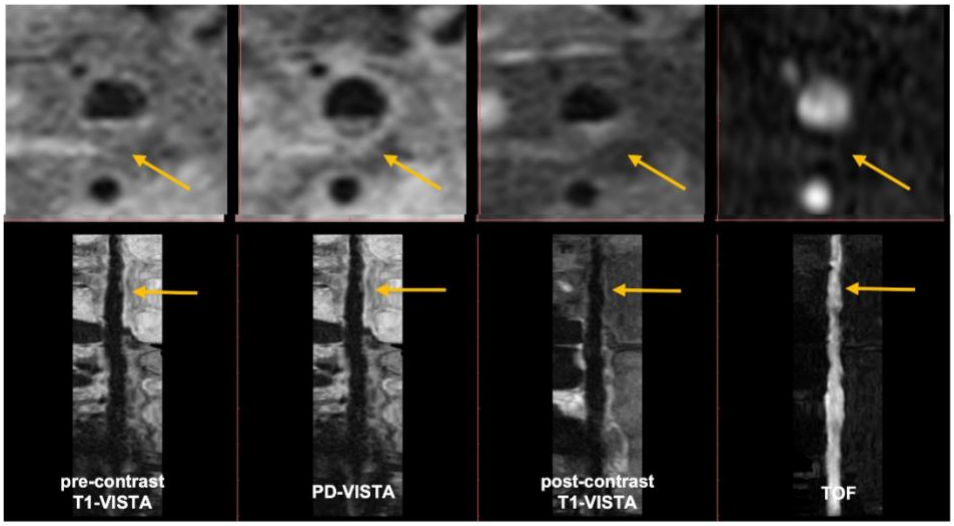

Figure 2.7 Representative non-stenotic supraclinoid ICA lesion identified using MOCHA (Top: cross-sectional view, bottom: longitudinal view)

Multi-contrast vessel wall imaging of the extracranial carotid artery has proven benefits for improved characterization and quantification of plaque features[31–33]. For intracranial arteries, besides whole-brain 3D isotropic black-blood T1 images, TOF MRA and post-contrast T1 images are often acquired as part of a multi-sequence protocol to resolve plaque-mimicking artifacts and to provide additional information on lumen morphology and plaque characteristics.

The benefits of information synthesis of these contrasts are maximized through precise registration by MOCHA. The pipeline design will allow easy inclusion of other 3D IVW sequences acquired to be reviewed together, such as T_2 and/or proton density weighted sequences. Furthermore, the MOCHA setup will allow easy comparison of the performance of different sequences for identifying vessel wall and other anatomic features.

In addition, we may extend the concept of "multi-contrast" in MOCHA to "multi-modality". A clinical CTA scan of one subject was obtained and combined into MOCHA (Figure 2.8). The circumferential calcification close to the vessel lumen is apparent on CTA, whereas the hypointense signal of calcium is barely discernable from lumen on IVW. With the capability of MOCHA to robustly register contrast weightings and even modalities together, we expect a more comprehensive understanding of imaging biomarkers from the intracranial arterial wall and potentially more robust and comprehensive clinical and investigational vascular disease review.

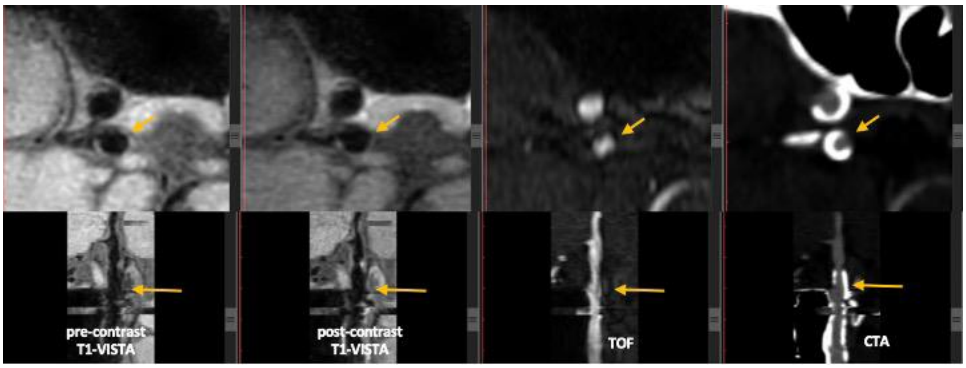

Figure 2.8 Example showing circumferential calcification when CTA is combined with MOCHA analysis (Top: cross-sectional view, bottom: longitudinal view).

Encroached vessel lumen was seen on CTA and TOF whereas the hypointense signal of calcium is barely discernable from lumen on IVW

There are a few limitations in this study. First, our study is a single-center study using only one type of MRI scanner and software for vessel wall analysis. Although reliability was not evaluated across different equipment vendors, MOCHA as a dedicated pipeline is vendor agnostic. Second, although reviewers analyzed major arterial segments in an efficient manner, the processing time to generate multi-contrast, multi-time point reformations for each subject was long. Image registration takes between 5 to 8 minutes (depending on how many contrast weightings and time points are available), and artery tracing and labeling (with potential manual editing) takes over 10 minutes on baseline TOF MRA. Nonetheless, this pre-processing can be done by a technologist and will not affect a clinician's image review. Future improvements may further cut down the pre-processing times. Finally, although the sample size in our study is still relatively small, the number of lesions (43) was adequate for analysis.

2.5 Conclusion

MOCHA enables an integrated, streamlined, and optimized workflow for IVW evaluation through multi-planar, multi-contrast and multi-time point analysis. MOCHA demonstrates excellent scan-rescan reproducibility in ICAD identification and measurement and with further validation, may be valuable for increased efficiency and accuracy in IVW review for clinical and investigational applications.

Bibliography

1. Virani, S. S. *et al.* Heart Disease and Stroke Statistics—2021 Update. *Circulation* **143**, E254–E743 (2021).
2. Yaghi, S., Prabhakaran, S., Khatri, P. & Liebeskind, D. S. Intracranial Atherosclerotic Disease. *Stroke* **50**, 1286–1293 (2019).
3. DM, M. *et al.* Intracranial Vessel Wall MRI: Principles and Expert Consensus Recommendations of the American Society of Neuroradiology. *AJNR. American journal of neuroradiology* **38**, 218–229 (2017).
4. Mossa-Basha, M. *et al.* Multicontrast High-Resolution Vessel Wall Magnetic Resonance Imaging and Its Value in Differentiating Intracranial Vasculopathic Processes. *Stroke* **46**, 1567–1573 (2015).
5. Mossa-Basha, M., Alexander, M., Gaddikeri, S., Yuan, C. & Gandhi, D. Vessel wall imaging for intracranial vascular disease evaluation. *Journal of NeuroInterventional Surgery* **8**, 1154–1159 (2016).
6. Qiao, Y. *et al.* Intracranial Plaque Enhancement in Patients with Cerebrovascular Events on High-Spatial-Resolution MR Images. *https://doi.org/10.1148/radiol.13122812* **271**, 534–542 (2014).
7. Qiao, Y. *et al.* Patterns and Implications of Intracranial Arterial Remodeling in Stroke Patients. *Stroke* **47**, 434–440 (2016).
8. Mossa-Basha, M. *et al.* Inter-rater and scan–rescan reproducibility of the detection of intracranial atherosclerosis on contrast-enhanced 3D vessel wall MRI. *https://doi.org/10.1259/bjr.20180973* **92**, (2019).

9. Qiao, Y. *et al.* MR Imaging Measures of Intracranial Atherosclerosis in a Population-based Study. *https://doi.org/10.1148/radiol.2016151124* **280**, 860–868 (2016).
10. Lindenholz, A., Van Der Kolk, A. G., Zwanenburg, J. J. M. & Hendrikse, J. The use and pitfalls of intracranial vessel wall imaging: How we do it. *Radiology* **286**, 12–28 (2018).
11. Fu, F. *et al.* Rapid vessel segmentation and reconstruction of head and neck angiograms using 3D convolutional neural network. *Nature Communications 2020 11:1* **11**, 1–12 (2020).
12. Chen, L. *et al.* Simultaneous Intracranial Artery Tracing and Segmentation from Magnetic Resonance Angiography by Joint Optimization from Multiplanar Reformation. *Lecture Notes in Computer Science (including subseries Lecture Notes in Artificial Intelligence and Lecture Notes in Bioinformatics)* **11794 LNCS**, 201–209 (2019).
13. Zhang, N. *et al.* 3D whole-brain vessel wall cardiovascular magnetic resonance imaging: a study on the reliability in the quantification of intracranial vessel dimensions. *Journal of Cardiovascular Magnetic Resonance 2018 20:1* **20**, 1–12 (2018).
14. Van Der Kolk, A. G. *et al.* Intracranial vessel wall imaging at 7.0-T MRI. *Stroke* **42**, 2478–2484 (2011).
15. van der Kolk, A. G. *et al.* Distribution and natural course of intracranial vessel wall lesions in patients with ischemic stroke or TIA at 7.0 tesla MRI. *European Radiology 2015 25:6* **25**, 1692–1700 (2015).
16. Zhang, X. *et al.* Scan-Rescan Reproducibility of High Resolution Magnetic Resonance Imaging of Atherosclerotic Plaque in the Middle Cerebral Artery. *PLOS ONE* **10**, e0134913 (2015).
17. Zhang, N., Liu, X., Xiao, J., Song, S. S. & Fan, Z. Plaque Morphologic Quantification Reliability of 3D Whole-Brain Vessel Wall Imaging in Patients With Intracranial

Atherosclerotic Disease: A Comparison With Conventional 3D Targeted Vessel Wall Imaging. *Journal of magnetic resonance imaging : JMRI* **54**, 166–174 (2021).

18. Yang, W. Q. *et al.* Reproducibility of high-resolution MRI for the middle cerebral artery plaque at 3 T. *European Journal of Radiology* **83**, e49–e55 (2014).
19. Qiao, Y. *et al.* Intracranial arterial wall imaging using three-dimensional high isotropic resolution black blood MRI at 3.0 Tesla. *Journal of Magnetic Resonance Imaging* **34**, 22–30 (2011).
20. Balu, N. *et al.* Accelerated multi-contrast high isotropic resolution 3D intracranial vessel wall MRI using a tailored k-space undersampling and partially parallel reconstruction strategy. *Magnetic Resonance Materials in Physics, Biology and Medicine 2019 32:3* **32**, 343–357 (2019).
21. Wang, J. *et al.* Joint blood and cerebrospinal fluid suppression for intracranial vessel wall MRI. *Magnetic Resonance in Medicine* **75**, 831–838 (2016).
22. Mattes, D., Haynor, D. R., Vesselle, H., Lewellyn, T. K. & Eubank, W. Nonrigid multimodality image registration. *https://doi.org/10.1117/12.431046* **4322**, 1609–1620 (2001).
23. Yaniv, Z., Lowekamp, B. C., Johnson, H. J. & Beare, R. SimpleITK Image-Analysis Notebooks: a Collaborative Environment for Education and Reproducible Research. *Journal of Digital Imaging 2017 31:3* **31**, 290–303 (2017).
24. Sarikaya, B. *et al.* Comparison of time-of-flight MR angiography and intracranial vessel wall MRI for luminal measurements relative to CT angiography. *https://doi.org/10.1259/bjr.20200743* **94**, (2020).

25. Chen, L. *et al.* Development of a quantitative intracranial vascular features extraction tool on 3D MRA using semiautomated open-curve active contour vessel tracing. *Magnetic Resonance in Medicine* **79**, 3229–3238 (2018).
26. Mossa-Basha, M. *et al.* Added value of vessel wall magnetic resonance imaging in the differentiation of moyamoya vasculopathies in a non-asian cohort. *Stroke* **47**, 1782–1788 (2016).
27. Mossa-Basha, M. *et al.* Added value of vessel wall magnetic resonance imaging for differentiation of nonocclusive intracranial vasculopathies. *Stroke* **48**, (2017).
28. Shi, Z. *et al.* Progression of Plaque Burden of Intracranial Atherosclerotic Plaque Predicts Recurrent Stroke/Transient Ischemic Attack: A Pilot Follow-Up Study Using Higher-Resolution MRI. *Journal of Magnetic Resonance Imaging* **54**, 560–570 (2021).
29. Guggenberger, K. *et al.* Intracranial vessel wall imaging framework – Data acquisition, processing, and visualization. *Magnetic Resonance Imaging* **83**, 114–124 (2021).
30. Wang, Y. *et al.* Culprit intracranial plaque without substantial stenosis in acute ischemic stroke on vessel wall MRI: A systematic review. *Atherosclerosis* **287**, 112–121 (2019).
31. Yuan, C. *et al.* Contrast-enhanced high resolution MRI for atherosclerotic carotid artery tissue characterization. *Journal of Magnetic Resonance Imaging* **15**, 62–67 (2002).
32. Cai, J. *et al.* In Vivo Quantitative Measurement of Intact Fibrous Cap and Lipid-Rich Necrotic Core Size in Atherosclerotic Carotid Plaque. *Circulation* **112**, 3437–3444 (2005).
33. Tartari, S. *et al.* High-Resolution MRI of Carotid Plaque With a Neurovascular Coil and Contrast-Enhanced MR Angiography: One-Stop Shopping for the Comprehensive Assessment of Carotid Atherosclerosis. *http://dx.doi.org/10.2214/AJR.10.4751* **196**, 1164–1171 (2012).

Chapter 3 Voxel-Wise Quantification and Multi-planar Visualization of Plaque Contrast Enhancement in Intracranial Vessel Wall MRI

This chapter presents the development and validation of a novel semi-automated method for visualization and quantification of contrast enhancement (CE) in intracranial atherosclerotic plaques.

The development process involved extensive optimization and refinement based on systematic evaluation of multiple approaches. A critical challenge addressed was the need for robust image signal intensity normalization to enable consistent CE quantification across patient cohorts. Through rigorous testing of various reference structures—including the corpus callosum, pituitary infundibulum, cerebrospinal fluid, and others— we identified the corpus callosum as the normalization approach that yielded the highest reproducibility, which confirmed findings from other research groups. The visualization methodology also underwent iterative refinement, as initial approaches including pixel-wise subtraction schemes produced overly noisy maps, while 3D volume rendering techniques, though visually intuitive, proved difficult to assess quantitively. Ultimately, we adopted a multi-planar design that balanced visualization clarity with quantitative precision. During the extensive image review process, multiple sources of CE artifacts were systematically identified and characterized by our team, leading to the development of robust artifact correction methods. Our final approach incorporates multi-contrast preprocessing, optimized image intensity normalization, comprehensive enhancement artifact adjustment, and an empirically derived signal intensity threshold to generate comprehensive and intuitive 3D CE maps.

The unique contributions of this work include a semi-automated workflow that performs both detection and visualization of CE, provides both intensity and volumetric quantitative features, and significantly reduces false positives due to imaging artifacts. Through extensive validation against expert review, the method demonstrated excellent diagnostic performance and strong correlation with manual measurements, while rigorous scan-rescan testing confirmed high reproducibility for both CE detection and quantification. These findings establish our CE map technique as a reliable tool for objective assessment of plaque vulnerability in intracranial atherosclerotic disease. The clinical utility of this approach is demonstrated in the subsequent longitudinal study (Chapter 4), where quantitative CE measurements showed strong associations with intracranial plaque progression, validating the biological relevance of our methodology.

This work presented here is being prepared for publication: Yin Guo, et al. "Voxel-Wise Quantification and Multi-planar Visualization of Plaque Contrast Enhancement in Intracranial Vessel Wall MRI."

3.1 Introduction

Intracranial atherosclerotic disease (ICAD) is a leading cause of ischemic stroke worldwide[1,2]. Three-dimensional intracranial vessel wall (IVW) magnetic resonance imaging (MRI) has enabled the direct characterization of vessel wall pathologies and is increasingly adopted in both research and clinical settings[3]. Among IVW imaging biomarkers, contrast enhancement (CE) of intracranial plaques has emerged as particularly valuable. Facilitated by gadolinium (Gd)-based contrast agents, plaque CE reflects pathological changes such as increased endothelial permeability and the development of vasa vasorum[4]. Recent meta-analyses[5,6] have highlighted the prevalence of plaque CE in symptomatic ICAD patients, identifying it as the most reliable imaging marker for culprit plaques - plaques most likely to be directly implicated in stroke.

While qualitative approaches have been commonly used in clinical practice[7], recent studies utilizing quantitative analyses of CE on IVW have provided deeper insights, revealing that CE represents a dynamic pathological process. For example, in recently symptomatic ICAD patients[8], CE signals in potentially culprit plaques have been shown to decrease over a one-year period, accompanied by an increase in vessel lumen area. Therefore, quantitative measures of CE signals may offer a more precise assessment of clinical risk, while also advancing our understanding of the disease process in ICAD.

A recent study developed a 3D enhancement color map for analyzing intracranial atherosclerotic plaques[9], establishing the genu of the corpus collosum (CC) as a preferred reference structure for image intensity normalization to ensure consistency when comparing plaque CE across patient cohorts. However, additional key capabilities are required to advance quantitative CE analysis. First, the method must effectively model complex, eccentric plaques to enable comprehensive characterization of CE intensity, volume, and other plaque morphological features. Additionally,

IVW is susceptible to multiple sources of enhancing artifacts[10], necessitating an adjustment strategy. A visualization framework is also crucial for intuitive depiction of the spatial extent of plaques and their CE characteristics. Finally, reproducible measurement methods for CE are necessary to precisely track subtle changes over time. While the reproducibility of other plaque morphologies has been extensively studied[11,12], few studies have reported scan-rescan reproducibility for quantitative CE measurements.

Therefore, this study aimed to develop a semiautomatic method for the visualization and quantification of intracranial plaque enhancement, building on a previously proposed multi-contrast, multi-planar framework for ICAD characterization, and to evaluate the accuracy and scan-rescan reproducibility of CE measurements.

3.2 Methods

3.2.1 Study Design

This retrospective study was conducted in compliance with the Health Insurance Portability and Accountability Act (HIPAA), and the study protocol was approved by the local Institutional Review Board. Written informed consent was obtained from all enrolled subjects, who were prospectively recruited as part of the 3D vessel WALL Imaging (WALLI) study. The study included two independent groups of subjects, all of whom had known intracranial atherosclerotic lesions based on clinical luminal imaging. Group A[8] consisted of 37 patients whose baseline IVW imaging was used to develop the quantitative CE map and establish the intensity threshold for identifying CE. Group B[12] consisted of 11 patients who underwent two IVW scans within two

weeks, to assess the scan-rescan reproducibility of CE measurements using the proposed framework.

3.2.2 MRI Protocol

All IVW examinations were performed on a 3T whole-body scanner (Ingenia CX, Philips Healthcare, Best, the Netherlands) with a 32-channel head coil. The IVW sequences utilized a 3D Volume ISotropic Turbo spin echo Acquisition (VISTA) protocol with fat suppression and Cartesian UnderSampling with Target Ordering Method (CUSTOM) acceleration, reconstructed using the Self-supporting Tailored k-space Estimation for Parallel imaging (STEP) technique[13]. Pre-contrast T1-VISTA (Pre-T1w) and 3D time-of-flight angiography (TOF-MRA) were obtained prior to administering a single-dose gadolinium contrast agent (Prohance, 0.1 mmol/kg at 2cc/s, followed by a bolus of equal volume of saline). Post-contrast T1-VISTA (Post-T1w) was acquired three minutes after contrast injection. MR imaging parameters have been described in previous studies[8,12].

3.2.3 IVW Preprocessing and Plaque Annotation

A detailed review protocol of IVW, along with extensive validation of this process, using a multi-contrast, multi-planar framework (MOCHA) has previously been reported[12]. Briefly, pre-T1w, post-T1w and TOF-MRA were spatially aligned using rigid image registration, and intracranial artery centerlines were automatically traced on TOF images. One reader identified atherosclerotic lesions on the MOCHA-generated longitudinal and cross-sectional multi-planar reformats (MPRs) across eight arterial segments. The luminal and outer wall boundaries were

delineated on the cross-sectional MPRs perpendicular to the luminal centerline. The results were then peer-reviewed by a second reader and disagreements were resolved by consensus. The analyzed arterial segments included the supraclinoid internal carotid arteries (ICA), M1/M2 middle cerebral arteries (MCA), A1/A2 anterior cerebral arteries (ACA), basilar artery (BA), V4 vertebral arteries (VA), and P1/P2 posterior cerebral arteries (PCA).

3.2.4 Development of the Quantitative Contrast Enhancement Map

Building upon MOCHA-based image preprocessing and plaque annotation, IVW images were further processed to generate the quantitative CE map. This process involved the following steps (Figure 3.1): 1) image intensity normalization, 2) adjustment for enhancement artifacts, including proximity to the sinus and venous flow, 3) deriving the signal intensity threshold for CE, and 4) display and feature calculation.

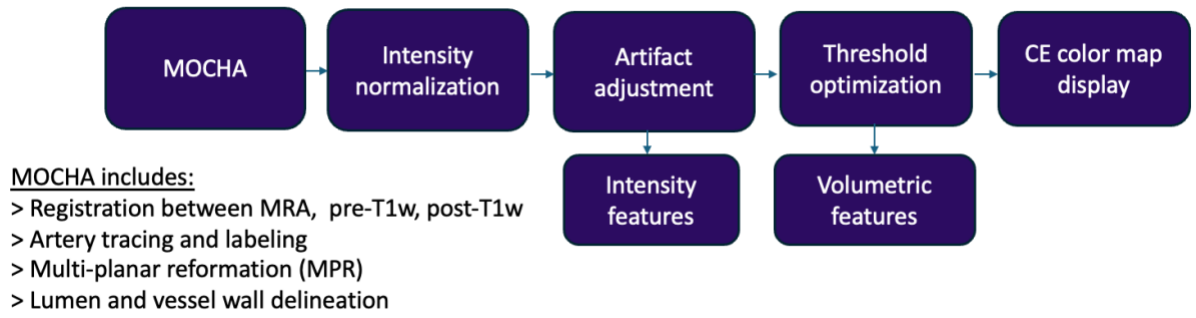

Figure 3.1 Flow chart of our proposed quantitative contrast enhancement map

Image intensity normalization. Following the method described by Omodaka et al.[14], for each subject, a region of interest (ROI) of 20mm^2 was drawn over a normal appearing region of the

genu of the corpus callosum (CC) on the co-registered pre- and post-T1w source images. The average signal intensities (SI) within the ROI were recorded as $SI\text{-}CC_{pre\text{-}T1w}$ and $SI\text{-}CC_{post\text{-}T1w}$, respectively. The CC was selected as it is a brain region with uniform signal intensity that is not influenced by contrast enhancement, and previous studies have demonstrated the superiority of CC as a normalizing reference structure compared to other brain regions[15,16]. The normalized pre-T1w and post-T1w maps were then calculated by normalizing each voxel's intensity to the $SI\text{-}CC_{pre\text{-}T1w}$ and $SI\text{-}CC_{post\text{-}T1w}$, respectively, and were applied across all arterial segments within this subject:

$$\text{pre-T1w map} = \text{pre-T1w image} / SI\text{-}CC_{pre\text{-}T1w}$$

$$\text{post-T1w map} = \text{post-T1w image} / SI\text{-}CC_{post\text{-}T1w}$$

Adjustment for enhancement artifacts. Hyperintense signals originating from sinuses and venous flows in post-T1w images were identified as major sources of enhancement artifact[10]. Arteries proximal to enhancing sinuses and veins often exhibit elevated CE values, which may not necessarily reflect true vessel wall enhancement, thus compromising the reliability of CE assessment in these regions. To address this issue, a 3D connected components-based algorithm was implemented to identify and isolate CE regions strictly confined within the vessel wall boundary.

Artery regions (R_{artery}) were defined by the plaque outer wall boundaries and dilated by 1mm. CE regions (R_{CE}) were defined by the 3D connected components where the SI of the post-T1w map exceed 1.0. The CE region within the arterial wall boundary ($R_{CE\text{-}wall}$) were derived using an intersection operation:

$$R_{CE-wall} = \{\forall(i,j,k) \in R_{CE} \mid R_{CE}(i,j,k) \cap R_{artery}(i,j,k) = R_{artery}(i,j,k)\}$$

Artifact regions ($R_{CE\text{-}artifact}$) were then calculated as:

$$R_{CE-artifact} = R_{CE} - R_{CE-wall}$$

For regions calculated as artifacts ($R_{CE\text{-}artifact}$), the post-T1w signal intensity values were adjusted to 0.5. This value represents an estimate of normal, non-enhancing vessel wall signal intensity rather than a high CE value that may artificially stand out during analysis. These regions (with value of 0.5) were excluded from subsequent steps of CE detection, segmentation, and feature extraction, as their CE values were deemed unreliable.

Illustrations of the algorithm and examples of common artifacts are shown in Figure 3.2.

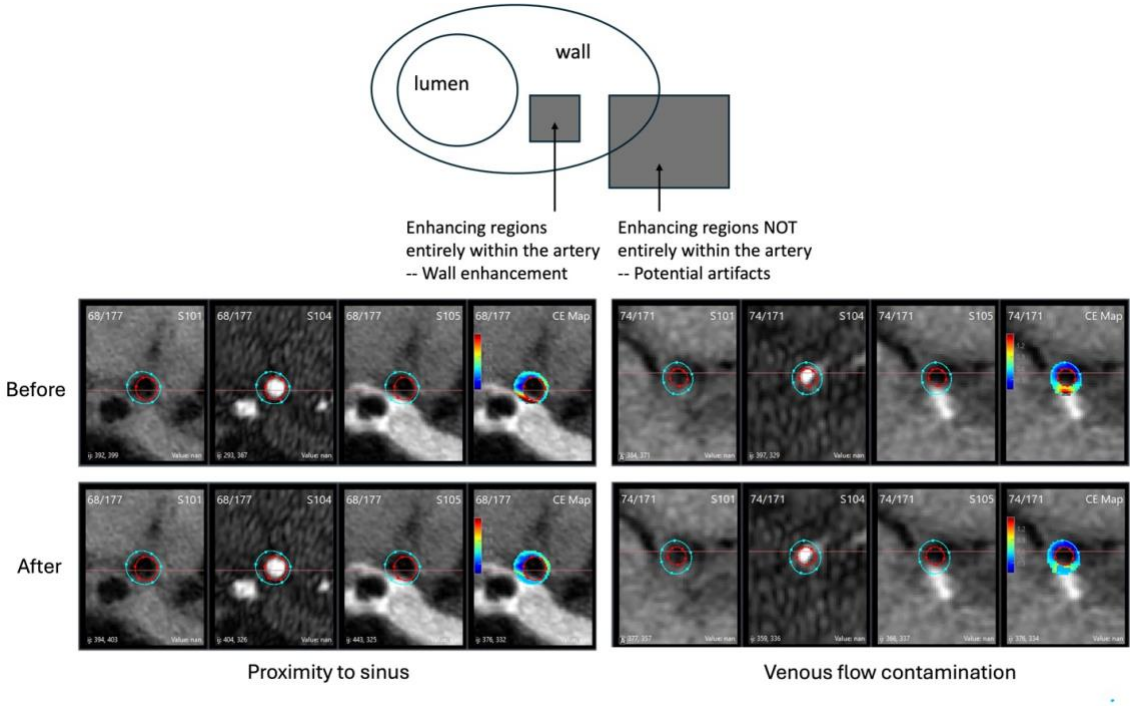

Figure 3.2 Artifact adjustment.

Upper: Illustration of the artifact adjustment process, where a 3D connected component-based algorithm identifies and excludes enhancing regions that extend beyond the arterial wall boundary, reducing false-positive detections from imaging artifacts. Lower: Examples of

common artifacts, including proximity to the sinus and venous flow contamination. The proposed algorithm effectively adjusts for these false-positive plaque enhancement signals.

Deriving signal intensity threshold for CE. In group A, an expert reader reviewed all identified plaques on the pre- and post-T1w source images, first assessing the presence of CE by visually inspecting for distinct enhancing signals within the artery wall. For plaques with enhancement, the reader classified CE as either grade 1 (enhancement higher than the normal vessel wall but lower than the pituitary infundibulum (PI)) or grade 2 (enhancement similar to or exceeding that of the PI), and further categorized it as focal (localized, well-defined enhancement) or diffuse (widespread, homogeneous enhancement). Additionally, plaque wall regions exhibiting CE were manually segmented using the open-sourced software ITK-SNAP. CE volume within each plaque was then calculated, and the segmentation masks were automatically converted into cross-sectional views in MOCHA. Examples of manual annotation on source images are shown in Figure 3.3.

A second reader independently performed CE detection using the same procedure to assess inter-rater reliability.

To identify the optimal signal intensity threshold for CE, the maximum intensity of the arterial wall from each post-T1 map slice, subtracted by the median intensity of the pre-T1w plaque wall, was compared with the manually determined CE presence or absence (see Statistical Analysis below).

Display and feature calculation. The CE color map (within the plaque wall region) was incorporated as an additional contrast weighting in MOCHA's multi-contrast, multi-planar display, overlaid on the post-T1w images (Figure 3.3).

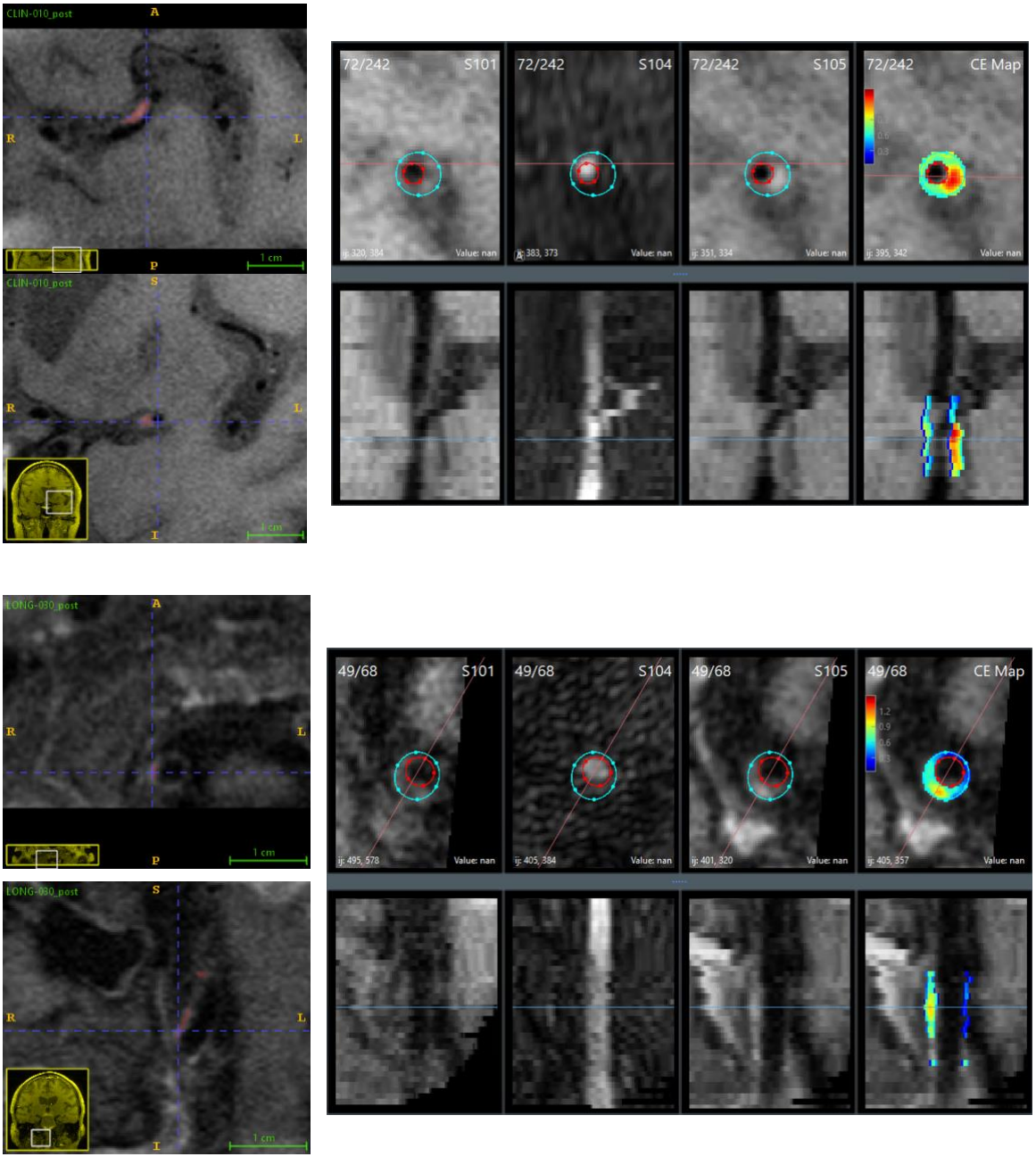

Figure 3.3 Multiplanar enhancement map visualization.

Examples of contrast-enhancing plaques in the upper: left middle cerebral artery and lower: right vertebral artery. The manually segmented enhancement, labeled in the 3D source image (upper: axial view, lower: coronal view), is shown on the left, while the corresponding multiplanar enhancement map visualization is displayed on the right.

We defined the following CE metrics:

1) Mean enhancement ratio: the mean SI on post-T1w map (mean SI on post-T1w images normalized to the CC) within the plaque area

The derived signal intensity threshold for CE was applied to all voxels within the plaque area to identify enhancing regions.

2) Gd uptake: the difference between the mean SI on the post-T1w map and the mean SI on the pre-T1w map within the enhancing area.
3) Enhancement volume: the total number of voxels in all enhancing regions, multiplied by the voxel size.
4) Percent enhancement volume: enhancement volume / plaque wall volume * 100%.

3.2.4 Reproducibility Studies

In group B, an additional image registration step was incorporated into the MOCHA framework to account for the two-week spaced scans. The CC signal intensity was measured separately for each scan. Subsequently, the enhancement metric was calculated automatically.

3.2.5 Statistical Analysis

In group A, the diagnostic performance of the quantitative CE map was assessed using the area under the curve (AUC) of the receiver operating characteristic curve (ROC). The optimal intensity threshold for CE detection on the normalized post-T1w map was determined by maximizing the Youden index (sensitivity + specificity – 1). Sensitivity and specificity for CE detection using the optimal threshold were estimated at the slice level, with the manual reader annotations as the reference standard.

At the plaque level, the correlation between CE volumes measured on the CE map and manual segmentation was assessed using Spearman's correlation coefficient, which is less affected by volume changes during MPR processing than measurements of absolute agreement such as the intraclass correlation coefficient (ICC). Additionally, Gd uptake was compared between Grade 1 and Grade 2 enhancement, and CE volume was compared between focal and diffuse enhancement, using generalized estimating equation (GEE)-based regression to account for multiple enhancing plaques within the same subject.

In Group B, scan-rescan reproducibility of CE detection was assessed using Cohen's kappa. The reproducibility of enhancement ratio, Gd uptake, enhancement volume, and percent enhancement volume was evaluated using the ICC and coefficient of variation (CV).

The nonparametric bootstrap and percentile method was employed to calculate 95% confidence intervals (CIs). Statistical significance was defined as $p < 0.05$. All statistical analyses were performed using statsmodels 0.13.5 with Python 3.10.

3.3 Results

A total of 37 subjects were included in group A (mean age: 69 ± 12 years, 12 females), and 10 subjects were included in group B (mean age: 69 ± 11 years, 5 females). Clinical characteristics for both groups are presented in Table 3.1. In total, 82 plaques were identified in the IVW scans of the 37 subjects in Group A, while 23 plaques were detected in both IVW scans of the 10 subjects in Group B.

Table 3.1 Study population

Characteristics	Group A (n = 37)	Group B (n = 10)
Age (years)	69 ± 12	69 ± 11
Male sex	25 (68)	5 (50)
Symptomatic	24 (65)	0 (0)
Hypertension	29 (78)	8 (80)
Hyperlipidemia	25 (68)	5 (50)
Diabetes	9 (24)	5 (50)
Statins use	29 (78)	8 (80)

In group A, there were a total of 673 cross-sectional post-T1w slices from 82 plaques, of which 90 (13%) slices from 17 (21%) plaques were identified as CE-positive by the reader. The overall AUC for CE detection was 0.91 (95% CI: 0.87, 0.94). The signal intensity threshold, determined using the Youden index on the normalized post-T1 map, was derived as 0.4 plus the median intensity of the pre-T1 map (Figure 3.4a). Applying this threshold, 134 (20%) slices from 23

plaques (28%) were identified as CE-positive. The sensitivity and specificity for CE detection at the slice level were 0.83 and 0.90, respectively.

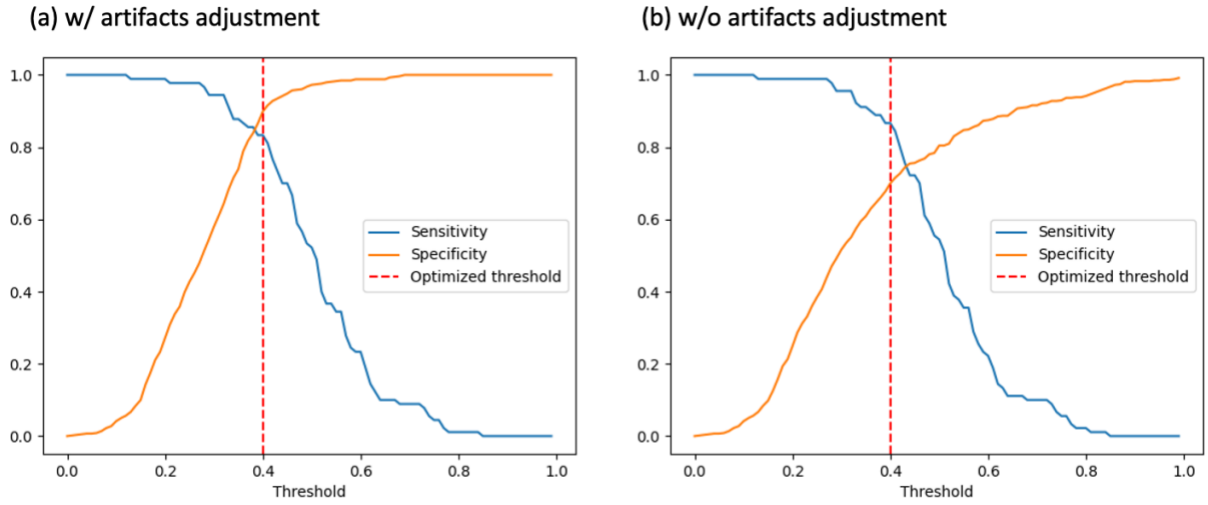

Figure 3.4 Signal intensity threshold optimization for the presence of contrast enhancement (CE).

(a) The optimal signal intensity threshold for CE detection on the post-T1w map was determined as 0.4 plus the median plaque wall intensity of the pre-T1w map, maximizing the sum of sensitivity and specificity. (b) When artifact adjustment was disabled, the same intensity threshold applied; however, this resulted in a substantial decline in detection specificity with only a marginal increase in sensitivity.

At the plaque level, 16/82 plaques were identified as CE-positive by both manual annotation and the quantitative CE map. CE volume measured using the optimal threshold on the CE map strongly correlated with reader measurements (Spearman's rho = 0.82, $p < 0.001$). Plaques with Grade 2 enhancement (n = 6) exhibited significantly higher Gd uptake compared to Grade 1 plaques (n = 10, $p < 0.001$, Figure 3.5a). Plaques with diffuse enhancement (n = 5) had

significantly larger enhancement volume than those with focal enhancement (n = 11, p = 0.03, Figure 3.5b).

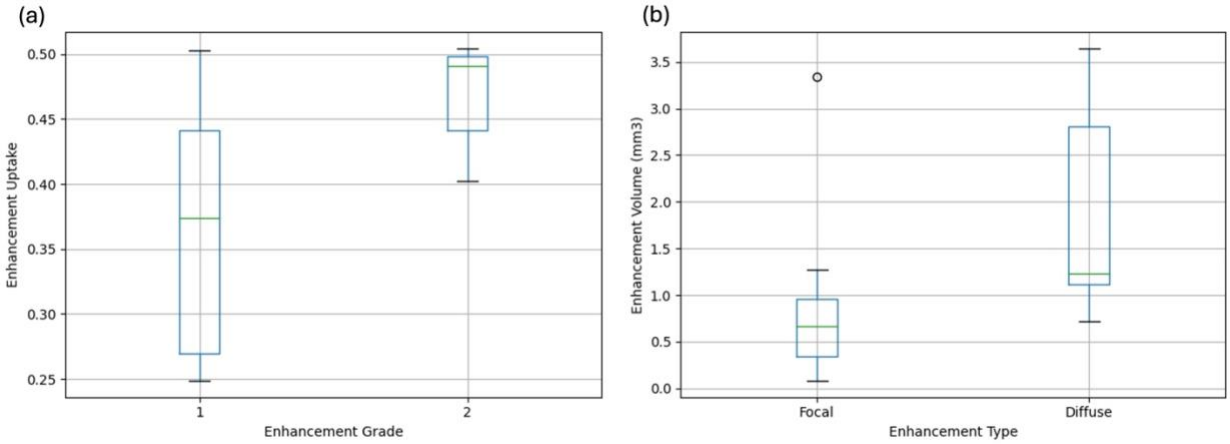

Figure 3.5 Box plot comparing CE map metrics and rater assessment.

(a) Box plot showing that plaques with Grade 2 enhancement (n = 6) had significantly higher Gd uptake than those with Grade 1 enhancement (n = 10, p < 0.001). (b) Box plot showing that plaques with diffuse enhancement (n = 5) had significantly larger enhancement volumes than those with focal enhancement (n = 11, p = 0.03).

When the modules for artifact adjustment were disabled, with the same threshold (Figure 3.4b), there was a decline in CE detection performance, with the overall AUC for dropping to 0.78 (95% CI: 0.74, 0.82). Sensitivity and specificity were 0.87 and 0.70, respectively. A total of 253 slices from 39 plaques were identified as enhancing. As signal intensity adjustment only reduces the measured CE values, we observed only a slight decrease in sensitivity after adjustment but a substantial increase in specificity, effectively reducing CE false positives caused by artifacts.

When assessing inter-rater reliability of CE detection, 16 plaques (20%) were categorized as CE-positive by both readers, while 7 plaques (9%) were categorized as CE-positive by only one reader. The remaining 59 plaques (72%) were categorized as CE-negative by both readers, resulting in a kappa coefficient of 0.76 (95% CI: 0.57, 0.92).

In Group B, the scan-rescan reproducibility of CE signals demonstrated robust agreement. The average histogram overlap (intersection over union, IoU) between the two scans was 0.73 ± 0.12 for pre-T1w maps and 0.75 ± 0.12 for post-T1w maps. The enhancement ratio showed high scan-rescan reproducibility, with an ICC of 0.92 (95% CI: 0.82, 0.96). Example of scan and rescan CE maps of an internal carotid artery plaque, and their overlapping histograms, are shown in Figure 3.6.

Applying the signal intensity threshold, 9 plaques (39%) were categorized as CE-positive in both scans, 2 plaques (9%) were categorized as CE-positive in only one scan, and 12 plaques (52%) were categorized as CE-negative in both scans, yielding a kappa coefficient of 0.82 (95%CI: 0.55, 1). Among the 9 plaques categorized as CE-positive in both scans, quantitative CE measures showed high reproducibility and small measurement variability (Table 3.2). The CV statistic favored enhancement ratio, while the ICC statistics favored Gd uptake and volumetric CE measurements. Bland-Altman plots (Figure 7) revealed no apparent relationship between variance and the mean for all the quantitative metrics.

Table 3.2 Assessment of scan-rescan reproducibility of the quantitative contrast enhancement metrics

	All Plaques (n = 23)				CE-detected plaques in both scans (n = 9)			
	Scan	Rescan	ICC (95% CI)	CV	Scan	Rescan	ICC (95% CI)	CV
Enhancement ratio	0.55 ± 0.10	0.54 ± 0.11	0.92 (0.82, 0.96)	4.4%	0.57 ± 0.05	0.55 ± 0.04	0.81 (0.39, 0.95)	3.0%
Enhancement uptake	NA				0.31 ± 0.15	0.31 ± 0.12	0.94 (0.76, 0.99)	10.7%
Enhancement volume (mm^3)	NA				0.71 ± 0.34	0.60 ± 0.28	0.86 (0.51, 0.97)	12.2%
Percent enhancement volume (%)	NA				3.7 ± 2.8	3.3 ± 2.6	0.98 (0.90, 0.99)	10.8%

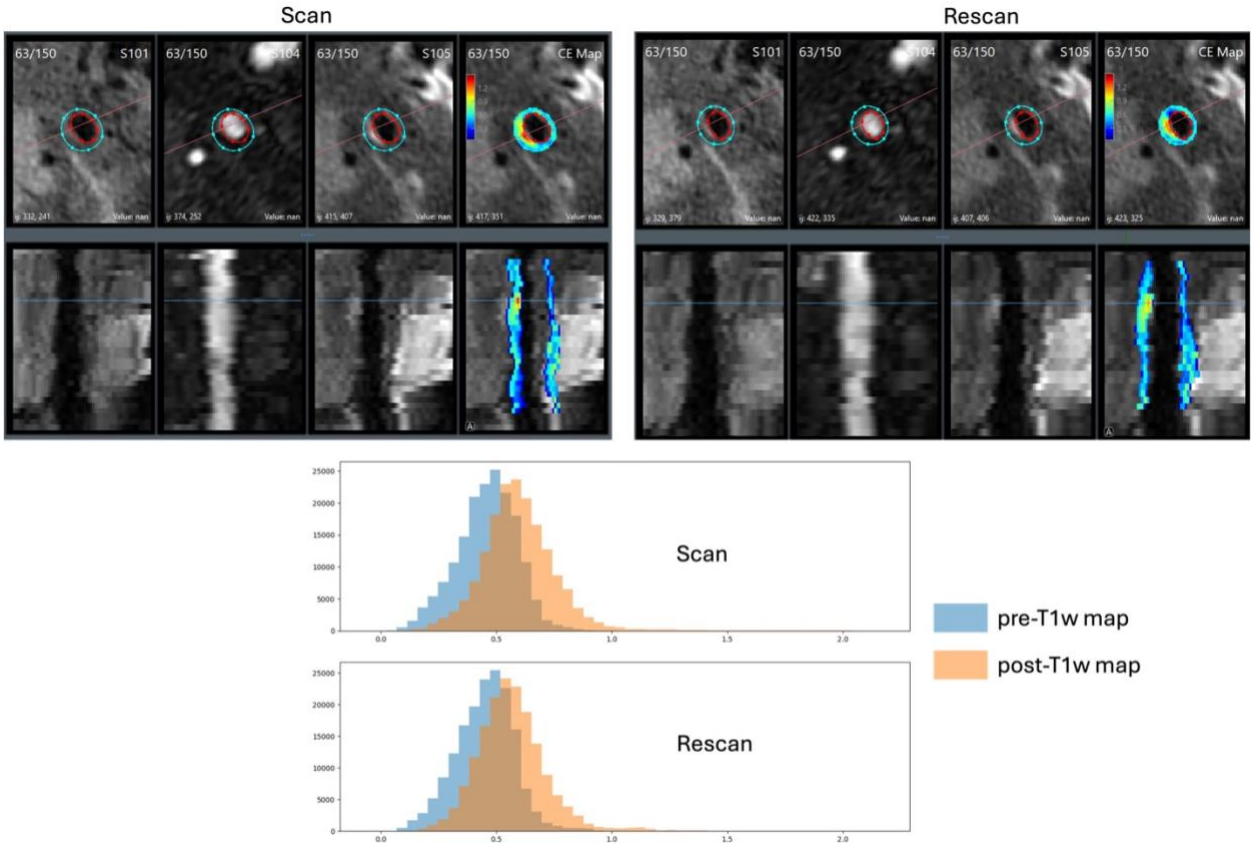

Figure 3.6 CE map reproducibility.

Upper: Example of co-registered scan and rescan intracranial vessel wall images with the corresponding CE map, presented in both cross-sectional and longitudinal views. A supraclinoid internal carotid plaque displaying CE is highlighted. Lower: Histograms of pre-T1w and post-T1w maps demonstrate good overlap between scan and rescan, indicating consistency in normalized signal intensity distributions.

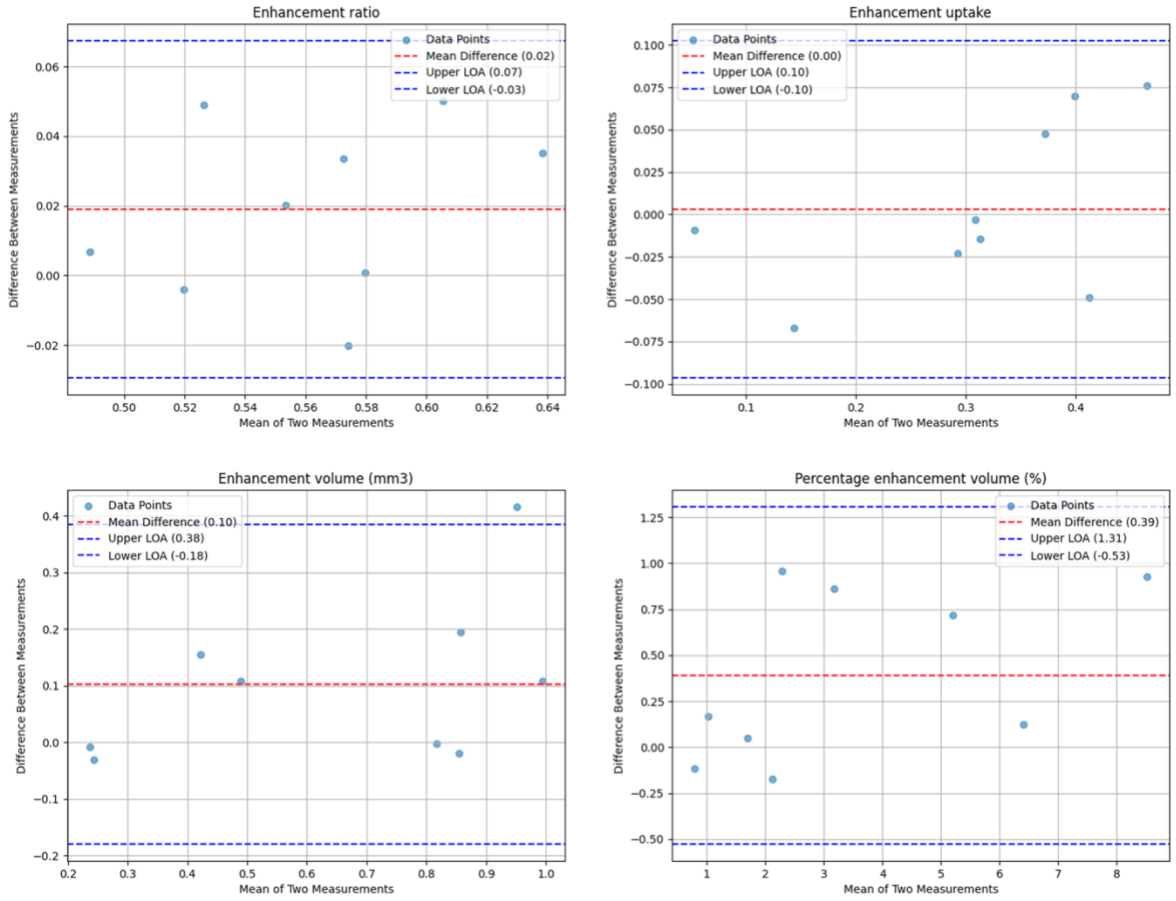

Figure 3.7 Bland-Altman plots illustrate the reproducibility of enhancement ratio, enhancement uptake, enhancement volume, and percent enhancement volume in the 9 plaques categorized as CE-positive in both scan and rescan sessions.

3.4 Discussion

We developed and validated an image processing method for quantitative characterization of contrast enhancement (CE) in intracranial atherosclerotic plaques, building upon a previously proposed multi-contrast, multi-planar framework for analyzing intracranial vessel wall (IVW) MRI[12]. Our method integrated intensity normalization across pre- and post-T1w scans,

mitigation of enhancing artifacts, and an optimized signal intensity threshold for CE detection, demonstrating strong agreement with expert reader assessments of CE presence and volume. In addition, the scan-rescan reproducibility of CE detection and measurement was high using the quantitative CE map. Incorporating this method into clinical practice could standardize IVW review and streamline radiologist workflows, enabling comprehensive plaque characterization while improving stroke risk assessment and treatment planning.

Despite the promise of IVW for improving the diagnosis and characterization of intraplaque atherosclerotic diseases, the small caliber of intracranial vessels and the limited resolution of imaging pose significant challenges in identifying specific plaque components, such as intraplaque hemorrhage and necrotic core—features commonly associated with high-risk plaques in larger arterial beds[17,18]. Despite these limitations, CE of intracranial plaques has emerged as a valuable biomarker in imaging ICAD. Upon the administration of gadolinium (Gd)-based contrast agents, plaque CE occurs through two primary mechanisms: direct diffusion from the arterial lumen or infiltration via the vasa vasorum in the adventitia. Intriguingly, healthy intracranial arteries lack vasa vasorum[19], which only develops in response to pathological conditions[20]. Consequently, the presence of vasa vasorum and associated CE may serve as an indicator of increased endothelial permeability and vessel wall vulnerability. Therefore, CE has been strongly linked to downstream acute infarction[9,21], with plaques demonstrating CE being up to ten times more likely to cause infarction in their supplied tissue compared to non-enhancing plaques[5]. For patients presenting with acute ischemic stroke, integrating CE assessment into routine IVW examinations could serve as a valuable method for identifying high-risk plaques and guiding therapeutic strategies.

Clinicians often assess intracranial plaque enhancement through qualitative grading[21–24] as follows: grade 0 indicates no enhancement; grade 1, enhancement higher than the normal vessel wall but lower than the pituitary infundibulum (PI); and grade 2, enhancement similar to or exceeding that of the PI. Additionally, they qualitatively categorize CE morphology as either focal (localized, well-defined enhancement) or diffuse (widespread, homogeneous enhancement). However, especially in research settings, a broader range of quantitative metrics is desirable for a more detailed analysis of plaque properties. Most studies quantify CE in 2D, using a single image slice from a specific plane of view in the source images, typically selecting the slice with the most severe stenosis or the thickest plaque wall. The degree of CE is then normalized to that of a reference structure, such as the PI[22,23], gray matter[25,26], cerebrospinal fluid (CSF)[27], or the genu of the corpus callosum (CC)[9,28], with the CC shown to provide the most reliable reference for identifying culprit plaques in stroke patients[9].

Despite these advances, most studies have fallen short of achieving intuitive 3D visualizations and voxel-wise CE measurements. Sanchez et al.[9], by adapting a workflow originally designed for quantifying intracranial aneurysms[16,29], utilized signal intensity probes extending from the lumen into the vessel wall to create a 3D enhancement color map. However, this spoke-based approach often misrepresents eccentric plaques as thin CE surfaces, still requiring manual plaque morphology measurements from source images. Furthermore, a lack of an image registration module between pre- and post-T1w images requires separate measurements on each, doubling the manual efforts for plaques delineation. Our proposed quantitative CE map, built upon MOCHA, address these challenges by streamlining ICAD and CE characterization. This approach allows for simultaneous multi-contrast image review, and the organic integration of plaque morphological and enhancement assessments within a single workflow through multi-

planar reformation. Beyond MOCHA's plaque characterization, only the manual signal intensity measurement of the reference structure (CC) is required to generate the CE map, significantly improving efficiency. Moreover, the derived quantitative metrics, including Gd uptake and enhancement volume, were found to correlate well with the widely adopted qualitative metrics.

Additionally, previous quantitative CE maps lacked a definitive threshold for determining CE presence, and these measurements were often compromised by common enhancing artifacts, such as proximity to the sinus or venous flow. While clinicians performing qualitative assessments can often recognize and disregard these artifacts[10], prior quantitative methods have not addressed this issue, leading to false-positive detections and reduced specificity. In our study, we implemented an artifact adjustment module that significantly improved specificity by distinguishing true plaque enhancement from non-plaque-related signal elevations using a 3D connected component-based approach. By excluding enhancing regions extending beyond the arterial wall boundary—likely stemming from imaging artifacts rather than true CE—this adjustment markedly reduced false positives, increasing specificity from 0.70 to 0.90 while maintaining high sensitivity at 0.83. The increased specificity is significant because it ensures that the detected CE truly reflects a pathological process rather than capturing imaging noise, establishing CE as a more reliable IVW imaging biomarker.

The accurate assessment of CE is particularly critical for facilitating longitudinal follow-up studies on ICAD, which help understand the time course of intracranial plaque enhancement and its relationship with acute ischemic events[30,31]. Evidence suggests that both the degree and persistence of plaque enhancement may serve as promising biomarkers for predicting recurrent strokes[32–34]. Given that patients with stroke attributable to ICAD face the highest risk of recurrence among all stroke etiologies[1], this understanding is crucial for optimizing primary and

secondary stroke prevention strategies. Several IVW studies have reported different trends in CE changes: plaques associated with recurrent events often exhibit an increase in CE[35], while non-recurrent plaques generally show a decrease in CE[8,31], potentially indicating a favorable response to medical treatment. To further elucidate the relationship between ICAD and CE evolution, a broader adoption of longitudinal IVW studies is necessary. Our quantitative CE map offers an efficient and reliable method for IVW lesion quantification, which may help overcome the barriers to such future investigations.

Few studies have reported on the reproducibility of CE measurements, which is a critical requirement for reliably tracking changes in plaque enhancement over serial IVW examinations. Existing studies have reported inter-rater ICCs ranging from 0.77 to 0.92[23,36,37], although the definitions of the measured quantities vary widely, and these studies continued to rely on traditional 2D approaches to characterize CE intensity. One previous study[12] evaluated the scan-rescan reproducibility of CE signals on IVW, reporting an ICC of 0.94 (95% CI: 0.89, 0.97) for the enhancement ratio in patients scanned twice within a two-week interval. However, that study did not perform intensity normalization, which may be sufficient in an experimental setting, where the same patient is scanned on the same scanner within a short timeframe, but fails to ensure comparability of CE values across patients. This limitation reduces its applicability in larger cohort studies. Importantly, our proposed method was developed and further validated against expert manual review, addressing reproducibility for broader applicability.

There are a few limitations in this study. First, while the number of plaques may be sufficient for analysis, this study remains limited by the small number of plaques with contrast enhancement. Additionally, scan-rescan validation was performed on a subset of asymptomatic patients, who may exhibit fewer CE features compared to clinical stroke cohorts. Second, the CE threshold was

developed and validated against manual review. Challenges remain in conducting histological studies to establish a definite ground truth for the presence of intracranial plaque CE. Third, this study was conducted at a single center using a single type of MRI scanner and IVW sequence, and CE intensity may also be influenced by factors such as the timing between gadolinium injection and IVW imaging[27]. Future studies are needed to evaluate the generalizability of the CE threshold across different imaging protocols and clinical settings.

3.5 Conclusion

We developed and validated a quantitative CE mapping method for intracranial atherosclerotic plaques, integrating a multi-contrast, multi-planar IVW MRI framework with intensity normalization, artifact mitigation, and an optimized signal intensity threshold for CE detection. Our approach demonstrated high accuracy and strong scan-rescan reproducibility for CE intensity and volumetric measurements. By offering an efficient and reliable means of assessing CE, this method has the potential to enhance stroke risk stratification, monitor disease progression, and guide treatment strategies for ICAD patients.

Bibliography

1. Yaghi, S., Prabhakaran, S., Khatri, P. & Liebeskind, D. S. Intracranial Atherosclerotic Disease. *Stroke* **50**, 1286–1293 (2019).
2. Martin, S. S. *et al.* 2024 Heart Disease and Stroke Statistics: A Report of US and Global Data From the American Heart Association. *Circulation* **149**, e347–e913 (2024).
3. Mandell, D. M. *et al.* Intracranial Vessel Wall MRI: Principles and Expert Consensus Recommendations of the American Society of Neuroradiology. *American Journal of Neuroradiology* **38**, 218–229 (2017).
4. Yuan, C. *et al.* Contrast-enhanced high resolution MRI for atherosclerotic carotid artery tissue characterization. *Journal of Magnetic Resonance Imaging* **15**, 62–67 (2002).
5. Gupta, A. *et al.* Gadolinium Enhancement in Intracranial Atherosclerotic Plaque and Ischemic Stroke: A Systematic Review and Meta-Analysis. *Journal of the American Heart Association* **5**, e003816 (2016).
6. Song, J. W. *et al.* Vessel Wall Magnetic Resonance Imaging Biomarkers of Symptomatic Intracranial Atherosclerosis. *Stroke* **52**, 193–202 (2021).
7. Mossa-Basha, M. *et al.* Survey of the American Society of Neuroradiology Membership on the Use and Value of Intracranial Vessel Wall MRI. *American Journal of Neuroradiology* **43**, 951–957 (2022).
8. Guo, Y. *et al.* Plaque Evolution and Vessel Wall Remodeling of Intracranial Arteries: A Prospective, Longitudinal Vessel Wall MRI Study. *Journal of Magnetic Resonance Imaging* **60**, 889–899 (2024).

9. Sanchez, S. *et al.* 3D Enhancement Color Maps in the Characterization of Intracranial Atherosclerotic Plaques. *American Journal of Neuroradiology* (2022) doi:10.3174/ajnr.A7605.
10. Lindenholz, A., van der Kolk, A. G., Zwanenburg, J. J. M. & Hendrikse, J. The Use and Pitfalls of Intracranial Vessel Wall Imaging: How We Do It. *Radiology* **286**, 12–28 (2018).
11. Zhang, N., Liu, X., Xiao, J., Song, S. S. & Fan, Z. Plaque Morphologic Quantification Reliability of 3D Whole-Brain Vessel Wall Imaging in Patients With Intracranial Atherosclerotic Disease: A Comparison With Conventional 3D Targeted Vessel Wall Imaging. *Journal of Magnetic Resonance Imaging* **54**, 166–174 (2021).
12. Guo, Y. *et al.* Multi-Planar, Multi-Contrast and Multi-Time Point Analysis Tool (MOCHA) for Intracranial Vessel Wall Characterization. *Journal of Magnetic Resonance Imaging* **56**, 944–955 (2022).
13. Balu, N. *et al.* Accelerated multi-contrast high isotropic resolution 3D intracranial vessel wall MRI using a tailored k-space undersampling and partially parallel reconstruction strategy. *Magn Reson Mater Phy* **32**, 343–357 (2019).
14. Omodaka, S. *et al.* Quantitative Assessment of Circumferential Enhancement along the Wall of Cerebral Aneurysms Using MR Imaging. *American Journal of Neuroradiology* **37**, 1262–1266 (2016).
15. Roa, J. A. *et al.* Objective quantification of contrast enhancement of unruptured intracranial aneurysms: a high-resolution vessel wall imaging validation study. *Journal of Neurosurgery* **134**, 862–869 (2020).
16. Raghuram, A. *et al.* Semiautomated 3D mapping of aneurysmal wall enhancement with 7T-MRI. *Sci Rep* **11**, 18344 (2021).

17. Ota, H. *et al.* Hemorrhage and Large Lipid-Rich Necrotic Cores Are Independently Associated With Thin or Ruptured Fibrous Caps. *Arteriosclerosis, Thrombosis, and Vascular Biology* **29**, 1696–1701 (2009).
18. Canton, G. *et al.* Pathophysiology of carotid atherosclerosis: Calcification, intraplaque haemorrhage and pulse pressure as key players. *European Journal of Radiology* **178**, 111647 (2024).
19. Aydin, F. Do human intracranial arteries lack vasa vasorum? A comparative immunohistochemical study of intracranial and systemic arteries. *Acta Neuropathol* **96**, 22–28 (1998).
20. Portanova, A. *et al.* Intracranial Vasa Vasorum: Insights and Implications for Imaging. *Radiology* **267**, 667–679 (2013).
21. Qiao, Y. *et al.* Intracranial Plaque Enhancement in Patients with Cerebrovascular Events on High-Spatial-Resolution MR Images. *Radiology* **271**, 534–542 (2014).
22. Wu, F. *et al.* Hyperintense Plaque on Intracranial Vessel Wall Magnetic Resonance Imaging as a Predictor of Artery-to-Artery Embolic Infarction. *Stroke* **49**, 905–911 (2018).
23. Wu, F. *et al.* Differential Features of Culprit Intracranial Atherosclerotic Lesions: A Whole-Brain Vessel Wall Imaging Study in Patients With Acute Ischemic Stroke. *Journal of the American Heart Association* **7**, e009705 (2018).
24. Lu, S.-S. *et al.* MRI of plaque characteristics and relationship with downstream perfusion and cerebral infarction in patients with symptomatic middle cerebral artery stenosis. *Journal of Magnetic Resonance Imaging* **48**, 66–73 (2018).

25. Wu, G. *et al.* Large Culprit Plaque and More Intracranial Plaques Are Associated with Recurrent Stroke: A Case-Control Study Using Vessel Wall Imaging. *American Journal of Neuroradiology* **43**, 207–215 (2022).
26. Ran, Y. *et al.* Higher Plaque Burden of Middle Cerebral Artery Is Associated With Recurrent Ischemic Stroke. *Stroke* **51**, 659–662 (2020).
27. Sun, B. *et al.* Delayed Enhancement of Intracranial Atherosclerotic Plaque Can Better Differentiate Culprit Lesions: A Multiphase Contrast-Enhanced Vessel Wall MRI Study. *American Journal of Neuroradiology* (2024) doi:10.3174/ajnr.A8132.
28. Sanchez, S., Miller, J. M., Jones, M. T., Ojeda, D. J. & Samaniego, E. A. Intracranial Atherosclerotic Plaque Morphologic Pattern and Enhancement Change With High-Intensity Statin Therapy. *Stroke: Vascular and Interventional Neurology* **3**, e000942 (2023).
29. Veeturi, S. S. *et al.* An Image-Based Workflow for Objective Vessel Wall Enhancement Quantification in Intracranial Aneurysms. *Diagnostics* **11**, 1742 (2021).
30. Skarpathiotakis, M., Mandell, D. M., Swartz, R. H., Tomlinson, G. & Mikulis, D. J. Intracranial Atherosclerotic Plaque Enhancement in Patients with Ischemic Stroke. *American Journal of Neuroradiology* **34**, 299–304 (2013).
31. Kwee, R. M., Qiao, Y., Liu, L., Zeiler, S. R. & Wasserman, B. A. Temporal course and implications of intracranial atherosclerotic plaque enhancement on high-resolution vessel wall MRI. *Neuroradiology* **61**, 651–657 (2019).
32. Kim, J.-M. *et al.* Intracranial plaque enhancement from high resolution vessel wall magnetic resonance imaging predicts stroke recurrence. *International Journal of Stroke* **11**, 171–179 (2016).

33. Song, X. *et al.* Incremental value of plaque enhancement in predicting stroke recurrence in symptomatic intracranial atherosclerosis. *Neuroradiology* **62**, 1123–1131 (2020).
34. Zhao, Y. *et al.* Plaque enhancement predicts recurrence in acute ischemic stroke patients with large artery intracranial atherosclerosis. *Journal of Stroke and Cerebrovascular Diseases* **32**, 107406 (2023).
35. Xiao, J. *et al.* Disparate trends of atherosclerotic plaque evolution in stroke patients under 18-month follow-up: a 3D whole-brain magnetic resonance vessel wall imaging study. *Neuroradiol J* **35**, 42–52 (2022).
36. Alexander, M. D., de Havenon, A., Kim, S.-E., Parker, D. L. & McNally, J. S. Assessment of quantitative methods for enhancement measurement on vessel wall magnetic resonance imaging evaluation of intracranial atherosclerosis. *Neuroradiology* **61**, 643–650 (2019).
37. Ryoo, S., Lee, M. J., Cha, J., Jeon, P. & Bang, O. Y. Differential Vascular Pathophysiologic Types of Intracranial Atherosclerotic Stroke. *Stroke* **46**, 2815–2821 (2015).

Chapter 4 Plaque Evolution and Vessel Wall Remodeling of Intracranial Arteries: A Prospective, Longitudinal Vessel Wall MRI study

This chapter presents a one of the first prospective, longitudinal investigations into the evolution of intracranial atherosclerotic disease (ICAD) using three-dimensional vessel wall MRI (IVW). Following 37 patients with angiography-confirmed ICAD over a one-year period, we employed our validated MOCHA workflow to jointly analyze baseline and follow-up imaging data. The majority of plaques (74%) remained stable during the observation period, with the regression group showing significant increases in minimum lumen area and the progression group exhibiting significant decreases. Our findings reveal significant associations between diabetes mellitus and plaque progression, with diabetic patients experiencing significant decrease in lumen area increase in wall thickness at one-year follow-up. Notably, baseline contrast enhancement emerged as a significant predictor of plaque progression, while culprit plaques demonstrated a distinctive pattern of luminal expansion. compared to non-culprit lesions. These results provide valuable insights into the natural history of ICAD and highlight potential imaging biomarkers for identifying high-risk plaques that may benefit from more aggressive intervention.

The work presented here is reproduced and adapted from: Yin Guo, et al. "Plaque evolution and vessel wall remodeling of intracranial arteries: a prospective, longitudinal vessel wall MRI study." Journal of Magnetic Resonance Imaging 60.3 (2024): 889-899.

4.1 Introduction

Intracranial atherosclerotic disease (ICAD) is a leading cause for ischemic stroke worldwide[1]. It represents a dynamic process, as evidenced by prior studies associating ICAD progression with both baseline and recurrent ischemic stroke events[2,3]. Therefore, there is a need for imaging techniques to investigate ICAD evolution and its associations with stroke.

Traditionally, ICAD evolution has been monitored with luminal stenosis changes on angiographic imaging such as computed tomography angiography (CTA) or magnetic resonance angiography (MRA)[4–6]. Three-dimensional (3D) intracranial vessel wall MRI (IVW), on the other hand, allows for morphological characterization of vessel wall lesions. IVW provides unique advantages in the longitudinal evaluation of ICAD as it can directly measure plaque evolution and vessel wall remodeling and identify both stenotic and non-stenotic lesions. Non-stenotic lesions are challenging to identify on angiography but are reported to account for 30%-70% of ICAD plaques[7,8].

Two longitudinal ICAD 3D IVW studies[9,10] monitored culprit plaques in stroke patients and documented regression under intensive medical treatment. However, these studies were limited in numbers, and as a result, ICAD evolution and its contributing factors remains relatively unknown. One of the challenges for longitudinal IVW studies is rater analysis of complex multi-contrast and multi-time point 3D datasets[11,12]. To address this limitation, our group previously developed MOCHA[13] (multi-planar, multi-contrast and multi-time point analysis tool for intracranial vessel wall characterization), a dedicated pipeline for efficient and reliable serial IVW lesion detection and quantification. MOCHA has shown excellent inter-rater and scan-rescan reproducibility for ICAD characterization, surpassing the reproducibility of standard rater review[14].

The objective of this study is to characterize imaging patterns of plaque evolution and vessel wall remodeling in ICAD, with longitudinal 3D IVW and MOCHA.

4.2 Methods

4.2.1 Study Population

This HIPAA-compliant study was approved by the Institutional Review Board. After written informed consent was obtained, patients were prospectively recruited as part of the WALLI study[8] between September 2016 and September 2020. The inclusion criterion was CTA- or MRA-confirmed intracranial artery stenosis or luminal irregularity after patients undergoing acute stroke workup. A board-certified radiologist conducted chart and clinical image review to determine eligibility of potential subjects. Exclusion criteria included: non-atherosclerotic vasculopathies, extracranial carotid stenosis >50%, recent stroke from atrial fibrillation or other potential cardioembolic sources, current or prior subarachnoid hemorrhage, intracranial stent or clip, history of radiation therapy to the head, any contraindication to MRI or intravenous gadolinium contrast, or inability to provide informed consent. During patient recruitment, demographic and clinical characteristics, including age, sex, hypertension, hyperlipidemia, diabetes mellitus and medications were collected. Patient management was determined by the clinical team and followed standard clinical care for medical management. No patients received intracranial stents.

After initial screening, 45 patients with evidence of ICAD on clinical luminal imaging were consecutively recruited in the WALLI study. To analyze atherosclerotic plaque evolution, subjects underwent IVW twice at a twelve-month interval. A total of 37 subjects (age 68.91 ±

11.74 years, 12 females) who completed longitudinal 3D IVW were included in this analysis. The study flow chart is provided in Figure 4.1(a). The mean interval between scans was 1.3 ± 0.4 years. A total of 29 subjects (78%) were on statins and 30 (81%) were on antiplatelet medications.

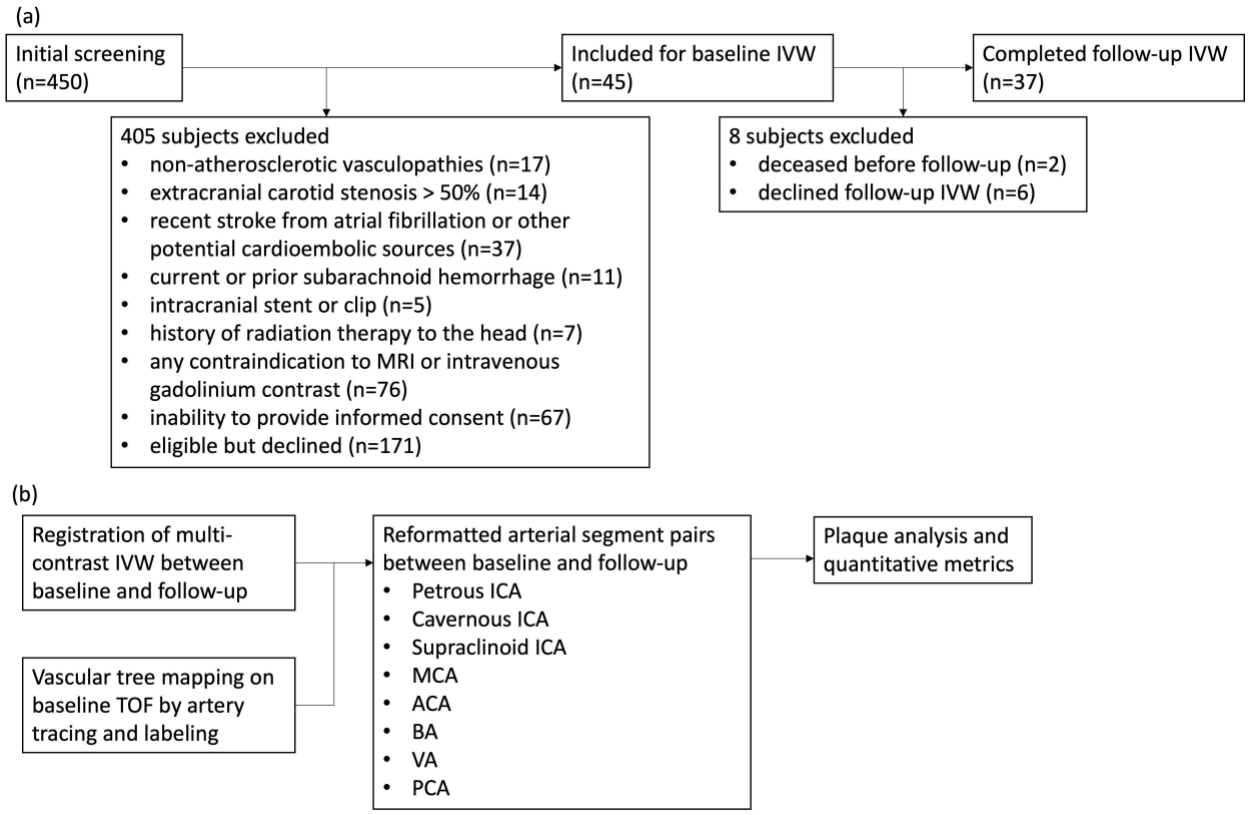

Figure 4.1 Flow chart for (a) the prospective WALLI longitudinal study and (b) IVW processing and interpretation by MOCHA.

4.2.2 MRI Protocol

Details of the 3D multi-contrast IVW protocol were previously reported[13,15]. Briefly, IVW was performed at two time points on a 3.0T scanner (Ingenia CX, Philips Healthcare, Best, The

Netherlands) with a 32- channel head coil. The imaging protocol included pre- and post-contrast T1 volumetric isotropic turbo spin echo (VISTA), delay alternating with nutation for tailored excitation (DANTE)- prepared blood-suppressed proton density (PD) weighted VISTA and time-of-flight MRA (TOF) sequences (see sequence parameters in Table 4.1). Conventional MRI sequences, including diffusion weighted imaging (DWI), susceptibility weighted imaging (SWI) and T2-fluid attenuated inversion recovery (FLAIR) were performed at both time points.

Table 4.1 MRI protocol sequence parameters

Sequence	Pre-T1 VISTA	PD VISTA	Post-T1 VISTA	3D-TOF
Orientation	Coronal	Coronal	Coronal	Axial
Field of view (mm)	180 × 180 × 40	180 × 180 × 40	180 × 180 × 40	190 × 190 × 72
Acquired resolution (mm)	0.5 × 0.5 × 0.5	0.5 × 0.5 × 0.5	0.5 × 0.5 × 0.5	0.5 × 0.5 × 1
Reconstructed resolution (mm)	0.25 × 0.25 × 0.25	0.25 × 0.25 × 0.25	0.25 × 0.25 × 0.25	0.25 × 0.25 × 0.5
Bandwidth (Hz/pixel)	620	625	620	289
Repetition time (msec)	800	2000	800	15
Echo time (msec)	26	36	26	3.5
Flip angle (°)	Varies	Varies	Varies	18
Echo train length	30	60	30	NA
Averages	2	2	2	1
Scan time (minutes:sec)	5:03	5:38	5:03	5:15

Pre- and Post-T1 VISTA = precontrast and postcontrast T1 volumetric isotropic turbo spin echo; PD VISTA = proton density weighted VISTA; 3D-TOF = three dimensional TOF magnetic resonance angiography.

4.2.3 IVW Interpretation and Morphological Measurements

The MOCHA workflow, as described previously[13,16], was used for the analysis of IVW images incorporating an image registration step to account for the multi-time point imaging data. Briefly, the baseline and follow-up contrast weightings (pre- and post-contrast T1

VISTA, PD VISTA and TOF, as mentioned above) were registered, and automated cross-sectional multi-planar reformats (MPRs) perpendicular to the luminal centerline were then created.

Cross-sectional MPRs were used for the detection of plaque and delineation of the luminal and outer wall boundaries of eight intracranial arterial segments. These included: petrous (PET), cavernous (CAV) and supraclinoid (SC) internal carotid arteries (ICA), M1/M2 middle cerebral artery (MCA), A1/A2 anterior cerebral artery (ACA), basilar artery (BA), V4 vertebral arteries (VA) and P1/P2 posterior cerebral arteries (PCA). A lesion was identified if it showed stenosis or irregularity on luminal imaging and/or wall thickening on T1 pre- and post-contrast VISTA[8], and the luminal and outer wall boundaries were manually traced by one reader (GC with 13 years of vascular imaging experience). The results were then peer-reviewed by a second reader (JS with 13 years of vascular imaging experience). Disagreement in the peer review was discussed with a third rater (MMB with 19 years of vascular imaging experience). Each arterial segment was analyzed independently after randomization, and plaques were traced on baseline and follow-up imaging side-by-side at the same session, with the order of the two scans randomized and timestamps removed. With the same readers, reproducibility of IVW plaque detection and measurements were extensively validated in a prior publication[13]. Per arterial segment with plaque, the manual analysis typically took 15 minutes for both studies. For segments without plaque, the analysis time was substantially shorter.

Plaque length was determined by counting consecutive cross-sectional slices with lesions. Plaque morphological measurements (including lumen area, wall area, total vessel area, maximum wall thickness, and normalized wall index) were derived based on the delineated

luminal and outer wall boundaries. In addition, we measured mean signal intensity within the vessel wall on pre-contrast and post-contrast T1-VISTA images to calculate the contrast enhancement ratio. Detailed definitions of these parameters can be found in a prior publication[13]. The flow chart for IVW processing and interpretation by MOCHA is provided in Figure 4.1(b).

Blinded to the IVW MPR images and interpretation, three neuroradiologists (MMB, DBG with 10 years of experience and MK with 5 years of experience) independently reviewed baseline TOF-MRA to record the location of stenoses across the different segments and measured the degree of stenosis with the Warfarin-Aspirin Symptomatic Intracranial Disease (WASID) criteria[17] using the RadiAnt DICOM Viewer (https://www.radiantviewer.com, Medixant, Poznan, Poland). Inter-reader agreement was assessed, and any disagreement was then resolved by consensus.

In a separate review session while blinded to all other imaging, one board-certified neuroradiologist (MMB) reviewed brain MRI performed in close temporal proximity to baseline IVW and determined the location of recent infarcts. Recent infarcts were lesions showing diffusion restriction. Medical charts and follow-up brain MRI were reviewed (MMB), and patient interviews were performed every 3 months over the one-year follow-up period for any recurrent ischemic events. These results were peer-reviewed and confirmed by one radiologist (NZ with 5 years of experience).

Detected atherosclerotic plaques were classified into two groups (culprit and non-culprit) based on their location, mean wall area, and the infarct territory, similar to approaches defined in prior studies[18–20]. A culprit plaque was identified when it was either the only lesion within the vascular territory upstream of the infarct, or it had the largest mean wall area when

multiple plaques were upstream within the same infarct territory. Other plaques were considered non-culprit. When deciding between possible culprit plaques all within a single infarcted vascular territory, wall area was used as the criterion rather than luminal stenosis, given the presence of non-stenotic or mildly stenotic culprit lesions in previous reports[21].

4.2.4 Statistical Analysis

Plaques were categorized as progressing, stable and regressing based on longitudinal changes in maximum wall thickness between the two scans. The threshold was determined using the measurement error in a previous scan-rescan reproducibility cohort[13] to establish meaningful changes in maximum wall thickness. A 15.2% change (two times the standard deviation of percentage measurement differences (7.6%), covering 95% of the confidence interval (CI)) in maximum wall thickness over one year was chosen as the threshold for determining whether a plaque had progressed, regressed, or remained stable. Plaque morphological measurements on IVW were compared between baseline and one-year scans within the three groups. Logistic regression was used to compare the differences in baseline plaque characteristics between regression versus stable/progression groups, and between progression versus stable/regression groups.

Regarding both baseline measurement and percentage changes of ICAD characteristics, we used univariate regression to study the associations with vascular risk factors and medications, and logistic regression to compare between culprit and non-culprit lesions. Specifically, culprit lesions were compared between both all non-culprit lesions from all patients, and to control for potential patient-specific confounders, with matched non-culprit lesions within patients where

culprit lesions were identified.

To assess the inter-reader reproducibility of luminal stenosis measurement, the intra-class coefficient (ICC) with 95% CI was calculated from a two-way mixed model.

Categorical variables were summarized as count (percentage). Continuous variables were summarized as mean ± standard deviation. To account for non-independent observations of multiple plaques detected in the same patient, generalized estimating equations (GEE)-based models were used throughout all above-mentioned analyses. Artery segment was included as a covariate in the regression models to account for properties of different artery beds.

All statistical analyses were performed using statsmodels[22] 0.13.5 with Python 3.10. A two-sided p-value<0.05 was considered statistically significant.

4.3 Results

Among 37 subjects, a total of 120 plaques were detected on IVW, with the ICA being the most frequently involved segment (n=64) and the ACA being the least frequently involved segment (n=1). The distribution of lesions among the above-mentioned eight segments and their changes in maximum wall thickness are shown in Figure 4.2. During the twelve-month follow-up, 89 (74%) plaques remained stable, 18 (15%) plaques regressed, and 13 (11%) plaques progressed. Specifically, 13/55 (24%) plaques progressed in 9/37 (24%) subjects, and 18/78 (23%) plaques regressed in 14/37 (38%) subjects. Example images of progressing and regressing plaques are shown in Figure 4.3.

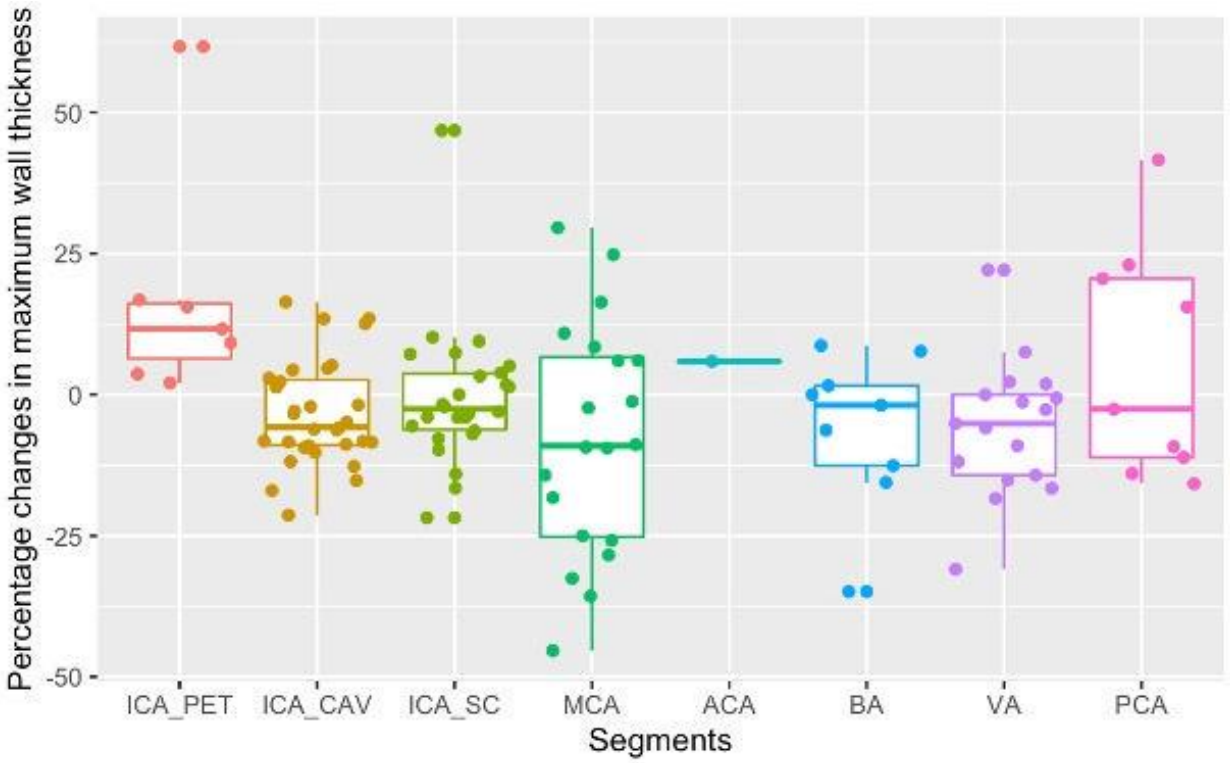

Figure 4.2 Percentage changes in maximum wall thickness grouped by intracranial artery segments.

ICA_PET: petrous internal carotid artery, ICA_CAV: cavernous internal carotid artery, ICA_SC: supraclinoid internal carotid artery, MCA: M1/M2 middle cerebral artery, ACA: A1/A2 anterior cerebral artery, BA: basilar artery, VA: V4 vertebral artery, PCA: P1/P2 posterior cerebral artery. Each dot represents one identified plaque.

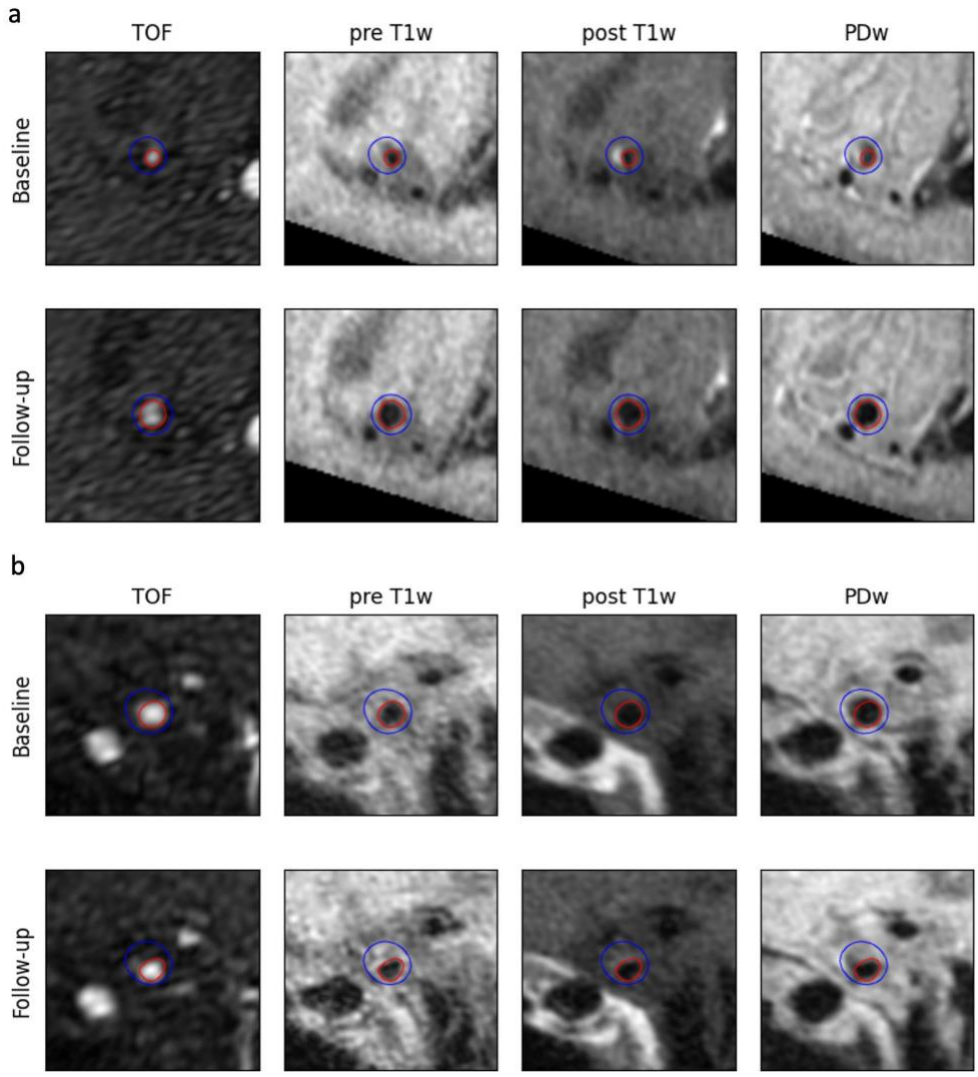

Figure 4.3 Examples of longitudinal evolution of intracranial plaques analyzed using MOCHA, showing multi-contrast IVW (columns) in cross sections with lumen (red) and outer wall (blue) contours.

(a) A culprit PCA plaque showing regression (thinning of arterial wall and expansion of lumen). (b) A non-culprit ICA supraclinoid plaque showing progression (thickening of arterial wall and contraction of lumen.

Ischemic infarcts were identified in 24 subjects (65%), and subsequently 18 culprit plaques were found. Two subjects experienced recurrent events during the follow-up period.

The three readers reached excellent reproducibility in measuring luminal stenosis, with the ICC value of 0.972 and 95% CI of (0.962, 0.979).

4.3.1 Associations of Plaque Morphology with Vascular Risk Factors

Table 4.2 presents the associations between patient demographics, clinical risk factors, medications, and baseline measurements and percentage changes in minimum lumen area and maximum wall thickness. We found that non-white race was significantly associated with smaller baseline lumen area. Presence of hypertension, hyperlipidemia, and diabetes were all significantly associated with larger arterial wall thickness measurements at baseline.

However only diabetes was significantly associated with ICAD progression, with 6.6% decrease in lumen area and 6.7% increase in wall thickness at one-year follow-up.

Table 4.2 Associations between patient demographics and clinical risk factors, and baseline characteristics and percentage changes of plaque lumen area and wall thickness

	Baseline Characteristics								Percentage Changes During Follow-up							
			Associations with Min Lumen Area			Associations with Max Wall Thickness			Associations with Min Lumen Area			Associations with Max Wall Thickness				
	No.	All	Coeff	(95% CI)	*P*-value	Coeff	(95% CI)	*P*-value	Coeff	(95% CI)	*P*-value	Coeff	(95% CI)	*P*-value
Age	120	70.9 ± 12.5	0.07	(−0.01, 0.14)	0.069	0.01	(−0.00, 0.02)	0.1	0.05	(−0.18, 0.28)	0.678	−0.02	(−0.28, 0.25)	0.886
Male sex	120	82 (68%)	1.85	(−0.47, 4.16)	0.118	0	(−0.21, 0.21)	0.994	−0.74	(−5.63, 4.15)	0.767	2.14	(−2.24, 6.51)	0.338
Non-white race	120	23 (19%)	−2.3	(−3.91, −0.69)	0.0052	0.08	(−0.34, 0.50)	0.712	0.37	(−7.20, 7.94)	0.923	4.33	(−1.43, 10.09)	0.141
Hypertension	120	106 (88%)	−1.36	(−3.93, 1.21)	0.3	0.26	(0.02, 0.51)	0.036	−2.34	(−10.96, 6.27)	0.594	2.57	(−4.34, 9.48)	0.466
Hyperlipidemia	120	91 (75%)	0.22	(−1.82, 2.26)	0.83	0.37	(0.21, 0.52)	<0.001	0.94	(−4.23, 6.11)	0.721	1.82	(−5.47, 9.11)	0.626
Diabetes	120	48 (40%)	−3.02	(−5.39, −0.66)	0.012	0.29	(0.00, 0.59)	0.05	−6.6	(−11.99, −1.22)	0.016	6.73	(2.01, 11.45)	0.0052
Statins	120	94 (78%)	0.9	(−1.59, 3.39)	0.48	0.1	(−0.08, 0.29)	0.282	−2.4	(−6.05, 1.26)	0.199	0.81	(−4.91, 6.53)	0.782
Antiplatelet	120	101 (84%)	1.35	(−0.99, 3.69)	0.259	0.03	(−0.18, 0.23)	0.788	3.65	(−2.56, 9.87)	0.249	1.58	(−2.90, 6.07)	0.49

4.3.2 Plaque Wall Remodeling Patterns

As shown in Table 4.3, we measured the minimum lumen area significantly increase from 7.4 mm^2 to 8.3 mm^2 and the mean wall area significantly decrease from 11.6 mm^2 to 10.1 mm^2 in the regression group. For the progression group, the minimum lumen area significantly decreased from 5.4 mm^2 to 4.3 mm^2 and the mean wall area significantly increased from 10.5 mm^2 to 11.5 mm^2. In the stable group, neither measurement differed significantly from baseline to follow-up ($p=1.00$ and 0.79, respectively). In all three groups, the changes in mean total vessel area were not statistically different ($p=0.23$, 0.42 and 0.49, respectively). Therefore, progressing plaques demonstrated inward remodeling with lumen loss, while regression was accompanied by luminal expansion.

We did not observe statistically significant changes in contrast enhancement in regression, stable and progression groups ($p=0.18$, 0.64 and 0.12, respectively).

Table 4.3 ICAD characteristics at baseline and 1-year follow-up

	Regression ($n = 18$)			Stable ($n = 89$)			Progression ($n = 13$)		
	Baseline	One year	*P*-value	Baseline	One year	*P*-value	Baseline	One year	*P*-value
Min lumen area (mm^2)	7.40 ± 4.14	8.34 ± 4.01	0.015	9.55 ± 6.18	9.54 ± 6.04	0.998	5.40 ± 3.21	4.28 ± 2.80	<0.001
Mean wall area (mm^2)	11.59 ± 4.07	10.05 ± 3.62	<0.001	13.85 ± 4.59	13.57 ± 4.52	0.788	10.48 ± 3.54	11.54 ± 3.93	0.003
Mean total vessel area (mm^2)	20.14 ± 8.31	19.58 ± 7.86	0.23	25.06 ± 10.44	24.86 ± 10.24	0.418	17.46 ± 7.23	17.59 ± 7.08	0.488
Max normalized wall index	63.51 ± 8.06	56.16 ± 5.59	<0.001	63.38 ± 11.72	62.69 ± 11.74	0.031	68.29 ± 9.60	75.37 ± 9.98	0.0056
Max enhancement ratio	0.72 ± 0.58	0.73 ± 0.40	0.18	1.26 ± 0.77	1.34 ± 0.70	0.641	1.05 ± 0.56	0.91 ± 0.61	0.116

4.3.3 Baseline Plaque Characteristics Across Plaque Evolution Categories

We did not find significant differences in the degree of baseline luminal stenosis comparing the regression or progression group to the other two corresponding groups combined (odds ratio=0.99 and 1.00, p=0.70 and 0.96), as shown in Table 4.4. Figure 4.4 further illustrates the relation of baseline luminal stenosis with percentage changes in minimum lumen area and maximum wall thickness.

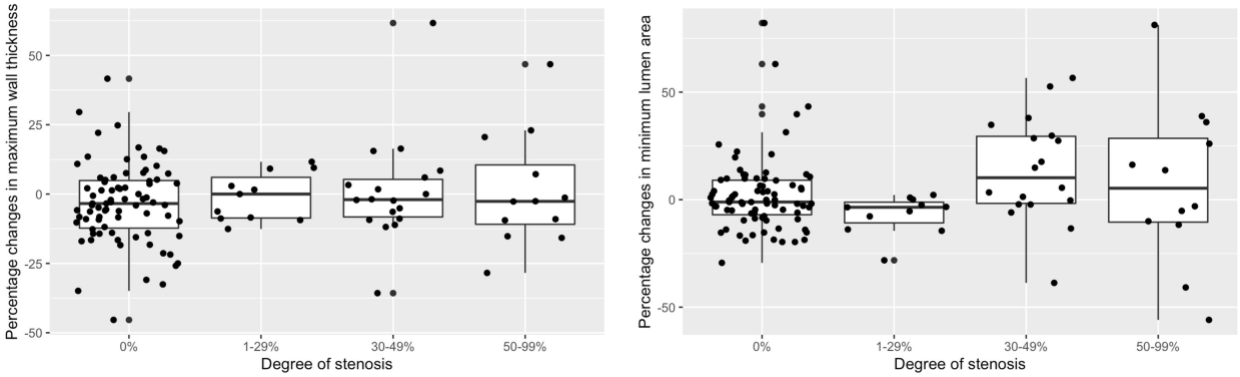

Figure 4.4 Percentage changes in minimum lumen area and maximum wall thickness by degree of baseline stenosis (measured on time-of-flight (TOF) based on Warfarin-Aspirin Symptomatic Intracranial Disease (WASID) criteria).

Each dot represents one identified plaque. Changes in vessel lumen and wall had substantial overlap between plaques with varying degree of stenosis.

Table 4.4 Predictabilities in baseline intracranial plaque characteristics when distinguishing between regression vs. stable and progression groups, or progression vs. stable and regression groups

	Regression vs. (Stable + Progression)			Progression vs. (Stable + Regression)		
	OR	(95% CI)	*P*-value	OR	(95% CI)	*P*-value
Stenosis (%)	0.98	(0.95, 1.01)	0.223	1	(0.97, 1.03)	0.993
Plaque length (mm)	0.91	(0.75, 1.09)	0.288	1.01	(0.92, 1.12)	0.798
Min lumen area (mm^2)	1.06	(0.93, 1.19)	0.393	0.92	(0.82, 1.02)	0.102
Mean wall area (mm^2)	1.07	(0.92, 1.24)	0.39	0.91	(0.83, 1.01)	0.064
Mean total vessel area (mm^2)	1.03	(0.98, 1.09)	0.246	0.94	(0.88, 1.00)	0.06
Max wall thickness (mm)	1.4	(0.41, 4.75)	0.593	0.69	(0.28, 1.72)	0.425
Max normalized wall index	0.96	(0.89, 1.04)	0.332	1.01	(0.95, 1.07)	0.829
Max enhancement ratio	0.36	(0.12, 1.12)	0.079	3.61	(1.06, 12.30)	0.04

No baseline plaque morphological features predicted progression. However, when controlled for arterial segment, maximum contrast enhancement ratio at baseline was significantly higher in the progression group than in the stable and regression groups (odds ratio=3.61). We also observed a trend of lower contrast enhancement in the regression group (odds ratio=0.36, p=0.08).

4.3.4 Culprit vs. Non-culprit Plaque Comparison

Four of the 18 culprit plaques underwent regression and 14 remained stable. Table 4.5 shows that there were no significant differences in baseline plaque characteristics between culprit and non-culprit lesions. However, we observed luminal increase (Figure 4.3(a)) in percentage changes within culprit lesions (n=18, 10.93 ± 19.06), the degree of which was significantly higher compared with non-culprit lesions (n=102, 2.25 ± 21.24). The comparison with matched culprit lesions confirmed the same association (10.93 ± 19.06 vs. 2.72 ± 24.09).

Table 4.5 Differences in baseline characteristics and percentage changes of ICAD between culprit and non-culprit plaques

	Baseline Characteristics					Percentage Changes During Follow-Up				
	Culprit ($n = 18$)	All Non-Culprit ($n = 102$)	*P*-Value	Matche d Non-Culprit ($n = 62$)	*P*-Value	Culprit ($n = 18$)	All Non-Culprit ($n = 102$)	*P*-Value	Matched Non-Culprit ($n = 62$)	*P*-Value
Min lumen area (mm)	8.91 ± 5.33	8.90 ± 5.99	0.924	7.21 ± 5.11	0.26	10.93 ± 19.06	2.25 ± 21.24	0.018	2.72 ± 24.09	0.014
Mean wall area (mm^2)	13.58 ± 4.73	13.20 ± 4.56	0.808	12.61 ± 4.42	0.898	−2.67 ± 8.17	−2.04 ± 9.69	0.934	−1.60 ± 10.99	0.98
Mean total vessel area (mm^2)	23.98 ± 9.80	23.71 ± 10.33	0.699	21.28 ± 9.17	0.636	−0.06 ± 5.72	−0.49 ± 6.54	0.609	−0.49 ± 7.50	0.534
Max wall thickness (mm)	1.90 ± 0.62	1.84 ± 0.58	0.773	1.84 ± 0.60	0.644	−6.02 ± 11.34	−1.41 ± 16.01	0.314	−1.52 ± 18.74	0.451
Max normalized wall index	64.24 ± 10.14	63.77 ± 11.39	0.693	67.18 ± 10.92	0.469	−3.52 ± 7.04	−0.80 ± 7.27	0.067	−0.43 ± 8.49	0.054
Max enhancement ratio	1.18 ± 0.93	1.17 ± 0.72	0.843	0.97 ± 0.65	0.406	−7.00 ± 55.80	6.91 ± 38.03	0.134	8.65 ± 40.08	0.106

We identified 18 culprit plaques from 37 subjects. "All non-culprit" plaques were defined as all 102 non-culprit plaques from all 37 subjects and "matched non-culprit" plaques were limited to the 62 non-culprit plaques within the 18 subjects where culprit plaques were identified.

4.4 Discussion

In this study, we reported a prospective study assessing the longitudinal evolution of ICAD on 3D IVW using a standardized quantification pipeline of 3D multi-planar, multi-contrast, multi-time point imaging review, and identified plaque contrast enhancement and diabetes mellitus, rather than stenosis, to be biomarkers indicating progression. We found that, after one-year follow-up, a quarter of all ICAD plaques evolved. Progressing plaques exhibited inward remodeling with lumen loss, while regression was accompanied by luminal expansion. Total vessel area, which represents changes in the outer wall boundary, remained stable in all three groups. This indicates there were no significant changes of outward remodeling in our study cohort, which differs from findings in the carotid plaque literature where outward remodeling was demonstrated in progressing plaques[23,24]. For example, Underhill et al. observed increases in wall and total vessel area but no changes in lumen area, demonstrating outward remodeling in 24 asymptomatic subjects with carotid atherosclerosis. Investigators and clinicians frequently infer ICAD behavior based on the carotid literature; however, this study suggests potential differential evolution that, with further validation, may better inform clinical longitudinal ICAD evaluation.

This study also demonstrated the limitations of using luminal angiography alone when assessing ICAD evolution. The changes in minimum lumen area and maximum wall thickness, indicative of plaque burden evolution, correlated poorly with the degree of baseline stenosis and had substantial overlap between stenotic and non-stenotic lesions. Additionally, the degree of baseline luminal stenosis did not predict future progression or regression of ICAD lesions. IVW-derived plaque features, however, could differentiate progressing plaques, which had higher contrast enhancement at baseline compared to plaques that regressed or remained stable.

Plaque contrast enhancement has been identified as a biomarker for increased neovascularization and inflammation[19,25], and our study further presented evidence highlighting the value of monitoring plaque enhancement.

Culprit ICAD lesions showed an expansion in lumen area. One possible explanation for this regression post-stroke is that, compared with non-culprit ICAD, culprit lesions may be more dynamic and more responsive to aggressive medical treatment. Another potential explanation is that before or immediately after the event, plaques may grow and the lumen size may be reduced secondary to inflammation, which subsides over time to baseline levels. Supporting this theory, culprit lesions showed a decrease in contrast enhancement over one year in our study.

The evolution of culprit lesions in symptomatic patients was the focus of four previous IVW longitudinal studies[9,10,25,26]. These studies imaged stroke patients with IVW over six to eighteen months, and divided patients into recurrent and non-recurrent stroke groups based on subsequent stroke events. The culprit plaques of the primary stroke were followed up, and they experienced plaque regression, especially in non-recurrent stroke patients, in agreement with our findings. However, when attempting to identify which plaque features are critical to predict future stroke events, each study pointed to different characteristics, such as stenosis, maximum wall thickness, plaque burden or enhancement ratio. The lack of consensus may be due to variable study designs: the two prospective studies used 2D IVW imaging acquisitions[25,26], which has its limitations in IVW coverage and lesion assessment[27], while the two 3D IVW imaging studies were retrospective[9,10]. The current study benefits from a prospective cohort with 3D IVW imaging protocols and a standardized analysis workflow. Moreover, comprehensive assessment and monitoring of all arterial segments and ICAD lesions, rather

than only one culprit plaque per patient, may further elucidate the risk of recurrent events and relationships in plaque behavior.

In the current study, the efficient identification and evaluation of all intracranial plaques in major vascular territories was facilitated by the dedicated MOCHA pipeline. MOCHA performed automated registration and arterial reconstruction into straight and curved planar reformats, allowing reviewers to navigate and identify lesions through all eight major intracranial arteries in an interactive, multi-planar display. Moreover, MOCHA was conceived as a tool dedicated to characterizing changes in ICAD over time with a built-in step to perform multi-time point image registration. Its excellent scan-rescan measurement reproducibility[13] has served as a firm quantitative basis in this longitudinal study. Previous investigative studies and patient monitoring of ICAD relied almost exclusively on luminal imaging modalities like transcranial Doppler[3,28], rotational angiography[29,30] and MRA[4,5,31,32]. As demonstrated in this study, more than half of the intracranial plaques that showed no appreciable stenosis would have been neglected on luminal imaging. With the advantages of MOCHA in both identifying and quantifying vessel wall abnormalities, through implementation into clinical workflows, we would expect increased IVW usage both in research and clinical settings to facilitate comprehensive evaluation of the intracranial vasculature. A recent survey of the ASNR membership indicated that more than 50% of institutions surveyed were performing IVW. Amongst those not using IVW, more than 50% indicated challenges of interpretation as an obstacle, and if these challenges were overcome, 55% indicated their institution would perform IVW[33]. MOCHA can help facilitate more efficient and automated imaging review with software-enabled lesion detection and characterization.

Vascular risk factors for ICAD traditionally include older age, male sex, race, smoking,

hypertension, diabetes, and hyperlipidemia. None of our 37 subjects were current smokers, so the effect of smoking on ICAD evolution could not be tested. Consistent with prior research, our study showed that non-white race was associated with smaller lumen area at imaging baseline, and the presence of hypertension, hyperlipidemia and diabetes were all significantly associated with thicker plaques. Diabetes mellitus was significantly associated with plaque progression, with an annualized 6.7% increase in wall thickness. However, we were not sufficiently powered to discriminate the effects of diabetes control on ICAD.

There are a few limitations in this study. First, the study sample size was limited. Although the number of identified lesions was adequate for plaque-level analysis, detailed segment-level analysis was precluded by the uneven distribution of lesions between artery segments. Larger studies are needed to determine if plaques involving the various intracranial arterial segments evolve differently. Moreover, due to sample size limitations we could not perform analysis on the impact of medications or vascular risk factor control. Second, most plaques in our cohort remained stable after one year of follow-up. Longer follow-up may provide further information on ICAD evolution patterns as plaques may take longer to change. Third, two subjects dropping out of the study due to death before follow-up imaging could bias the results. However, the subject number was small (2) compared to those whose follow-up imaging was completed (37), and therefore likely would not have a major impact on the study findings. Fourth, we did not investigate plaque composition and its contribution to evolution. As lipid core and intraplaque hemorrhage have been reported to be strongly associated with extracranial carotid artery plaque progression[34,35], investigation of these features with improved IVW techniques may provide additional information on ICAD evolution.

4.5 Conclusion

ICAD plaque evolution might be quantitatively assessed on longitudinal IVW and showed remodeling on the lumen side. Culprit plaques demonstrated longitudinal luminal expansion compared to their non-culprit counterparts. Baseline stenosis did not predict lesion changes, but baseline plaque contrast enhancement and diabetes mellitus were found to be significantly associated with ICAD changes.

Bibliography

1. Yaghi, S., Prabhakaran, S., Khatri, P. & Liebeskind, D. S. Intracranial Atherosclerotic Disease. *Stroke* **50**, 1286–1293 (2019).
2. Liu, L. *et al.* Dual antiplatelet therapy in stroke and ICAS: Subgroup analysis of CHANCE. *Neurology* **85**, 1154–1162 (2015).
3. Wong, K. S., Li, H., Lam, W. W. M., Chan, Y. L. & Kay, R. Progression of Middle Cerebral Artery Occlusive Disease and Its Relationship With Further Vascular Events After Stroke. *Stroke* **33**, 532–536 (2002).
4. Kwon, S. U. *et al.* Cilostazol Prevents the Progression of the Symptomatic Intracranial Arterial Stenosis. *Stroke* **36**, 782–786 (2005).
5. Kwon, S. U. *et al.* Efficacy and Safety of Combination Antiplatelet Therapies in Patients With Symptomatic Intracranial Atherosclerotic Stenosis. *Stroke* **42**, 2883–2890 (2011).
6. Zhu, J., Wang, Y., Li, J., Deng, J. & Zhou, H. Intracranial artery stenosis and progression from mild cognitive impairment to Alzheimer disease. *Neurology* **82**, 842–849 (2014).
7. Suri, M. F. K. *et al.* Prevalence of Intracranial Atherosclerotic Stenosis Using High-Resolution Magnetic Resonance Angiography in the General Population. *Stroke* **47**, 1187–1193 (2016).
8. Sun, J. *et al.* Characterization of non-stenotic plaques in intracranial arteries with multi-contrast, multi-planar vessel wall image analysis. *Journal of Stroke and Cerebrovascular Diseases* **31**, 106719 (2022).
9. Xiao, J. *et al.* Disparate trends of atherosclerotic plaque evolution in stroke patients under 18-month follow-up: a 3D whole-brain magnetic resonance vessel wall imaging study. *Neuroradiol J* **35**, 42–52 (2022).

10. Shen, Z.-Z. *et al.* Temporal changes in plaque characteristics after treatment and their relationship with stroke recurrence: a quantitative study using magnetic resonance imaging. *Quantitative Imaging in Medicine and Surgery* **12**, 4559569–4554569 (2022).
11. Zhang, N. *et al.* 3D whole-brain vessel wall cardiovascular magnetic resonance imaging: a study on the reliability in the quantification of intracranial vessel dimensions. *Journal of Cardiovascular Magnetic Resonance* **20**, 39 (2018).
12. Zhang, N., Liu, X., Xiao, J., Song, S. S. & Fan, Z. Plaque Morphologic Quantification Reliability of 3D Whole-Brain Vessel Wall Imaging in Patients With Intracranial Atherosclerotic Disease: A Comparison With Conventional 3D Targeted Vessel Wall Imaging. *Journal of Magnetic Resonance Imaging* **54**, 166–174 (2021).
13. Guo, Y. *et al.* Multi-Planar, Multi-Contrast and Multi-Time Point Analysis Tool (MOCHA) for Intracranial Vessel Wall Characterization. *Journal of Magnetic Resonance Imaging* **56**, 944–955 (2022).
14. Mossa-Basha, M. *et al.* Inter-rater and scan–rescan reproducibility of the detection of intracranial atherosclerosis on contrast-enhanced 3D vessel wall MRI. *Brit. J. Radiol.* **92**, 20180973 (2019).
15. Balu, N. *et al.* Accelerated multi-contrast high isotropic resolution 3D intracranial vessel wall MRI using a tailored k-space undersampling and partially parallel reconstruction strategy. *Magn Reson Mater Phy* **32**, 343–357 (2019).
16. Chen, L. *et al.* Development of a quantitative intracranial vascular features extraction tool on 3D MRA using semiautomated open-curve active contour vessel tracing. *Magnetic Resonance in Medicine* **79**, 3229–3238 (2018).

17. Samuels, O. B., Joseph, G. J., Lynn, M. J., Smith, H. A. & Chimowitz, M. I. A Standardized Method for Measuring Intracranial Arterial Stenosis. *American Journal of Neuroradiology* **21**, 643–646 (2000).
18. Kwee, R. M., Qiao, Y., Liu, L., Zeiler, S. R. & Wasserman, B. A. Temporal course and implications of intracranial atherosclerotic plaque enhancement on high-resolution vessel wall MRI. *Neuroradiology* **61**, 651–657 (2019).
19. Qiao, Y. *et al.* Intracranial Plaque Enhancement in Patients with Cerebrovascular Events on High-Spatial-Resolution MR Images. *Radiology* **271**, 534–542 (2014).
20. Wu, F. *et al.* Differential Features of Culprit Intracranial Atherosclerotic Lesions: A Whole-Brain Vessel Wall Imaging Study in Patients With Acute Ischemic Stroke. *Journal of the American Heart Association* **7**, e009705 (2018).
21. Wang, Y. *et al.* Culprit intracranial plaque without substantial stenosis in acute ischemic stroke on vessel wall MRI: A systematic review. *Atherosclerosis* **287**, 112–121 (2019).
22. Seabold, S. & Perktold, J. Statsmodels: Econometric and Statistical Modeling with Python. *Proceedings of the 9th Python in Science Conference* 92–96 (2010) doi:10.25080/Majora-92bf1922-011.
23. Underhill, H. R. *et al.* Arterial Remodeling in the Subclinical Carotid Artery Disease. *JACC: Cardiovascular Imaging* **2**, 1381–1389 (2009).
24. Saam, T. *et al.* Expansive arterial remodeling of the carotid arteries and its effect on atherosclerotic plaque composition and vulnerability: an in-vivo black-blood 3T CMR study in symptomatic stroke patients. *J Cardiovasc Magn Reson* **18**, 11 (2016).

25. Zhang, X. *et al.* Enhancement Characteristics of Middle Cerebral Arterial Atherosclerotic Plaques Over Time and Their Correlation With Stroke Recurrence. *Journal of Magnetic Resonance Imaging* **53**, 953–962 (2021).
26. Shi, Z. *et al.* Progression of Plaque Burden of Intracranial Atherosclerotic Plaque Predicts Recurrent Stroke/Transient Ischemic Attack: A Pilot Follow-Up Study Using Higher-Resolution MRI. *Journal of Magnetic Resonance Imaging* **54**, 560–570 (2021).
27. Lindenholz, A., van der Kolk, A. G., Zwanenburg, J. J. M. & Hendrikse, J. The Use and Pitfalls of Intracranial Vessel Wall Imaging: How We Do It. *Radiology* **286**, 12–28 (2018).
28. Arenillas, J. F. *et al.* Progression and Clinical Recurrence of Symptomatic Middle Cerebral Artery Stenosis. *Stroke* **32**, 2898–2904 (2001).
29. Akins, P. T., Pilgram, T. K., Cross, D. T. & Moran, C. J. Natural History of Stenosis From Intracranial Atherosclerosis by Serial Angiography. *Stroke* **29**, 433–438 (1998).
30. Leung, T. W. *et al.* Evolution of intracranial atherosclerotic disease under modern medical therapy. *Annals of Neurology* **77**, 478–486 (2015).
31. Ryu, W.-S. *et al.* Long-Term Natural History of Intracranial Arterial Stenosis: An MRA Follow-Up Study. *CED* **38**, 290–296 (2014).
32. Zhang, K. *et al.* Alterations in cerebral distal vascular features and effect on cognition in a high cardiovascular risk population: A prospective longitudinal study. *Magnetic Resonance Imaging* (2022) doi:10.1016/j.mri.2022.12.011.
33. Mossa-Basha, M. *et al.* Survey of the American Society of Neuroradiology Membership on the Use and Value of Intracranial Vessel Wall MRI. *American Journal of Neuroradiology* **43**, 951–957 (2022).

34. Zhao, X.-Q. *et al.* MR Imaging of Carotid Plaque Composition During Lipid-Lowering Therapy: A Prospective Assessment of Effect and Time Course. *JACC: Cardiovascular Imaging* **4**, 977–986 (2011).
35. Sun, J. *et al.* Sustained Acceleration in Carotid Atherosclerotic Plaque Progression With Intraplaque Hemorrhage: A Long-Term Time Course Study. *JACC: Cardiovascular Imaging* **5**, 798–804 (2012).

Chapter 5 Long-Term Carotid Plaque Progression and the Role of Intraplaque Hemorrhage: A Deep Learning-Based Analysis of Longitudinal Vessel Wall Imaging

This chapter investigates the long-term impact of intraplaque hemorrhage (IPH) on carotid atherosclerosis progression through a comprehensive longitudinal study utilizing novel deep learning-based segmentation approaches. A key methodological contribution of this work is the development and validation of deep learning algorithms for automatic quantification of carotid plaque burden and intraplaque hemorrhage from multi-contrast vessel wall imaging. These automated segmentation pipelines demonstrate excellent reproducibility, and therefore facilitate efficient, consistent measurements that are particularly valuable for longitudinal studies where manual analysis would be prohibitively time-intensive and subject to inter-observer variability.

The unprecedented scope of our longitudinal investigation—following 28 asymptomatic subjects over nearly six years with up to five imaging timepoints per patient—vastly exceeds the duration and frequency of follow-up reported in most studies in the current literature, thereby providing novel insights into the long-term natural history of atherosclerosis that were previously unattainable. Through this extensive follow-up, we demonstrate that carotid plaque progression exhibits bilateral correlation under normal circumstances, but this symmetry is disrupted in the presence of IPH. Our analysis reveals that while arteries without IPH showed minimal progression (-0.001%/year) under contemporary medical therapy, the presence of IPH was associated with significant plaque burden increase (2.3% absolute increase in wall volume percentage). Furthermore, we observed that IPH can persist for extended periods, with greater IPH volume directly correlating with accelerated plaque growth. These findings, enabled by our

validated deep learning segmentation pipelines and unprecedented longitudinal data collection, highlight IPH as a critical biomarker for identifying high-risk atherosclerotic lesions that warrant more aggressive monitoring and intervention despite being asymptomatic.

This work presented here is being prepared for publication: Yin Guo, et al. "Long-Term Carotid Plaque Progression and the Role of Intraplaque Hemorrhage: A Deep Learning-Based Analysis of Longitudinal Vessel Wall Imaging."

5.1 Introduction

Stroke remains the fifth leading cause of mortality in the United States, with an 8.4% increase in the age-adjusted death rate from 2011 to 2021[1]. Carotid atherosclerosis is a leading etiology in stroke[2]. The progression of carotid atheroma, which leads to a reduction in vessel lumen and eventual plaque rupture, is closely related to the risk of cerebrovascular ischemic events[3,4]. Understanding the mechanisms driving plaque evolution is essential for improving stroke prevention strategies.

A recent meta-analysis demonstrated the prevalence of intraplaque hemorrhage (IPH) in patients with both symptomatic and asymptomatic carotid stenosis and identified IPH as a stronger predictor of stroke than any known clinical risk factors[5]. Moreover, IPH is associated with increasing lumen stenosis and rapid vessel wall growth[6–9]. Despite this, little is known about the long-term behavior of IPH, including its occurrence, resolution, and distribution over extended periods, as most studies have been limited to follow-ups of one to two years[7–9]. Its long-term impact on plaque progression also remains inadequately explored.

Carotid magnetic resonance (MR) vessel wall imaging (VWI) is a noninvasive imaging technique validated with histology for the accurate in vivo detection of IPH and has become an established approach for measuring IPH and plaque growth in longitudinal studies[10–12]. Traditionally, manual analysis of longitudinal VWI has limited the ability to study carotid atherosclerosis due to its labor-intensive and expertise-dependent nature. Advances in deep learning-based segmentation have now enabled automated, reproducible measurements of the carotid vessel wall[13–15] and IPH, facilitating comprehensive studies of plaque dynamics over longer follow-up periods.

This study leverages these tools to analyze carotid atherosclerosis in an initially asymptomatic cohort over approximately six years. By investigating both systemic and localized trends in plaque evolution, this work provides novel insights into the natural history of carotid atherosclerosis, emphasizing the critical role of IPH in driving plaque burden progression and its implications for stroke prevention.

5.2 Methods

5.2.1 Study Population

Participants for this study were recruited as part of a prospective cohort study over a ten-year period (2012-2022), aimed at examining the natural history of carotid atherosclerosis through serial VWI. Eligible participants included patients aged 35 years and older with clinically identified atherosclerosis in at least one carotid artery and without cerebrovascular events in the six months prior to enrollment. Study procedures and consent forms were reviewed and approved by the institutional review board, and all participants provided written informed consent prior to enrollment. Detailed information on cohort recruitment has previously been published[16].

To monitor the evolution of atherosclerotic plaque, serial VWI scans with consistent parameters (detailed below) were conducted up to five times during the study period. For the analysis of long-term plaque burden progression and the effects of IPH, we conducted a retrospective analysis of a subset of participants. Inclusion criteria for this retrospective analysis required subjects who had undergone at least three VWIs over a minimum span of five years. Arteries with a history of carotid endarterectomy (CEA) or stenting at study entry were excluded. Scans of arteries performed after CEA or stenting were also excluded.

5.2.2 MR Imaging Protocol

Two large-coverage three-dimensional isotropic VWI sequences were performed using a 3.0T Philips Ingenia CX scanner (Philips Healthcare, Best, The Netherlands): 1) Motion-sensitized driven equilibrium prepared rapid gradient echo sequence (MERGE[17]) was used to delineate vessel wall morphology; 2) an inversion-recovery gradient echo sequence with phase-sensitive reconstruction (simultaneous non-contrast angiography and intraplaque hemorrhage imaging, SNAP[18]) was used to detect and measure IPH. Detailed description of both sequences and imaging parameters can be found elsewhere[9,16].

5.2.3 *Ischemic Infarct Assessment*

Conventional brain MRI examinations, including diffusion weighted imaging (DWI), susceptibility weighted imaging (SWI), and T2-fluid attenuated inversion recovery (FLAIR), were performed at all VWI time points. A board-certified neuroradiologist directly compared the baseline and follow-up brain MRI images and scored for any incident infarcts (FLAIR and DWI images) or hemorrhages (SWI images). Vascular territory and signs of acuity or associated hemorrhage were noted for the infarcts.

5.2.4 *Deep Learning-based Vessel Wall and IPH segmentation*

5.2.4.1 Model Design

Two deep learning-based imaging analysis pipelines were developed to bilaterally segment the carotid vessel wall and IPH on MERGE and SNAP sequences, respectively. Each scan was segmented independently.

For the segmentation of carotid lumen and outer wall boundary using MERGE[19], the location of the left and right common carotid bifurcations was identified automatically. On each side, a 3D bounding box encompassing the bifurcation area as well as the distal and proximal segments of the bifurcation was extracted and then used for a preliminary 3D lumen segmentation. A trained radiologist reviewed the preliminary segmentation to assess image quality and ensure that the lumen from all slices encompassing the bifurcation region were correctly localized. Finally, 2D patches along both carotids were segmented slice-by-slice using a 2.5D convolutional neural network.

To segment IPH from SNAP, a similar bifurcation detection module was first applied to locate the left and right carotid bifurcations. A 3D bounding box was then generated on each side to focus on the bifurcation area, ensuring that IPH detection was performed within the anatomically relevant region. A 2D nnUNet[20]-based algorithm was trained to segment IPH slice-by-slice by identifying hyperintense signals on axial reformatted images with 2mm spacing.

For each MERGE image, after obtaining lumen and outer wall segmentations of the same artery, the range of slices with wall thickness greater than 2mm in any scan was included as atherosclerotic plaque. This threshold aligns with the criteria used in the Rotterdam[21], PARISK[22]

and other established researches. Plaque burden was defined as the percent wall volume (%WV), calculated as wall volume divided by total vessel volume, multiplied by 100.

For each SNAP image per artery per time point, IPH was categorized as present (IPH+) or absent (IPH-). IPH volume was aggregated as the sum of IPH areas per slice multiplied by 2mm, and percent hemorrhage volume (%HV) was defined as IPH volume divided by wall volume, multiplied by 100.

5.2.4.2 Training Datasets

For the segmentation of carotid lumen and outer wall boundary using MERGE, the training data was provided by the 2020 and 2021 Grand Challenge hosted by the Society of Magnetic Resonance Angiography: the CARE-II dataset and the COSMOS dataset. The CARE-II dataset includes VWI data from 50 participants with expert annotations. The imaging was conducted on a 3T Philips MRI scanner using the MERGE sequence, producing isotropic voxels with a 0.35 mm resolution. Similarly, the COSMOS dataset offers VWI data from 50 participants with annotations. This data was collected using a 3T Philips MRI scanner with a 3D VISTA sequence, achieving isotropic voxels with a 0.35 mm resolution.

To segment IPH on SNAP, the training data were derived from the full study cohort of 98 subjects, using manually annotated IPH contours on baseline SNAP images[9]. These images were axially reformatted into 2mm spacing. IPH was identified based on visual inspection, defined as hyperintense areas on SNAP in comparison to the sternocleidomastoid muscle.

5.2.4.3 Validation Datasets

In a separate validation cohort, group A consisted of 14 subjects who were scheduled for carotid endarterectomy (CEA). Histological specimens were available and were matched with axially reformatted SNAP images, for assessment of IPH detection and segmentation[23]. Group B consisted of 33 patients who underwent baseline MRI (MERGE and SNAP) twice within one month. For each scan, the vessel wall and IPH were segmented from the MERGE and SNAP images, using the two abovementioned deep learning-based pipelines, for analysis of scan-rescan reproducibility. Detailed information on this validation cohort can be found in Figure 5.1 and the referenced publication[23].

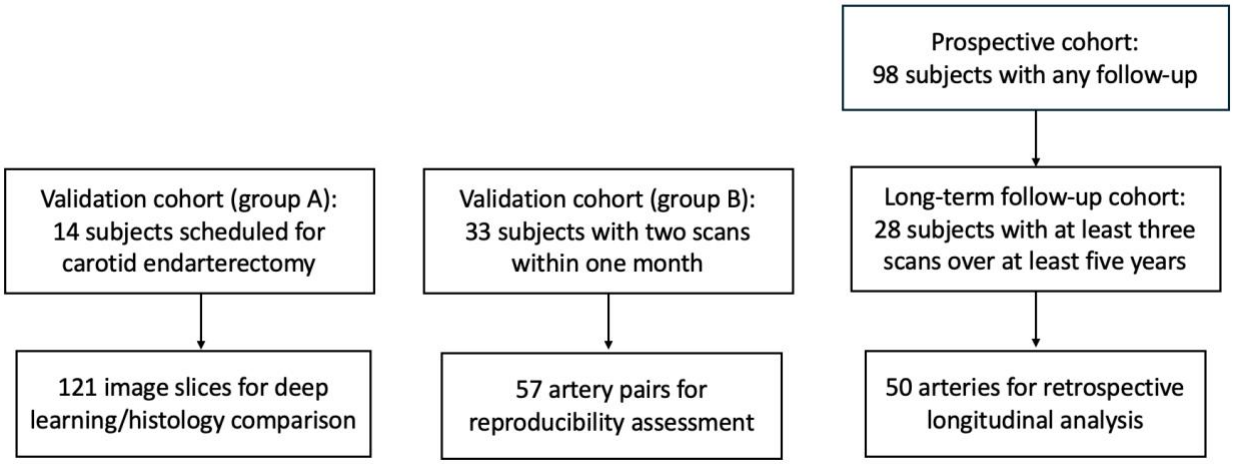

Figure 5.1 Flow chart of the study cohort.

5.2.4.4 Statistical Analysis

In group A, sensitivity and specificity for IPH detection were estimated at the slice level, and agreement in IPH detection between deep learning and histological analysis was evaluated using

Cohen's kappa. Agreement in IPH area quantification between SNAP and histology was assessed using Spearman's correlation coefficient, as it is less affected by shrinkage of histological specimen during processing compared to absolute agreement measures like the intraclass correlation coefficient (ICC) and the Bland-Altman plot.

In group B, Cohen's kappa was used for evaluating the scan-rescan reproducibility of IPH detection of the deep learning-based image segmentation pipeline, and the ICC was used for evaluating the reproducibility of plaque burden and IPH volume (within arteries identified as IPH+ in either scan). The nonparametric bootstrap and percentile method was used to calculate 95% confidence intervals (CI).

5.2.4.5 Assessment Results of Deep Learning-based Plaque Segmentation

In the 14 arteries in group A, a total of 121 SNAP slices were matched with histological specimens, of which 49 (40%) slices from 13 (93%) plaques had histology-detected IPH. Deep learning-based analysis had moderate overall agreement with histology in detecting IPH (kappa: 0.62, 95% CI: 0.48 - 0.76). The sensitivity and specificity for IPH detection at the slice level were 61% and 97%, respectively. In these 30 slices where both methods agreed on IPH presence, IPH area measured using deep learning (mean ± SD: 16.4 ± 12.6 mm^2) and histology (mean ± SD: 12.0 ± 7.3 mm^2) were strongly correlated (Spearman's rho = 0.63, $p < 0.001$).

In the 33 subjects with 66 arteries in validation group B, eight pairs of MERGE images were excluded due to low image quality on either scan, and one artery was lesion-free. In the remaining 57 pairs of arteries, %WV characterized by MERGE showed high scan-rescan reproducibility, with an ICC of 0.88 (95% CI: 0.80 - 0.93).

In SNAP from group B, 15 (26.3%) arteries were categorized as IPH+ in both scans, 3 (5.3%) were categorized as IPH+ either scan, and 39 (68.4%) were categorized as IPH- in both scans, yielding a kappa of 0.87 (95% CI: 0.71 - 0.99). Of the 18 arteries categorized as IPH+ in at least one scan, IPH volume showed high reproducibility, demonstrated by an ICC of 0.93 (95% CI: 0.82 - 0.97).

Bland-Altman plots indicated no apparent relationship between variance and mean for measurements of both %WV and IPH volume (Figure 5.2).

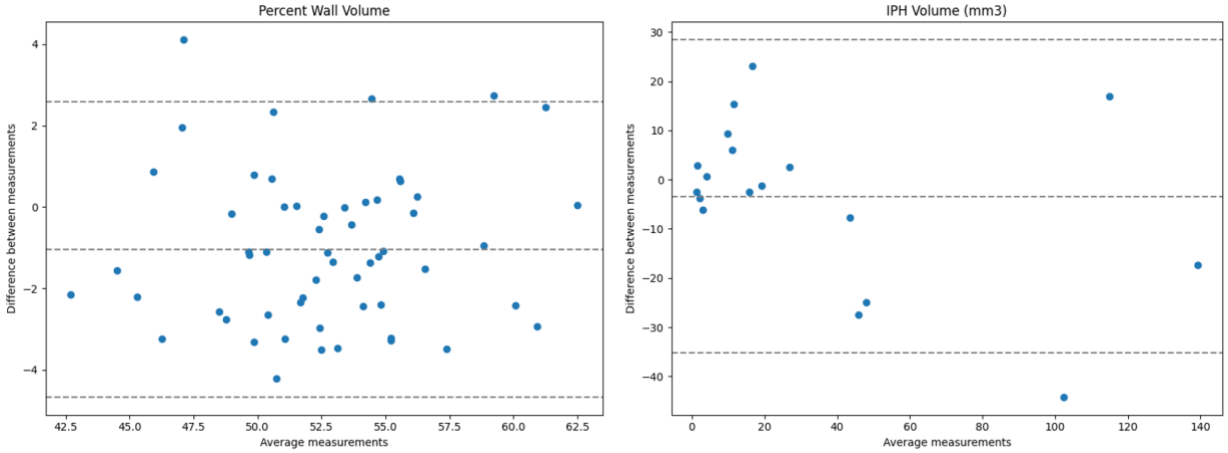

Figure 5.2 Bland-Altman plots demonstrate scan-rescan reproducibility for deep learning-based measurements of percent wall volume and IPH volume.

5.2.5 Statistical Analysis

Summary statistics of baseline demographics are presented as mean ± standard deviations (SDs) for continuous variables and counts with percentage for categorical variables.

For each analyzable plaque, a linear model was fitted across all available time points to determine the long-term growth rate of plaque burden[24], defined as annualized absolute change in %WV, expressed in units of percent per year. The method for deriving the long-term plaque growth rate is illustrated in Figure 5.3. Generalized estimating equation (GEE)-based linear regression models were used to evaluate associations of the long-term growth rate of each side with the contralateral side, adjusted for potential confounding factors of age, sex, history of hypertension and statin use. The number of risk factors considered in the models was limited by the available sample size. Effect sizes were summarized using the partial correlation coefficient.

In all arteries, to investigate whether long-term progression rate in plaque burden depends on presence and volume of IPH, we employed a linear mixed-effects model. This model used %WV as the primary outcome variable and included random intercepts to account for within-subject and within-artery correlation. As fixed effects, the model included time as a continuous variable to estimate the growth rate of %WV and account for variation in scan intervals, a binary predictor indicating IPH presence, and %HV to assess the effect of IPH volume. %HV was log2-transformed to reduce right skewness, and further transformed such that it equals zero when IPH is absent, and equals the deviation from the population mean when IPH is present. The model setup was designed to disentangle the effects of the presence and volume of IPH on plaque burden progression. This model was further adjusted for age, sex, history of hypertension and statin use. The Wald method was used to compute 95% confidence intervals (CI) for the fixed-effect coefficients.

All statistical analyses were performed using R 4.4.0. A two-sided p-value < 0.05 was considered statistically significant.

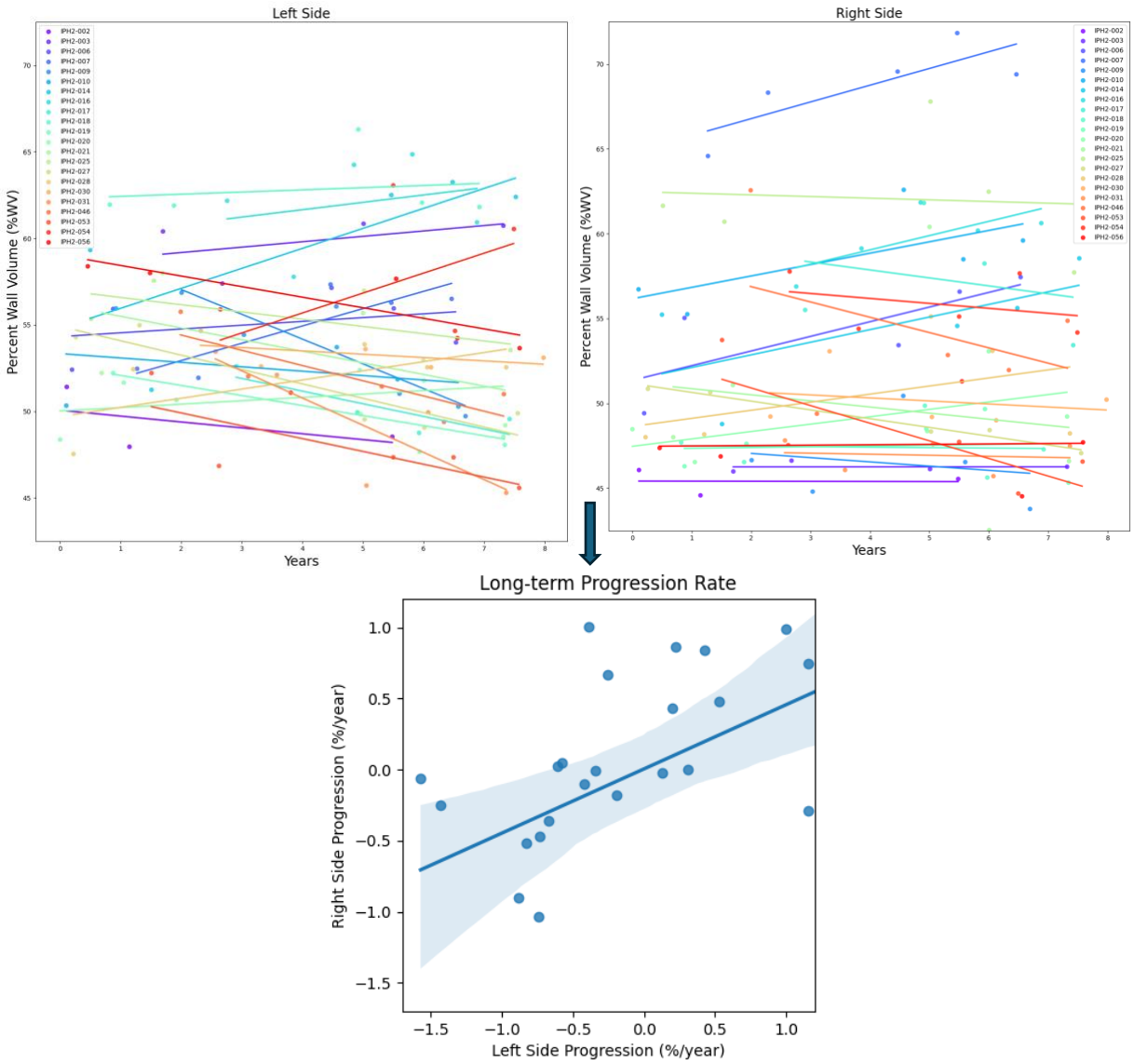

Figure 5.3 Assessing the symmetric evolution of carotid atherosclerosis.

Upper panel: for each plaque, a linear model was fitted across all available time points to determine the long-term growth rate of plaque burden (%/year). Lower panel: associations of long-term growth rate of plaque burden between bilateral carotid arteries.

5.3 Results

5.3.1 Patient Characteristics

A total of 98 subjects were recruited prospectively, and population demographics can be found in the referenced publication[9]. Among these, 28 subjects underwent at least three VWIs over a span of at least five years and were therefore included in this retrospective analysis. All subjects were under contemporary medical management, and the baseline clinical information of these 28 subjects is presented in Table 5.1. After three scans were excluded due to poor image quality, each subject had an average of 4.7 ± 0.6 scans within 5.8 ± 1.1 years, indicating a relatively uniform distribution of imaging time points and follow-up duration across the cohort. Figure 5.1 shows the study flow chart.

Among the 56 carotid arteries within the 28 subjects, six were excluded due to prior history of CEA or having fewer than three available scans due to CEA during the study period. The remaining 50 arteries from 28 subjects were included in artery-level analyses. Of these subjects, there were 22 with bilateral arteries available (44 arteries) for the subject-level analysis where plaque growth on each side was compared.

Table 5.1 Population demographics at baseline

Variable	Value
Age	71.3 ± 9.7
Male sex	20 (71%)
Current smoker	3 (10%)
History of hypertension	17 (60%)
History of hyperlipidemia	25 (89%)
History of diabetes	3 (10%)
Statins	21 (75%)
Antihypertensives	16 (57%)
Antiplatelets	21 (75%)

Values are no. (%) or mean ± standard deviation

5.3.2 IPH Presence, Occurrences, and Relation to New Infarcts

Among the 50 carotid arteries from 28 subjects, 23 arteries (46%) from 17 subjects (60.7%) showed presence of IPH on VWI at any time point during the study period. Of the 39 IPH- arteries at the baseline scan, eleven (28.2%) became IPH+ on all subsequent scans after the initial occurrence of IPH, and one artery (2.56%) developed new IPH on the second scan but reverted to IPH- on scans 3 to 5. Of the 11 arteries that were IPH+ at baseline, IPH persisted in five (45.5%) throughout the study, whereas six (54.5%) demonstrated resolution of IPH before the final scan.

During the follow-up, only three subjects (10.7%) developed new ischemic infarcts, with two (66.7%) occurring among the 17 subjects (60.7%) with either unilateral or bilateral IPH. One of these subjects consistently exhibited ipsilateral IPH and was IPH- on the contralateral side across all scans. In the other subject, a new infarct was detected at the third scan, coinciding with the appearance of new ipsilateral IPH. The third subject who developed an infarct had no detectable IPH in either carotid artery at any time point. Given the limited number of ischemic events, the association between IPH and ischemic stroke in this study remains exploratory in nature.

5.3.3 Bilateral Symmetry in Plaque Evolution and the Disruptive Role of IPH

In the 22 subjects with bilateral analyzable arteries, the baseline %WV was 54.4 ± 3.8% for the left carotid artery and 53.2 ± 6.2% for the right. The average %WV absolute growth rate was -0.19 ± 0.74 %/year on the left side and 0.04 ± 0.54 %/year on the right. The long-term plaque growth rate of one side was moderately correlated ($r = 0.54$, $p < 0.001$) with the contralateral side, suggesting that plaque progression may be influenced by systemic factors. The significant correlation remained after adjusting for age, sex, history of hypertension and statin use ($r = 0.38$, $p = 0.016$). Figure 5.4 provides an example of bilateral plaque burden increases over five scans. The association between plaque progression on the left and right sides is visualized in Figure 5.5.

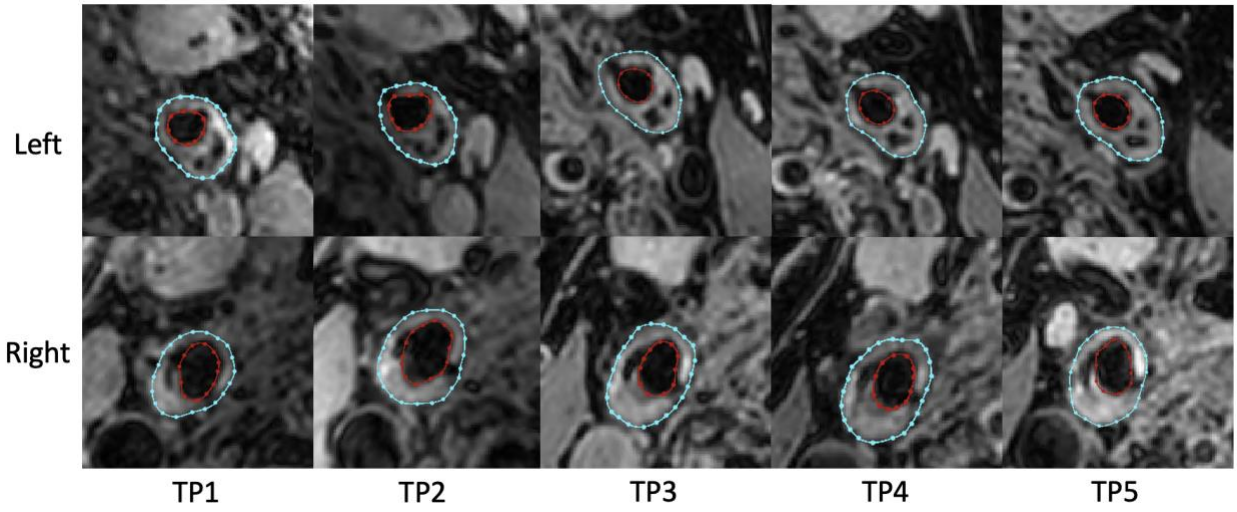

Figure 5.4 Example of bilateral plaque burden increases over five vessel wall imaging sessions spanning five years, demonstrating symmetrical plaque progression on both the left and right sides.

The vessel wall contours were generated using deep learning-based segmentation, with red contours delineating the vessel lumen and blue contours delineating the vessel outer wall boundary. 'TP' denotes 'time point'.

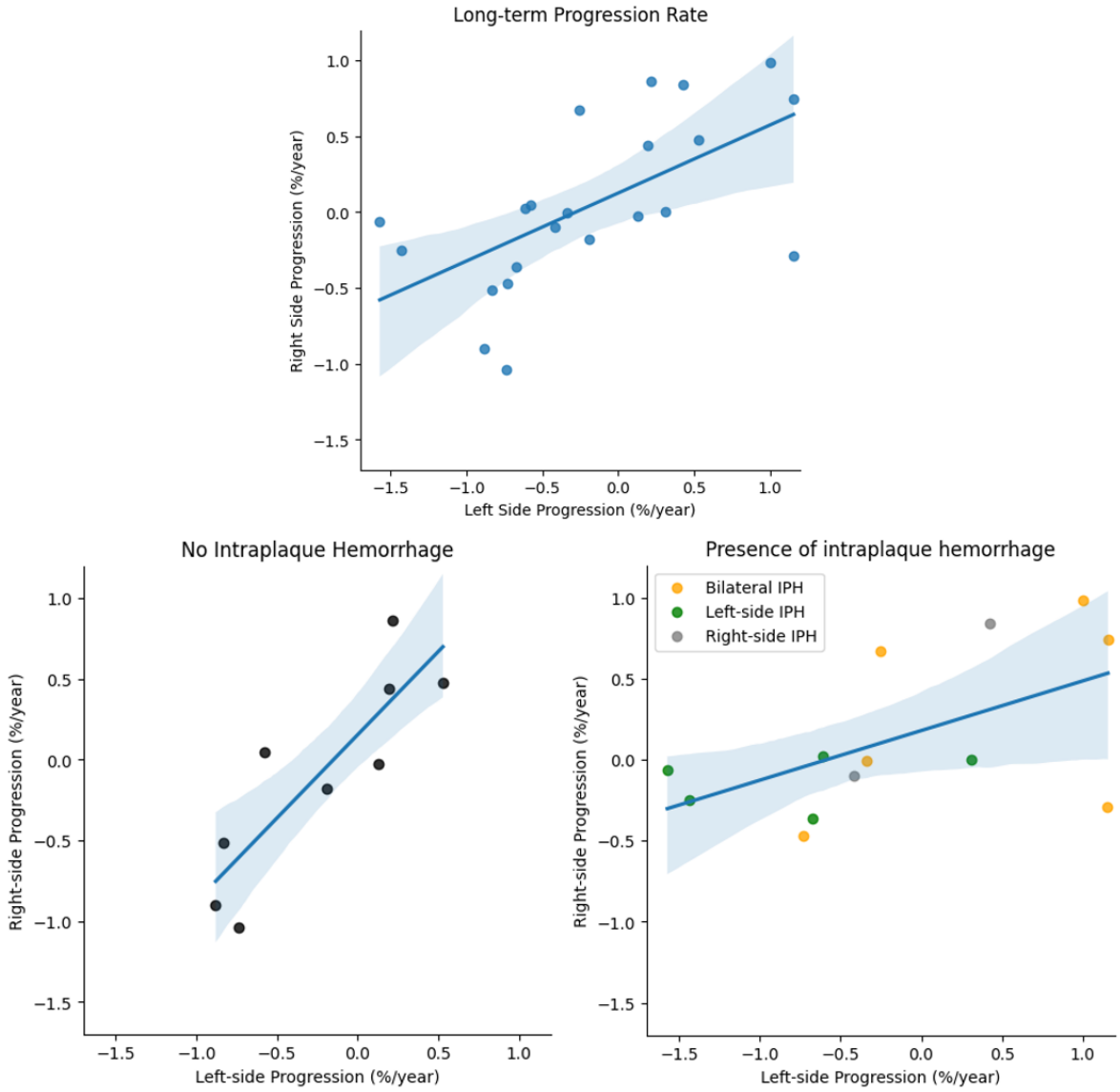

Figure 5.5 Correlation of long-term growth rate of plaque burden between bilateral carotid arteries in groups.

Upper panel: Correlation of long-term growth rate of plaque burden between bilateral carotid arteries, demonstrating systemic influences on bilateral plaque progression. Lower panel: Correlation of bilateral long-term progression in the two subgroups of carotid arteries with (right) and without IPH (left). Due to the limited number of subjects with bilateral IPH, a separate subgroup analysis for this cohort is not shown.

To further explore the potential effects of IPH, the 22 subjects were further divided into two sub-groups based on its presence. In nine subjects, IPH was not detected at any time point, and in this IPH- subgroup, significant associations of plaque progression between one side and its contralateral part were found ($r = 0.57$, $p < 0.001$). However, among the 13 subjects with either unilateral or bilateral IPH during the study period, the correlation coefficient decreased, and the association no longer remained significant ($r = 0.28$, $p = 0.19$). These findings suggest that the presence of IPH may be associated with a disruption of the systemic symmetry in bilateral plaque evolution. The correlation of bilateral long-term plaque progression in the two subgroups is visualized in Figure 5.5.

5.3.4 IPH's Long-term Impact on Plaque Progression

Building on these findings, we further evaluated both the presence and the volume of IPH on %WV progression using a linear mixed-effects model. In the unadjusted model, the random effects for patients and arteries accounted for individual variability, with SDs of 4.3% and 1.9%, respectively. The SD of the residual term is 3.1%. This suggests considerable variability in %WV progression among patients and between bilateral arteries within the same patient.

The progression of %WV over time in arteries without IPH was minimal, with an average absolute growth rate of -0.001 %/year (95% CI: -0.18 - 0.16, $p = 0.90$). However, the presence and occurrence of IPH at any point was a significant predictor, associated with a 2.34% absolute increase in %WV on average (95% CI: 1.02 - 3.67, $p < 0.001$). This indicates that patients with IPH had higher %WV compared to those without IPH and that the development of new IPH was significantly associated with an increase in plaque burden.

Furthermore, within the IPH+ arteries, %HV was further associated with %WV ($p = 0.005$). Each doubling of the %HV – reflected by a 1-unit increase in the log2-transformed %HV – was associated with an additional 0.73% absolute increase in %WV (95% CI: 0.23 - 1.23), corresponding to a 31% increase relative to the average IPH effect ([2.34% + 0.73%] / 2.34% = 1.31). This underscored the significant impact of both the presence and volume of IPH on the progression of carotid plaque burden over time, as illustrated in Figure 5.6. Figure 5.7 provides an example of plaque progression over four scans, highlighting the increasing plaque burden alongside the occurrence (scan 3) and subsequent volume expansion (scan 4) of IPH.

When adjusted for age, sex, history of hypertension and statin use, the linear mixed-effects model continued to show strong associations between IPH and %WV progression. The presence of IPH was associated with an adjusted 2.29% absolute increase in %WV (95% CI: 0.95 - 3.64, $p < 0.001$), and the %HV association persisted, with a coefficient of 0.74% (95% CI: 0.24 - 1.24, $p = 0.004$), similar to the unadjusted model. Age, sex, history of hypertension and statin use did not have statistically significant associations with %WV progression ($p > 0.33$ for each).

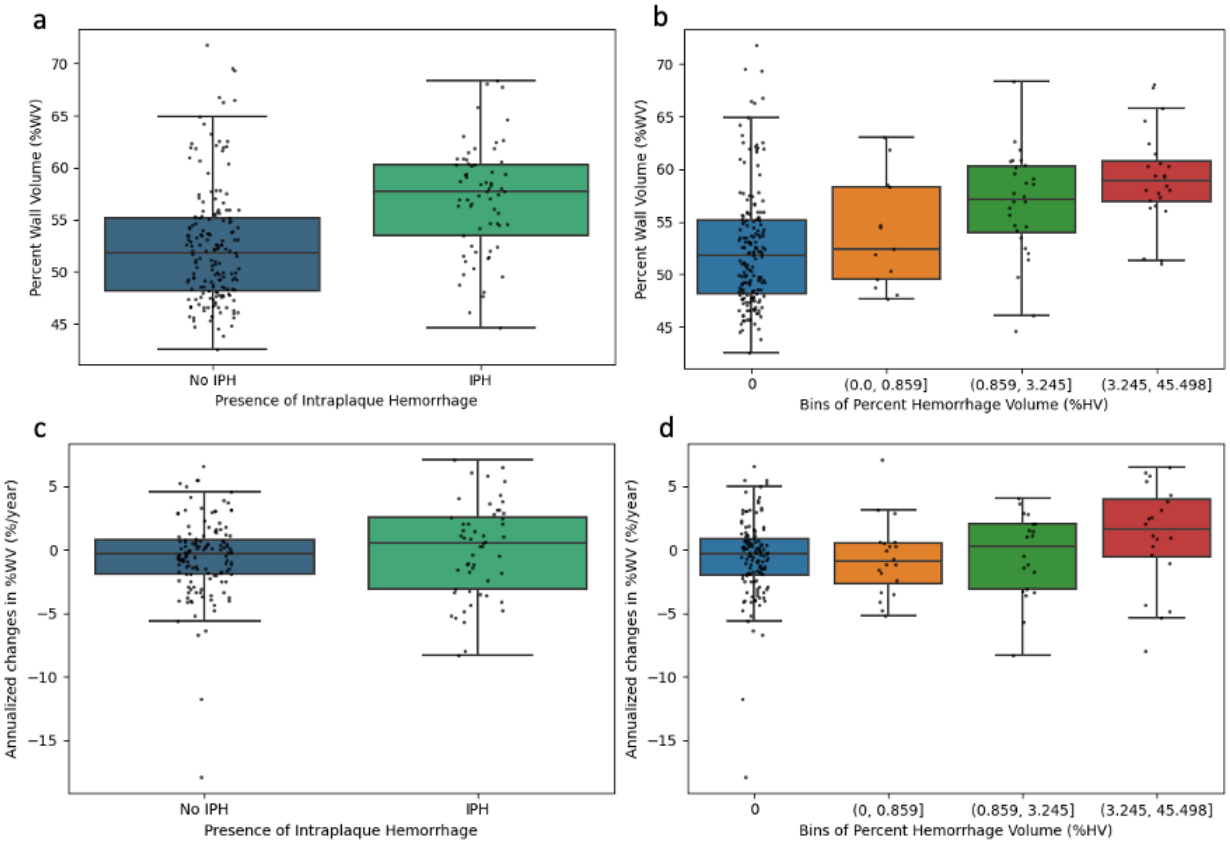

Figure 5.6 Box plots demonstrating the effects of presence and volume of IPH on plaque burden.

In (a) and (c), %WV and annualized changes in %WV were compared based on presence or not of IPH. In (b) and (d), %HV was divided into three equal-sized bins, comparing %WV and annualized changes in %WV across different degrees of IPH volume.

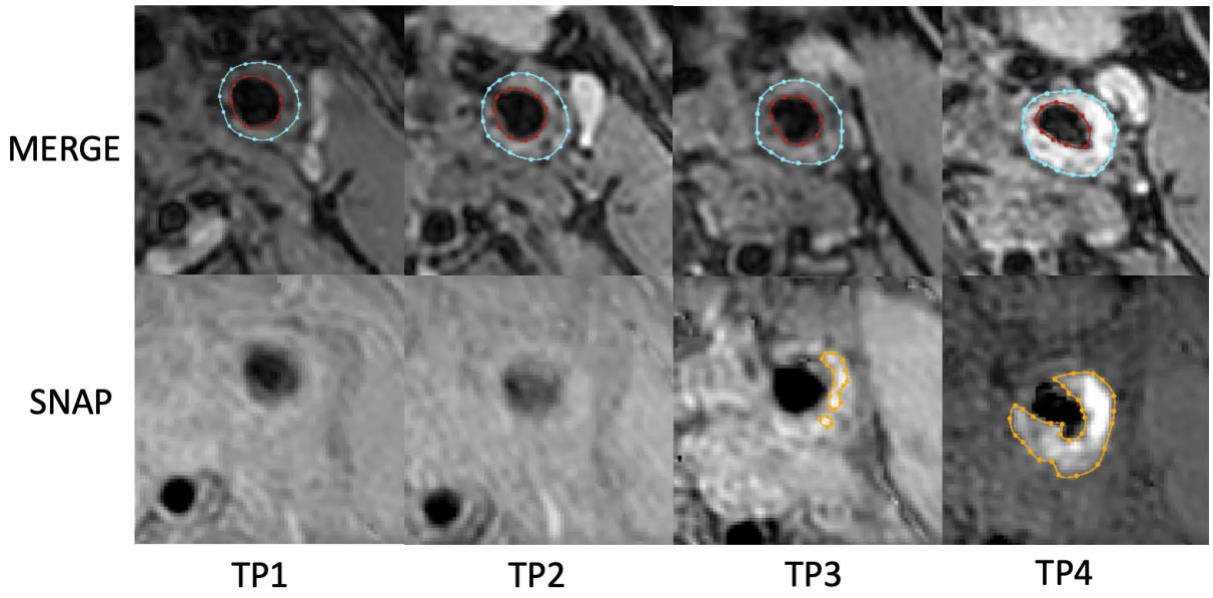

Figure 5.7 Example of plaque progression over four vessel wall imaging sessions spanning five years.

This figure demonstrated an increase in plaque burden, marked by the occurrence of intraplaque hemorrhage (IPH) at TP3 and subsequent volume expansion at TP4. The vessel wall and IPH contours were generated using deep learning-based segmentation, with red and blue contours delineating the vessel lumen and vessel outer wall boundary on MERGE, and orange contours delineating IPH boundary on SNAP. 'TP' denotes 'time point'.

5.4 Discussion

By leveraging two deep learning-based segmentation pipelines on two large-coverage 3D MR vessel wall imaging (VWI) sequences, we comprehensively evaluated carotid plaque features across an average of five scans over six years in an asymptomatic patient cohort. The role of intraplaque hemorrhage (IPH) in long-term plaque progression can be characterized in two

critical ways. First, while plaque progression on one side was significantly correlated with the contralateral side, reflecting the systemic nature of atherosclerotic disease, this symmetry was notably weakened in subjects with IPH, suggesting an association between IPH and more localized effects. Second, despite contemporary medical management, the occurrence and volume of IPH were strongly associated with plaque burden increase, whereas plaques without IPH remained stable over the study period. These findings deepen our understanding of the long-term and pivotal role IPH plays in the natural history of carotid atherosclerosis and underscore the importance of early IPH detection for optimized strategies in managing atherosclerosis.

Previous studies have demonstrated carotid plaque symmetry by comparing cross-sectional measurements of plaque burden between bilateral carotid arteries, as observed in ex vivo imaging studies[25] and in vivo assessments using ultrasound[26] and VWI[27]. Our study extends this understanding with longitudinal follow-up over a six-year period, which reveals not just static morphological symmetry but also symmetrical trends in bilateral plaque progression. While our results suggest that monitoring the more advanced plaque could provide prognostic insights into the less advanced contralateral plaque, the clinical implications of bilateral plaque progression remain an area for further investigation. Specifically, it is unclear whether patients with plaque disruption in one carotid artery are more likely to develop similar disruptions in the contralateral artery or other vascular beds. Evidence from prior studies, such as the AIM-HIGH sub-study[28], suggests that patients with high-risk carotid plaque features may have an increased risk of systemic cardiovascular events, highlighting the need for further research into the relationship between local plaque progression and broader vascular instability.

Notably, as demonstrated by Li et al.[27], IPH exhibits low concordance between left and right carotid plaques, with unilateral or bilateral IPH frequently reported in the current and other

studies, underscoring the role of localized factors in its pathogenesis. Studies showed that IPH development, likely driven by the rupture of neo-vessels, is shaped by conditions such as hemodynamic forces[29], calcification[9], and inflammation[30] within the plaque microenvironment. At the same time, systemic factors still significantly contribute to the development of IPH. For instance, the Rotterdam Study[31], in a cross-sectional analysis, identified pulse pressure as the most significant predictor of IPH, independent of plaque burden and other cardiovascular risk factors. Similarly, another longitudinal study associated male sex and hypertension with an increase in IPH[9]. Understanding the interplay between these localized and systemic influences is critical for advancing our understanding of pathophysiology of IPH development and its impact on plaque stability.

IPH is a dynamic process with the potential for growth or resolution over time. Longitudinal follow-up studies have shown that its hyperintense signal on VWI, likely attributable to methemoglobin from hemoglobin breakdown after erythrocyte extravasation, can persist throughout the course of atherosclerotic disease. Previous studies[7,32,33] using T1-weighted sequences reported IPH resolution rates of 0%, 0%, and 6% over 17 to 18 months of follow-up. More recently, one study[9] found that IPH resolved in only 3 out of 89 scan pairs (3.4%) over an average of 1.8 years, utilizing the SNAP sequence which combines inversion-recovery gradient echo with phase-sensitive acquisition to enhance IPH-to-wall contrast and measurement accuracy[34,35]. Similarly, our study, using SNAP to detect IPH, demonstrated that all but one newly developed IPH persisted to the study end, around half arteries with pre-existing IPH continued to exhibit it throughout the study period, and hyperintense IPH signals may be observed for as long as six years. This persistence may be explained by ongoing erythrocyte extravasation from leaky neo-vessels[36].

IPH is widely recognized as a strong indicator of carotid plaque vulnerability, with its presence linked to an increased risk of future ischemic cerebrovascular events[37], independent of symptom status[38] or degree of stenosis[5,39]. In our study, despite more than half of subjects exhibited IPH at some point during follow-up, the incidence of ischemic symptoms over at least five years was low. Histological studies[36,40] have supported this observation by identifying neovasculature, a potential source of IPH, predominantly located in the adventitia away from the plaque surface, thus preserving surface integrity. This suggests that assessing plaque surface disruption[41,42] could be an important additional metric for stratifying stroke risk, particularly in asymptomatic patients. Nonetheless, IPH has been consistently associated with a rapid increase in plaque burden[7,9], and our findings added to the body of evidence by further highlighting the sustained and long-term impact of IPH presence and volume on the progression of atherosclerotic disease.

Statin therapy improves cardiovascular outcomes and has demonstrated plaque regression[43–45] in multiple imaging studies, by the mechanism of modulating inflammation and decreasing or even depleting the lipid content within plaques[46–49]. However, the recent AIM-HIGH MRI sub-study[49] showed that, despite two years of intensive lipid-lowering therapy, carotid arteries with IPH experienced larger increases in lipid core size and greater reductions in lumen area compared to plaques without hemorrhage, which exhibited stabilized plaque burden and significant reductions in lipid content. This suggests the IPH's interplay with a potential non-lipid-driven pathway of plaque progression. One study[50] identified CD163+ macrophages, induced by IPH, as potential contributors to a positive feedback loop involving increased vascular permeability, inflammation, and further IPH increase. Our findings similarly highlighted the role of IPH in counteracting the systemic stabilizing effects of contemporary medical treatment. While non-IPH plaques remained stable, current therapies may be insufficient to prevent IPH-associated plaque burden

increase. Further investigation into the mechanisms behind this non-lipid-driven pathway is essential and could pave the way for novel therapeutic approaches specifically targeting IPH.

Overall, there remains a significant gap in longitudinal imaging studies investigating the pathophysiology of carotid atherosclerosis and IPH, as most studies are either short-term[7,9,51] or involve long-term clinical follow-up without repeated imaging[22,38]. To the best of our knowledge, the longest imaging follow-up duration reported is 54 months[6]. However, this study was limited by a very small sample size and the use of 2D VWI, which provided inadequate coverage of the carotid bifurcation. This limitation was further compounded by challenges in identifying consistent imaging coverage for bilateral arteries and comparing multiple time points. Indeed, Geleri et al. reported that, when using the large-coverage 3D VWI sequence MERGE, only 54% of lesions were fully covered and 25% partially covered by 2D VWI in their analysis of 381 advanced plaques from the CARE-II study[52]. Recognizing these limitations, our study utilized MERGE, which provided adequate imaging coverage for bilateral and longitudinal analysis.

The emergence of deep learning-based imaging analysis also offers a promising solution to the labor-intensive nature of longitudinal VWI studies, reducing the need for extensive reviewer training and minimizing bias, as well-validated deep learning tools provide consistent and reproducible analyses across time points. While significant efforts have been made in segmenting the vessel wall on VWI[13–15], robust algorithms for detailed plaque composition segmentation remain underdeveloped[53,54]. In our study, we successfully utilized deep learning to integrate multi-contrast VWI, demonstrating its potential to deliver more detailed and comprehensive assessments of plaque morphology and composition[55].

Our study has a few limitations. First, although each patient underwent an average of five scans, the requirement to analyze the long-term evolution of atherosclerosis over more than five years

restricted the number of participants in this retrospective analysis. Second, the retrospective nature of this analysis resulted in a relatively healthy and stabilized patient cohort, as individuals with severe symptoms—indicative of plaques experiencing dramatic reductions in stability—were more likely to drop out of the prospective cohort early. Third, despite extensive follow-up, the absolute number of newly detected or resolved hemorrhages remained relatively low, underscoring the need for larger studies to better understand these potentially course-altering events in the plaque natural history. Finally, future research should aim to develop more advanced deep learning algorithms capable of simultaneously segmenting additional plaque components, such as lipid contents and calcification[56], to further elucidate the complex interplay between these plaque components and the pathobiology of atherosclerosis.

5.5 Conclusion

By leveraging deep learning-based segmentation on multi-contrast VWI, we successfully monitored long-term plaque dynamics across an average of five scans over a follow-up of six years in an asymptomatic cohort. Around half of the arteries with pre-existing IPH continued to exhibit it throughout the study period, while newly developed IPH also persisted, yet caused few new ischemic symptoms. Importantly, the presence of IPH was associated with disruption of the systemic symmetry of bilateral plaque progression: arteries without IPH demonstrated minimal growth under contemporary medical treatment, whereas the occurrence and volume of IPH were strongly associated with accelerated plaque burden progression.

Bibliography

1. Martin, S. S. *et al.* 2024 Heart Disease and Stroke Statistics: A Report of US and Global Data From the American Heart Association. *Circulation* **149**, e347–e913 (2024).
2. Cheng, S. F., Brown, M. M., Simister, R. J. & Richards, T. Contemporary prevalence of carotid stenosis in patients presenting with ischaemic stroke. *British Journal of Surgery* **106**, 872–878 (2019).
3. Mortimer, R., Nachiappan, S. & Howlett, D. C. Carotid artery stenosis screening: where are we now? *British Journal of Radiology* **91**, 20170380 (2018).
4. Zhao, X. *et al.* Prevalence and Characteristics of Carotid Artery High-Risk Atherosclerotic Plaques in Chinese Patients With Cerebrovascular Symptoms: A Chinese Atherosclerosis Risk Evaluation II Study. *Journal of the American Heart Association* **6**, e005831.
5. Schindler, A. *et al.* Prediction of Stroke Risk by Detection of Hemorrhage in Carotid Plaques: Meta-Analysis of Individual Patient Data. *JACC: Cardiovascular Imaging* **13**, 395–406 (2020).
6. Sun, J. *et al.* Sustained Acceleration in Carotid Atherosclerotic Plaque Progression With Intraplaque Hemorrhage: A Long-Term Time Course Study. *JACC: Cardiovascular Imaging* **5**, 798–804 (2012).
7. Takaya, N. *et al.* Presence of Intraplaque Hemorrhage Stimulates Progression of Carotid Atherosclerotic Plaques. *Circulation* **111**, 2768–2775 (2005).
8. Simpson, R. J. *et al.* MR Imaging–Detected Carotid Plaque Hemorrhage Is Stable for 2 Years and a Marker for Stenosis Progression. *American Journal of Neuroradiology* **36**, 1171–1175 (2015).

9. Canton, G. *et al.* Pathophysiology of carotid atherosclerosis: Calcification, intraplaque haemorrhage and pulse pressure as key players. *European Journal of Radiology* **178**, 111647 (2024).
10. Yuan, C. *et al.* In Vivo Accuracy of Multispectral Magnetic Resonance Imaging for Identifying Lipid-Rich Necrotic Cores and Intraplaque Hemorrhage in Advanced Human Carotid Plaques. *Circulation* **104**, 2051–2056 (2001).
11. Moody, A. R. *et al.* Characterization of Complicated Carotid Plaque With Magnetic Resonance Direct Thrombus Imaging in Patients With Cerebral Ischemia. *Circulation* **107**, 3047–3052 (2003).
12. Cappendijk, V. C. *et al.* In vivo detection of hemorrhage in human atherosclerotic plaques with magnetic resonance imaging. *Journal of Magnetic Resonance Imaging* **20**, 105–110 (2004).
13. Chen, L. *et al.* Automated Artery Localization and Vessel Wall Segmentation Using Tracklet Refinement and Polar Conversion. *IEEE Access* **8**, 217603–217614 (2020).
14. Chen, L. *et al.* Domain adaptive and fully automated carotid artery atherosclerotic lesion detection using an artificial intelligence approach (LATTE) on 3D MRI. *Magnetic Resonance in Medicine* **86**, 1662–1673 (2021).
15. Li, X. *et al.* Carotid Vessel Wall Segmentation Through Domain Aligner, Topological Learning, and Segment Anything Model for Sparse Annotation in MR Images. *IEEE Transactions on Medical Imaging* 1–1 (2024) doi:10.1109/TMI.2024.3424884.
16. Sun, J. *et al.* Blood Pressure Is a Major Modifiable Risk Factor Implicated in Pathogenesis of Intraplaque Hemorrhage. *Arteriosclerosis, Thrombosis, and Vascular Biology* **36**, 743–749 (2016).

17. Balu, N. *et al.* Carotid plaque assessment using fast 3D isotropic resolution black-blood MRI. *Magnetic Resonance in Medicine* **65**, 627–637 (2011).
18. Wang, J. *et al.* Simultaneous noncontrast angiography and intraPlaque hemorrhage (SNAP) imaging for carotid atherosclerotic disease evaluation. *Magnetic Resonance in Medicine* **69**, 337–345 (2013).
19. HashemizadehKolowri, S. *et al.* Automated Localization of the Extracranial Carotid Artery in Black Blood Contrast MR Images Using a Deep Learning Approach. in *Proc. Intl. Soc. Mag. Reson. Med* 3068 (2023).
20. Isensee, F., Jaeger, P. F., Kohl, S. A. A., Petersen, J. & Maier-Hein, K. H. nnU-Net: a self-configuring method for deep learning-based biomedical image segmentation. *Nat Methods* **18**, 203–211 (2021).
21. van den Bouwhuijsen, Q. J. A. *et al.* Determinants of magnetic resonance imaging detected carotid plaque components: the Rotterdam Study. *European Heart Journal* **33**, 221–229 (2012).
22. Nies, K. P. H. *et al.* Signal intensity and volume of carotid intraplaque hemorrhage on magnetic resonance imaging and the risk of ipsilateral cerebrovascular events: The Plaque At RISK (PARISK) study. *Journal of Cardiovascular Magnetic Resonance* **26**, 101049 (2024).
23. Liu, J. *et al.* Semiautomatic carotid intraplaque hemorrhage volume measurement using 3D carotid MRI. *Journal of Magnetic Resonance Imaging* **50**, 1055–1062 (2019).
24. Guo, Y. *et al.* Abstract TP143: Longitudinal Evaluation of Vessel Wall MRI Demonstrates Bilaterally Symmetric Evolution of Carotid Atherosclerosis. *Stroke* **55**, ATP143–ATP143 (2024).

25. Adams, G. J. *et al.* Bilateral Symmetry of Human Carotid Artery Atherosclerosis. *Stroke* **33**, 2575–2580 (2002).
26. Howard, G. *et al.* Relations of intimal-medial thickness among sites within the carotid artery as evaluated by B-mode ultrasound. ARIC Investigators. Atherosclerosis Risk in Communities. *Stroke* **25**, 1581–1587 (1994).
27. Li, F. & Wang, X. Bilateral symmetry of human carotid artery atherosclerosis: a multi-contrast weighted MR study. *Int J Cardiovasc Imaging* **32**, 1219–1226 (2016).
28. Sun, J. *et al.* Carotid Plaque Lipid Content and Fibrous Cap Status Predict Systemic CV Outcomes. *JACC: Cardiovascular Imaging* **10**, 241–249 (2017).
29. Shen, R. *et al.* Slice-based and time-specific hemodynamic measurements discriminate carotid artery vulnerable atherosclerotic plaques. *Computer Methods and Programs in Biomedicine* **225**, 107050 (2022).
30. Sun, J. *et al.* Adventitial Perfusion and Intraplaque Hemorrhage. *Stroke* **44**, 1031–1036 (2013).
31. Selwaness, M. *et al.* Blood Pressure Parameters and Carotid Intraplaque Hemorrhage as Measured by Magnetic Resonance Imaging. *Hypertension* **61**, 76–81 (2013).
32. Underhill, H. R. *et al.* Arterial Remodeling in the Subclinical Carotid Artery Disease. *JACC: Cardiovascular Imaging* **2**, 1381–1389 (2009).
33. van den Bouwhuijsen, Q. J. A. *et al.* Change in Carotid Intraplaque Hemorrhage in Community-dwelling Subjects: A Follow-up Study Using Serial MR Imaging. *Radiology* **282**, 526–533 (2017).

34. Ota, H. *et al.* Carotid Intraplaque Hemorrhage Imaging at 3.0-T MR Imaging: Comparison of the Diagnostic Performance of Three T1-weighted Sequences. *Radiology* **254**, 551–563 (2010).
35. Li, D. *et al.* Histological validation of simultaneous non-contrast angiography and intraplaque hemorrhage imaging (SNAP) for characterizing carotid intraplaque hemorrhage. *Eur Radiol* **31**, 3106–3115 (2021).
36. Virmani, R. *et al.* Atherosclerotic Plaque Progression and Vulnerability to Rupture. *Arteriosclerosis, Thrombosis, and Vascular Biology* **25**, 2054–2061 (2005).
37. Gupta, A. *et al.* Carotid Plaque MRI and Stroke Risk. *Stroke* **44**, 3071–3077 (2013).
38. Takaya, N. *et al.* Association Between Carotid Plaque Characteristics and Subsequent Ischemic Cerebrovascular Events. *Stroke* **37**, 818–823 (2006).
39. Saam, T. *et al.* Meta-Analysis and Systematic Review of the Predictive Value of Carotid Plaque Hemorrhage on Cerebrovascular Events by Magnetic Resonance Imaging. *Journal of the American College of Cardiology* **62**, 1081–1091 (2013).
40. Sluimer, J. C. *et al.* Thin-Walled Microvessels in Human Coronary Atherosclerotic Plaques Show Incomplete Endothelial Junctions: Relevance of Compromised Structural Integrity for Intraplaque Microvascular Leakage. *Journal of the American College of Cardiology* **53**, 1517–1527 (2009).
41. Ota, H. *et al.* Hemorrhage and Large Lipid-Rich Necrotic Cores Are Independently Associated With Thin or Ruptured Fibrous Caps. *Arteriosclerosis, Thrombosis, and Vascular Biology* **29**, 1696–1701 (2009).

42. Chen, S. *et al.* Evaluation of carotid atherosclerotic plaque surface characteristics utilizing simultaneous noncontrast angiography and intraplaque hemorrhage (SNAP) technique. *Journal of Magnetic Resonance Imaging* **47**, 634–639 (2018).
43. Corti, R. *et al.* Effects of Aggressive Versus Conventional Lipid-Lowering Therapy by Simvastatin on Human Atherosclerotic Lesions: A Prospective, Randomized, Double-Blind Trial With High-Resolution Magnetic Resonance Imaging. *Journal of the American College of Cardiology* **46**, 106–112 (2005).
44. Underhill, H. R. *et al.* Effect of rosuvastatin therapy on carotid plaque morphology and composition in moderately hypercholesterolemic patients: A high-resolution magnetic resonance imaging trial. *American Heart Journal* **155**, 584.e1-584.e8 (2008).
45. Lee, J. M. S. *et al.* Early changes in arterial structure and function following statin initiation: Quantification by magnetic resonance imaging. *Atherosclerosis* **197**, 951–958 (2008).
46. Zhao, X.-Q. *et al.* MR Imaging of Carotid Plaque Composition During Lipid-Lowering Therapy: A Prospective Assessment of Effect and Time Course. *JACC: Cardiovascular Imaging* **4**, 977–986 (2011).
47. Dong, L. *et al.* Carotid Artery Atherosclerosis: Effect of Intensive Lipid Therapy on the Vasa Vasorum—Evaluation by Using Dynamic Contrast-enhanced MR Imaging. *Radiology* **260**, 224–231 (2011).
48. Kini, A. S. *et al.* Changes in Plaque Lipid Content After Short-Term Intensive Versus Standard Statin Therapy: The YELLOW Trial (Reduction in Yellow Plaque by Aggressive Lipid-Lowering Therapy). *Journal of the American College of Cardiology* **62**, 21–29 (2013).

49. Zhao, X.-Q. *et al.* Magnetic Resonance Imaging of Intraplaque Hemorrhage and Plaque Lipid Content With Continued Lipid-Lowering Therapy: Results of a Magnetic Resonance Imaging Substudy in AIM-HIGH. *Circulation: Cardiovascular Imaging* **15**, e014229 (2022).
50. Guo, L. *et al.* $CD163^{+}$ macrophages promote angiogenesis and vascular permeability accompanied by inflammation in atherosclerosis. *J Clin Invest* **128**, 1106–1124 (2018).
51. Guo, Y. *et al.* Plaque Evolution and Vessel Wall Remodeling of Intracranial Arteries: A Prospective, Longitudinal Vessel Wall MRI Study. *Journal of Magnetic Resonance Imaging* **60**, 889–899 (2024).
52. Baylam Geleri, D. *et al.* Detection of Advanced Lesions of Atherosclerosis in Carotid Arteries Using 3-Dimensional Motion-Sensitized Driven-Equilibrium Prepared Rapid Gradient Echo (3D-MERGE) Magnetic Resonance Imaging as a Screening Tool. *Stroke* **53**, 194–200 (2022).
53. Guo, Y. *et al.* Carotid plaque composition segmentation in multi-contrast MRI with U-net. in *Proc. Intl. Soc. Mag. Reson. Med* 2145 (2019).
54. Guo, Y. *et al.* AI-based Computer-Aided System for Cardiovascular Disease Evaluation (AI-CASCADE) for carotid tissue quantification. in *Proc. Intl. Soc. Mag. Reson. Med* 2666 (2021).
55. Cai, J.-M. *et al.* Classification of Human Carotid Atherosclerotic Lesions With In Vivo Multicontrast Magnetic Resonance Imaging. *Circulation* **106**, 1368–1373 (2002).
56. Wang, X. *et al.* Automated MRI-based segmentation of intracranial arterial calcification by restricting feature complexity. *Magnetic Resonance in Medicine* **93**, 384–396 (2025).

Chapter 6 Conclusion

This dissertation advances the field of vascular imaging through innovative methodological developments and clinically relevant investigations of atherosclerotic disease across two distinct arterial beds. My contributions are two-fold, encompassing both methodological innovations and advancements in clinical knowledge.

For intracranial atherosclerosis, I developed and validated MOCHA, a reproducible image analysis pipeline for multi-contrast vessel wall MRI that enables precise plaque characterization across multiple arterial segments. Building on this foundation, I introduced a novel semi-automated method for quantifying contrast enhancement in intracranial plaques, demonstrating excellent accuracy against expert assessment and high reproducibility. These methodological advances enabled me to conduct the first prospective longitudinal study of intracranial atherosclerosis using 3D vessel wall MRI, revealing significant associations between diabetes, baseline contrast enhancement, and plaque progression, while identifying distinctive remodeling patterns in culprit versus non-culprit lesions.

In the carotid artery bed, I developed and implemented deep learning-based segmentation pipelines capable of accurately identifying vessel walls and intraplaque hemorrhage from multi-contrast vessel wall MRI. Utilizing these advanced techniques, I conducted the longest-duration study with the most follow-up timepoints to date, demonstrating that intraplaque hemorrhage persists over extended periods and significantly accelerates plaque growth compared to lesions without hemorrhage, which showed minimal progression under contemporary medical therapy. Collectively, these studies establish advanced imaging biomarkers across both arterial territories that may improve risk stratification and guide targeted interventions for stroke prevention.

VITA

Yin Guo was born in Suzhou, Jiangsu, China and received a Bachelor of Engineering in Biomedical Engineering with a minor in Industrial Engineering from Tsinghua University in 2018. Following this, he earned a Master of Science in Biomedical Engineering from Yale University in 2019, before pursuing doctoral studies at the University of Washington.

During his Bioengineering PhD program, he worked as a Graduate Research Assistant in the Vascular Imaging Lab in the Department of Radiology, focusing on developing AI-driven quantitative imaging pipelines for multi-modality medical imaging in longitudinal studies. His research contributions include designing automated and interactive quantification and visualization tools for magnetic resonance vessel wall imaging, and conducting pioneering longitudinal studies on cerebrovascular atherosclerosis progression.

Beyond academic research, Yin has gained valuable industry experience through internships at Global Health Labs and Subtle Medical Inc, where he applied his expertise in AI and medical imaging to solve real-world healthcare challenges. Additionally, he served as Chair of the Society of Magnetic Resonance Angiography Early Career Committee, contributed as a reviewer for several prestigious scientific journals including the American Journal of Neuroradiology, and volunteered at the Seattle Symphony.